AD NUMBER

AD877209

LIMITATION CHANGES

TO:

Approved for public release; distribution is unlimited.

FROM:

Distribution authorized to U.S. Gov't. agencies and their contractors; Critical Technology; OCT 1970. Other requests shall be referred to U.S. Aviation Materiel Laboratories, Fort Eustis, VA 23604. This document contains export-controlled technical data.

AUTHORITY

USAAMRDL ltr, 17 May 1971

AD

USAAVLABS TECHNICAL REPORT 70-56

SINGLE-STAGE AXIAL COMPRESSOR STATOR REDESIGN INVESTIGATION

By

C. Muller

October 1970

U. S. ARMY AVIATION MATERIEL LABORATORIES
FORT EUSTIS, VIRGINIA

CONTRACT DAAJ02-69-C-0085
CURTISS-WRIGHT CORPORATION
WOOD-RIDGE, NEW JERSEY

DISCLAIMERS

The findings in this report are not to be construed as an official Department of the Army position unless so designated by other authorized documents.

When Government drawings, specifications, or other data are used for any purpose other than in connection with a definitely related Government procurement operation, the United States Government thereby incurs no responsibility nor any obligation whatsoever; and the fact that the Government may have formulated, furnished, or in any way supplied the said drawings specifications, or other data is not to be regarded by implication or otherwise as in any manner licensing the holder or any other person or corporation, or conveying any rights or permission, to manufacture, use, or sell any patented invention that may in any way be related thereto.

DISPOSITION INSTRUCTIONS

Destroy this report when no longer needed. Do not return it to the originator.

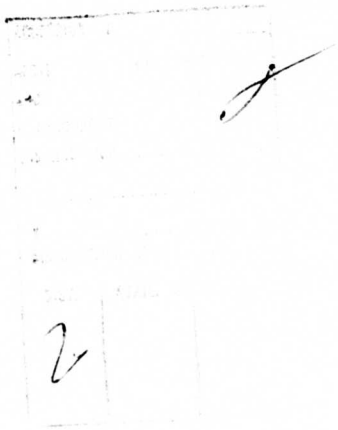

DEPARTMENT OF THE ARMY
HEADQUARTERS US ARMY AVIATION MATERIEL LABORATORIES
FORT EUSTIS, VIRGINIA 23604

The work described herein was conducted by the Curtiss-Wright Corporation under U. S. Army Contract DAAJ02-69-C-0085. The work was performed under the technical management of Mr. David B. Cale of the Propulsion Division, U. S. Army Aviation Materiel Laboratories.

Appropriate technical personnel of this Command have reviewed this report and concur with the conclusions contained herein. The findings and recommendations outlined herein will be used in the planning of any future supersonic axial compressor programs.

The work reported herein is essentially a follow-on effort to work performed under U. S. Army Contract DA 44-177-AMC-392(T) and reported in USAAVLABS Technical Reports 68-90A, 68-90B, and 68-90C.

Task 1G162203D14413
Contract DAAJ02-69-C-0085
USAAVLABS Technical Report 70-56
October 1970

SINGLE-STAGE AXIAL COMPRESSOR STATOR REDESIGN INVESTIGATION

Final Report

by

C. Muller

Prepared by

Curtiss-Wright Corporation
Wood-Ridge, New Jersey

for

U.S. ARMY AVIATION MATERIEL LABORATORIES
FORT EUSTIS, VIRGINIA

SUMMARY

The objectives of this program are to redesign the exit stators of the 2.8:1 pressure ratio supersonic axial compressor to provide an essentially cylindrical flow path aft of the rotor, and to fabricate and test the redesigned stators to evaluate their effect on overall stage performance.

The compressor stage performance from the test with the redesigned exit stators is as follows:

	Stage		
	Design Goals	Demonstrated	
Inlet Guide Vane Setting	Design	Design	-7 Degrees
Exit Stator Setting	Design	Design	Design
Pressure Ratio	2.8:1	2.68:1	2.57:1
Adiabatic Efficiency (Percent)	82.2	71.4	72.8
Corrected Airflow (Pounds per Second)	4.0	4.00	4.00
Corrected Speed (Revolutions per Minute)	50,700	50,700	50,700

This performance does not represent any improvement over the performance demonstrated under Contract DA 44-177-AMC-392(T) with the previous exit stators and reflects a two-point degradation in efficiency.

The demonstrated exit stator and duct total pressure loss at design speed peak stage performance points ranged from 7 to 12 percent. At the design stator setting, the loss was consistent with that demonstrated by the previous exit stators.

The measured axial static pressure gradient indicated that the flow accelerates from a Mach number under 0.9 at the rotor trailing edge to sonic or slightly supersonic Mach number at the stator leading edge. This acceleration was also evident in the test with the previous exit stator design. It is concluded that the insensitivity of the stator loss to the change in stator configuration is attributed to this acceleration and the high Mach number which results at the stator entrance.

Variation in the angle setting of the adjustable stator blades caused some movement of the surge line and flow range of the compressor but offered no improvement in the peak performance relative to the design setting.

FOREWORD

This work was performed under United States Army Contract DAAJ02-69-C-0085 by Curtiss-Wright Corporation to advance and demonstrate the performance of a high-pressure-ratio supersonic axial compressor stage by improving the exit stator design. The initial design of this compressor stage was performed under Contract DA 44-177-AMC-392(T) as a part of the advanced technology component program for small gas turbines. The subject contract was administered by the Propulsion Division of the U.S. Army Aviation Materiel Laboratories. The exit stators and associated stator housings of the compressor were redesigned, fabricated, and tested with the inlet guide vanes and rotor developed under the previous contract. The authority for this work was DA Task 1G162203D14413.

The manager of this compressor technology contract was C. H. Muller. Principal contributing engineers were S. Thirumalaisamy, W. Litke and H. Watts. The overall guidance and technical direction provided by Mr. J. Wiggins and the direction of Mr. D. Wagner, are gratefully acknowledged. The guidance of Mr. H. Morrow, Mr. E. Johnson and Mr. D. Cale of the U.S. Army Aviation Materiel Laboratories is also gratefully acknowledged.

BLANK PAGE

TABLE OF CONTENTS

LIST OF ILLUSTRATIONS

LIST OF ILLUSTRATIONS (Cont.)

LIST OF ILLUSTRATIONS (Cont.)

LIST OF TABLES

LIST OF SYMBOLS

A/A^*	isentropic area ratio - dimensionless
A^*	area at which sonic flow would occur - square inches
A_{ann}	annular area - square inches
A_{flow}	flow area - square inches
a	acoustic velocity (based on static temperature) - feet per second
a_t	acoustic velocity (based on total temperature) - feet per second
c	blade chord - inches
C_p	specific heat for a constant pressure process - BTU per pound per degree Rankine
C/I	inverse of the stiffness modulus - reciprocal of inches cubed
D	diameter - inches
D_m	mean diameter - inches
g	acceleration of gravity - feet per second squared
h	hub streamtube
IC	iron-constantan thermocouple
ID	inside diameter - inches
i	incidence angle - degrees
i'	modified incidence angle - degrees
J	work constant (778 foot-pounds per BTU)
K	continuity equation constant (0.26048 pound square root of degree Rankine per second per square inch per inch of mercury)
k	spring rate - pounds per inch
L	length of blade suction surface forming passage - inches
M	Mach number - dimensionless
m	mean streamtube
N	rotational speed - revolutions per minute

LIST OF SYMBOLS (Cont.)

OD	outside diameter - inches
P_s	static pressure - inches of mercury
P_T	total pressure - inches of mercury
R	radius of curvature in meridional plane - inches; (or gas constant, 53.4 foot-pounds per pound per degree Rankine, when it occurs in the expression $\sqrt{KgRT_s}$)
REC	total pressure recovery - ratio of total pressure remaining after losses through blade row passage to initial total pressure at blade row inlet - dimensionless
r	radius from compressor axis - inches
s	blade to blade pitch - inches
T_s	static temperature - degrees Rankine
T_T	total temperature - degrees Rankine
t	tip streamtube
t/c	ratio of maximum blade thickness to the chord length - dimensionless
U	rotor blade section speed - feet per second
V	velocity - feet per second
V_{ax}	axial velocity component - feet per second
V_{tan}	tangential velocity component - feet per second
W	airflow - pounds per second
w	width of blade passage at throat - inches
α	tangential airflow angle relative to the compressor axis - degrees
β	tangential angle to blade camber line - degrees
β'	tangential angle to blade suction surface - degrees
δ	deviation angle - degrees (or ratio of local total pressure to a reference pressure, when it occurs in $(W\sqrt{\theta})/\delta$ - dimensionless)
Δ	change of a quantity across a blade row - dimensionless

ξ	airflow slope angle in meridional plane - degrees
η_{ad}	adiabatic efficiency - dimensionless
γ	ratio of specific heats - dimensionless
σ	solidity (c/s) - dimensionless
ϕ	blade camber angle - degrees
ρ	density - pounds per cubic foot
θ	air turning angle through a blade row - degrees (or ratio of local total temperature to a reference temperature, when it occurs in either $N/\sqrt{\theta}$ or $(W\sqrt{\theta})/\delta$ - dimensionless)

Subscripts

amb	ambient conditions
0	station at entrance to inlet guide vanes
1	absolute conditions (relative to nonrotating reference) at a station representing exit of inlet guide vanes and inlet to rotor
2	entrance conditions to rotor relative to the rotating rotor blade
3	exit conditions from the rotor relative to the rotating rotor blade
4	absolute conditions (relative to nonrotating reference) at a station representing the rotor exit and inlet to the exit stator and duct
4'	absolute conditions at the leading edge of the stator blade
5'	absolute conditions at the trailing edge of the stator blade
5	absolute conditions at a station representing the exit of the exit stator and interconnecting duct

INTRODUCTION

The 2.8:1-pressure-ratio supersonic axial compressor has been under development as a part of the U.S. Army Aviation Materiel Laboratories advanced technology program for small gas turbines. This compressor is intended to serve as a boost stage in axial centrifugal compressors with overall pressure ratios of 16:1.

The preliminary engine and compressor design studies, the detailed design and fabrication of the supersonic axial stage, and the initial experimental development program for this stage were performed under Contract DA 44-177-AMC-392(T). The stage developed under that contract consisted of an inlet duct, inlet guide vanes, rotor, exit stators, and the interconnecting duct which connects to a following centrifugal stage at the entrance to its impeller.

The exit stator and interconnecting duct configuration involved an "S" shaped meridional flow path in order to match the scaled RF-1 (Reference 7) centrifugal compressor geometry. The stator vanes were incorporated within the "S" shaped duct to avoid an excessive overall stage length, and this made variable or adjustable stators impractical. The design goals and demonstrated performance for the overall stage were as follows:

	Goal	Demonstrated	
Inlet Guide Vane Setting	Design	Design	-4 Degrees
Pressure Ratio	2.8:1	2.69:1	2.62:1
Adiabatic Efficiency (Percent)	82.2	73.9	74.7
Corrected Airflow (Pounds per Second)	4.0	4.02	4.02

The inlet guide vane and rotor performances had essentially met their goals, and the deficiency in stage performance was attributed to the stator losses. The overall results were very encouraging, however, and it was expected that the elimination of the "S" shaped duct in the stator assembly would reduce the stator losses.

An investigation of a change in exit stator configuration has been pursued under Contract DAAJ02-69-C-0085. The objectives of this program were to redesign the exit stators of the 2.8:1-pressure-ratio supersonic axial compressor to provide an essentially cylindrical flow path aft of the rotor, and to fabricate and test the redesigned stators to evaluate their effect on overall stage performance. The results of this program are reported herein.

EXIT STATOR REDESIGN

CONFIGURATION

The redesign of the compressor stage performed in this program has been limited to the components downstream of the rotor and rotor shroud. The performance goals at the rotor exit were essentially met in the final test of Contract DA 44-177-AMC-392(T). The compressor configuration from the inlet to the rotor exit for this program has, therefore, been maintained as previously tested.

The exit stator and duct assembly has been redesigned to provide a cylindrical annular flow path from the rotor exit to the trailing edge of the exit stator (see **Figure** 1). The stator vanes have been designed so that the stagger angle can be adjusted to vary the flow incidence. Beyond the trailing edge of the stator vanes, the outer shroud wall becomes conical to form a diffusing passage with the cylindrical inner wall for further deceleration of the flow.

AERODYNAMIC REDESIGN

The approach to the aerodynamic redesign of the exit stator assembly was to investigate whether or not a stator could be designed within a truly cylindrical flow path and meet all of the desired criteria. The vane airfoil shapes were developed to satisfy passage flow criteria. Primary criteria considered in optimizing the stator design were area schedule, aspect ratio, solidity, choke margin, maximum thickness-to-chord ratio, turning, and loading distributions. The passages were initially established and evaluated with respect to these criteria as two-dimensional sections. Subsequently they were integrated into a three-dimensional passage and evaluated as such in the final analysis. The exit stator was designed to match the rotor exit flow conditions for the compressor design point, which are as follows:

	Hub	Mean	Tip
Corrected Airflow (Pounds Per Second) = 4.0			
Radius (Inches)	2.507	2.650	2.796
Pressure Ratio	2.86	2.91	2.90
Corrected Temperature Rise (Degrees Rankine)	207.2	217.0	223.0
Absolute Flow Angle	43.3	46.8	48.9
Absolute Mach Number	.900	.845	.798

Table I presents the blade data for the redesigned stator.

Turning Angle and Solidity

Stall data for two-dimensional diffusers were the criteria used to establish the blade solidity and overall turning angle. Reference 4 provides stall data for curved diffusers as a function of the turning angle, normalized inner wall length, and aspect ratio. Figure 2 presents the turning angle at which stall occurs as a function of the inner normalized wall length at the three aspect ratios appropriate for the hub, mean and

2.8:1 Supersonic Compressor

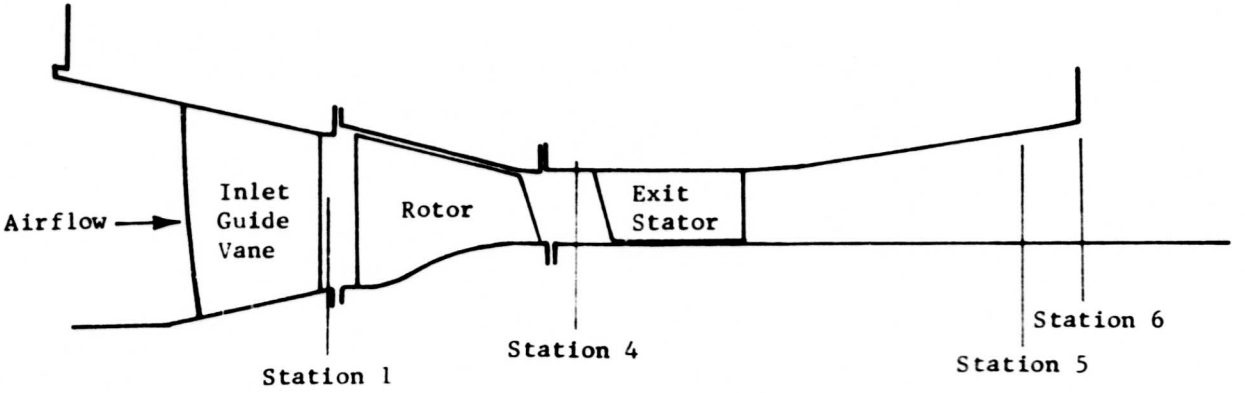

Figure 1. Meridional Flow Path With Redesigned Exit Stator.

TABLE I. BLADE DATA FOR REDESIGNED EXIT STATOR

Number of Blades		42	
Radius, r ~ in.	2.449	2.667	2.885
Pitch, s ~ in.	.3664	.3990	.4316
Chord, c ~ in.	.9179	1.0105	1.0920
Axial Chord, ~ in.	.8785	.9264	.9761
Inlet Throat Width, ~ in.	.2808	.2670	.2751
Leading Edge Radius, ~ in.	.005	.005	.005
Trailing Edge Radius, ~ in.	.008	.008	.008
Solidity, σ	2.51	2.53	2.53
Maximum Thickness to Chord Ratio, t/c	.05	.05	.05
Passage Area Ratio ~ $A_{\text{flow } 5'}/A_{\text{flow } 4'}$	1.222	1.375	1.433
Suction Surface Forming Passage, L ~ in.	0.74	0.78	0.84
Equivalent Diffuser Length, L/w	2.58	2.81	2.88
Inlet Air Angle, α 4' ~ deg	40.0	48.0	50.4
Exit Air Angle, α 5' ~ deg	0.0	3.0	6.0
Incidence to Suction Surface, i' ~ deg	1.0	1.0	1.0
Deviation, δ ~ deg	7.0	8.0	8.5
Unguided Turning Before Throat, θ ~ deg	7.3	8.2	8.2
Blade Passage Turning, $\Delta\beta$ ~ deg	43.1	49.2	49.1
Blade Inlet Angle, β 4', ~ deg	36.1	44.2	46.6
Blade Exit Angle, β 5', ~ deg	-7.0	-5.0	-2.5
Inlet Wedge Angle	5.7	5.5	5.5
Average Mach Number at Throat, M		0.76	
Choke Margin, (A/A*) -1		.057	

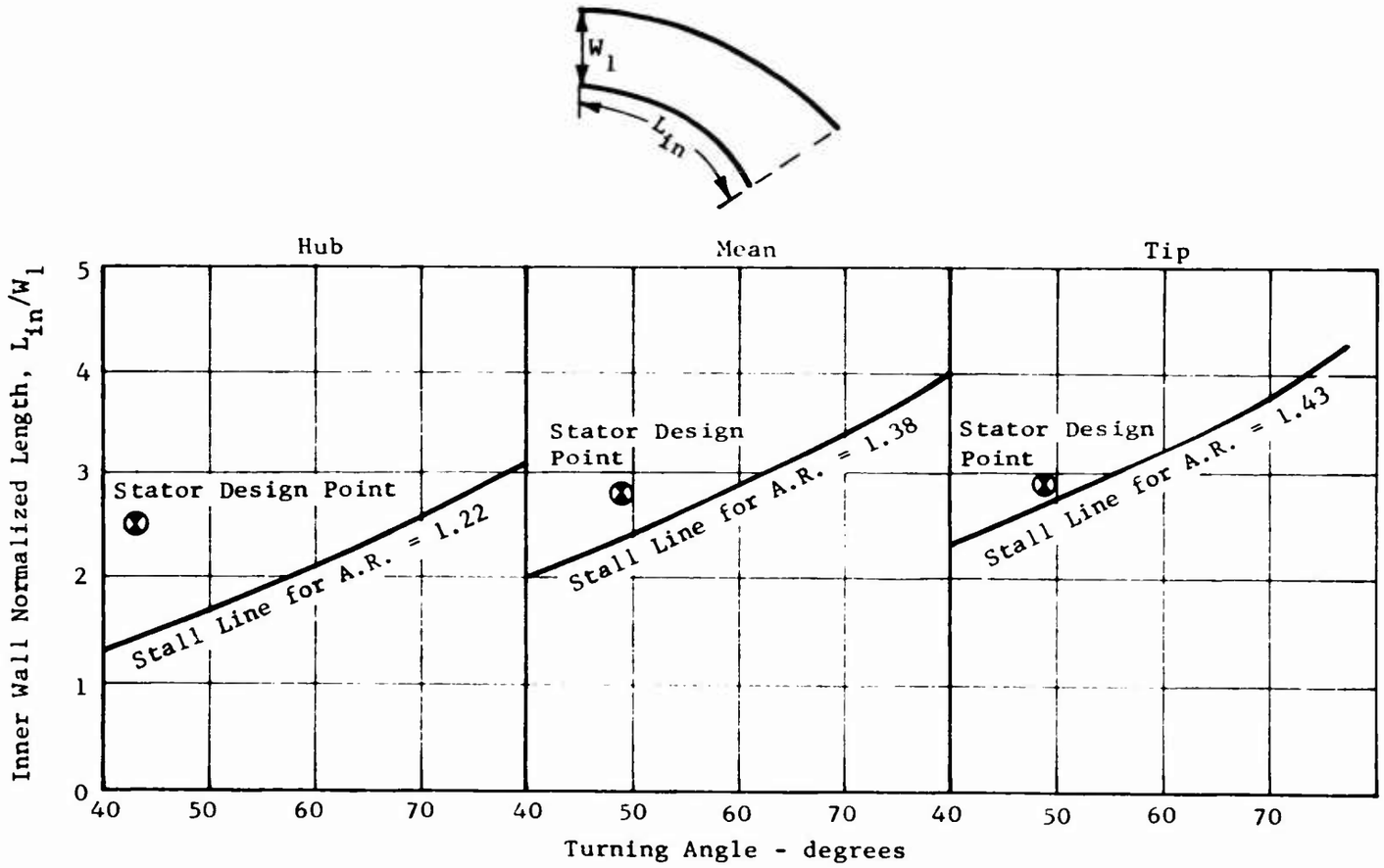

Figure 2. Stall Data for Curved Diffusers.

tip sections. The stator blade passages were equated to curved diffusers and evaluated with respect to these curves. The stator solidity ranging from 2.51 at the hub to 2.53 at the tip was established based on these curves so as to avoid stall. The initial intent was to turn the flow to an axial direction leaving the stator. At the hub section, the blade turning angle required to meet an axial exit flow is 61.1 degrees. It can be seen on Figure 2 that the stall margin for this turning at the specified solidity is sufficient to compensate for the three-dimensional effects which favor the tip at the expense of the hub. The tip section has a higher inlet angle and deviation angle and therefore would require a turning angle of 55.1 degrees to meet an axial exit flow. This high turning would require a tip solidity substantially higher than that at the hub in order to avoid tip stall. The blade taper and tip chord associated with such a tip solidity was considered excessive. Consequently, the tip flow was only turned to an exit angle 6 degrees shy of axial with a linear variation to the axial flow direction at the hub. This compromise required only a slight increase in tip solidity to provide an adequate stall margin as indicated on Figure 2.

Aspect Ratio

Two-dimensional diffuser data were utilized to evaluate the effects of aspect ratio (span/chord) on the stator performance and to establish the mean stator blade chord and the number of blades. Figure 3 shows the effect of aspect ratio on diffuser performance as derived from reference 5. These data indicate that below an aspect ratio of 3.0, the losses become sensitive to changes in aspect ratio and, below 1.0, increase rapidly as the aspect ratio is reduced. Consequently, it was desireable to design for an aspect ratio of greater than 1.0 and to approach 3.0 as closely as possible to minimize the stator pressure loss. Within the small size of the stator hardware, the blade attachment button considerations imposed a mechanical limitation at a maximum of 42 blades. At the designated solidity, a chord of 1.0 inch is established for the 42 blades, which results in an aspect ratio of 1.69.

Blade Passage and Blade Shape

The following considerations were taken into account in establishing the passages and developing the blade shapes.

The incidence angle to the suction surface was set equal to one degree since this value approximates the minimum loss incidence for transonic blading. The unguided surface turning between the stator leading edge and the throat reached a maximum of nine degrees at the tip section, resulting in a maximum suction surface Mach number of 1.4 with sonic inlet velocity, a condition which could be met at off-design operation. At design point, the tip inlet Mach number is 0.798 and average throat Mach number is 0.76.

The rate of change of mean camber line slope is made linear with axial distance to develop the balde sections aft of the throat. The variation of mean passage flow angle is shown in Figure 4.

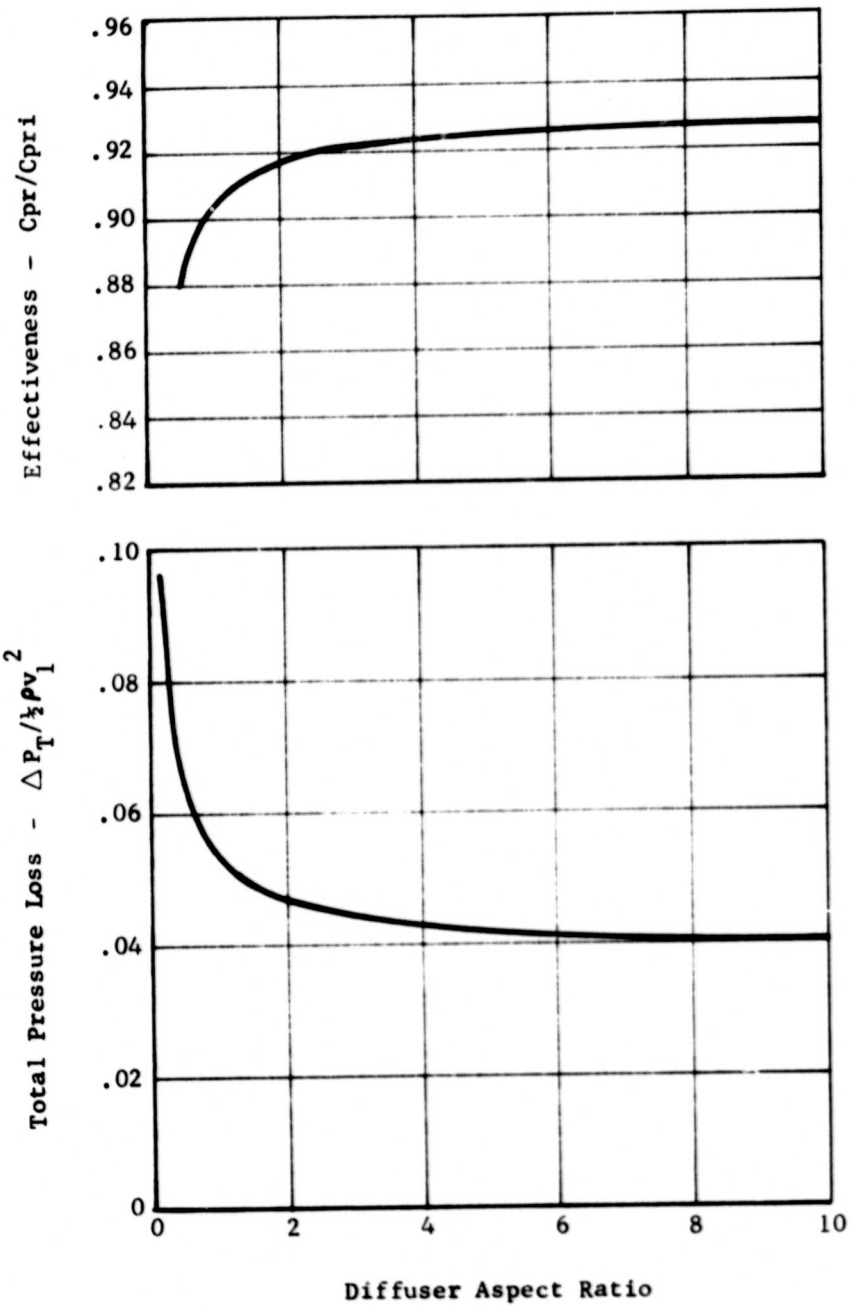

Figure 3. Diffuser Loss Versus Aspect Ratio.

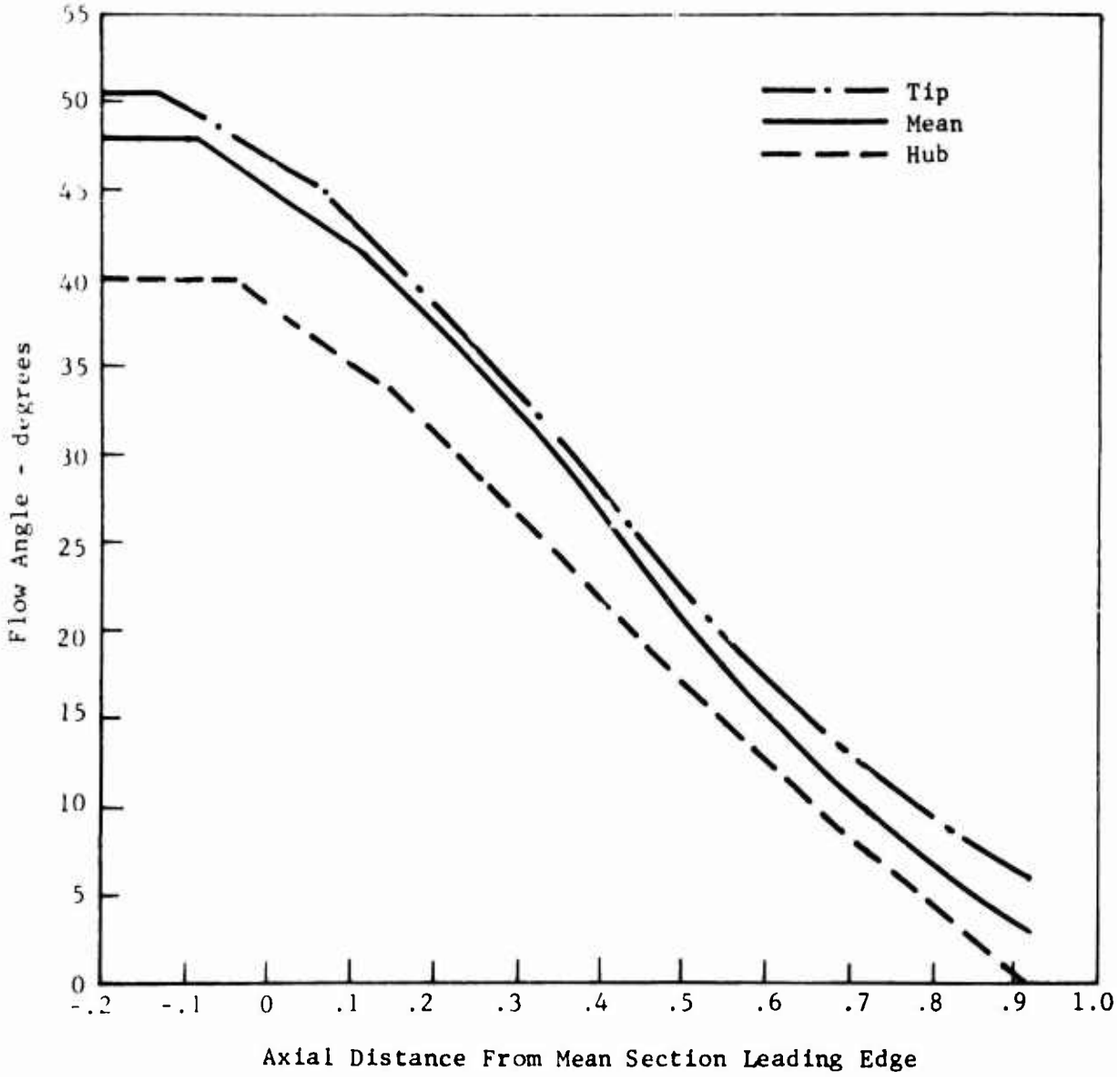

Figure 4. Variation of Flow Angle With Axial Distance in Redesigned Exit Stator.

The minimum value of maximum thickness-to-chord ratio was established at .05 for structural integrity. The thickness distribution was developed so as to achieve a relatively uniform increase in area as a function of mean camber length. Figure 5 shows the area schedules for the two-dimensional hub, mean and tip sections in terms of the ratio of local passage width to normalized axial length. Figure 6 shows the physical blockage of the blade thickness as a function of axial distance. The resultant blade airfoils are shown in Figures 7, 8, 9.

A computer program has been used to determine the variation in static pressure and velocity with axial distance in the resultant three-dimensional passage which satisfies continuity and radial equilibrium. The results are shown in Figure 10. The variation in tangential velocity is relatively linear with distance over most of the passage, indicating uniform blade loading and good blade velocity distribution (see reference 6). The rate of tangential velocity change is reduced at the exit to reduce deviation and equalize trailing edge blade surface velocities.

Aft of the blades the outer shroud is a cone of 6 degrees 25 minutes. This provides an annular diffuser with an equivalent circular diffuser cone angle of 10.8 degrees. In this section the flow is decelerated from a mean Mach number of .474 to a stage exit Mach number of .322.

Choke Margin

A choke margin of 5.7 percent was provided. The entire stator annulus area was made 3.1 percent larger than the rotor exit annulus area to attain this margin. The increase was accomplished by an equal increase of the tip shroud radius and decrease at the hub shroud radius of .007 inch in the stator assembly. The tip and hub radii were maintained constant from the leading edge of the stator housings to the trailing edge of the stator vane.

Table II summarizes the design velocity, Mach number and flow angle data at the key stations in the compressor.

STRUCTURAL DESIGN

The redesigned hardware for the exit stator assembly is shown in Figure 11. The exit outer housing, the exit stator blades (exit guide vanes), and the sleeve on the rear main bearing support are the newly designed components. The rear main bearing support was reworked to fit with the new sleeve. All of the other compressor components from the rotor and rotor shroud forward remained unchanged.

The two important aspects of the redesign were the change to a cylindrical annular flow path and the provision for adjustable stator vanes. The latter consideration required a change in exit stator design from an

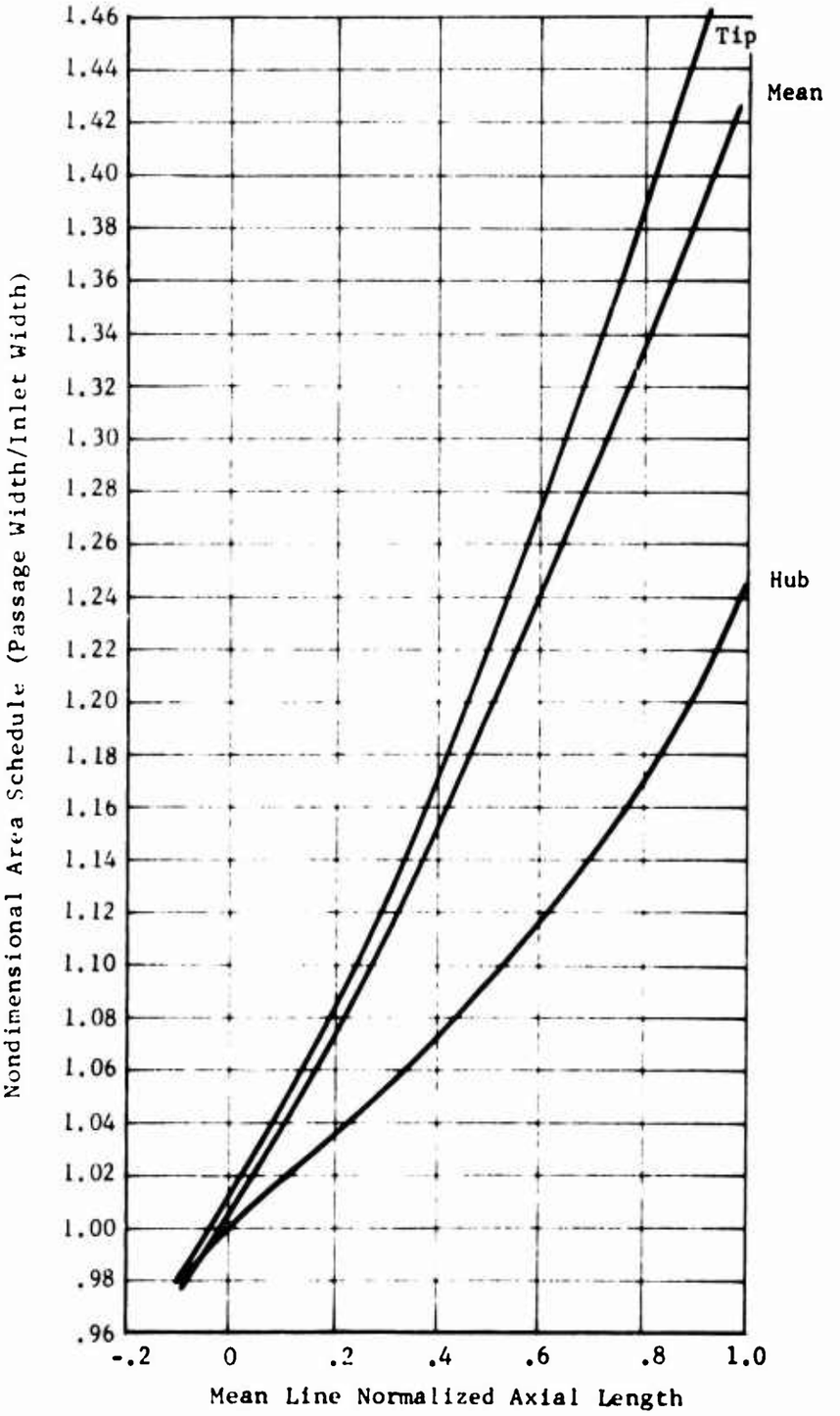

Figure 5. Area Schedule of Redesigned Stator Passage.

2.8:1 Supersonic Compressor

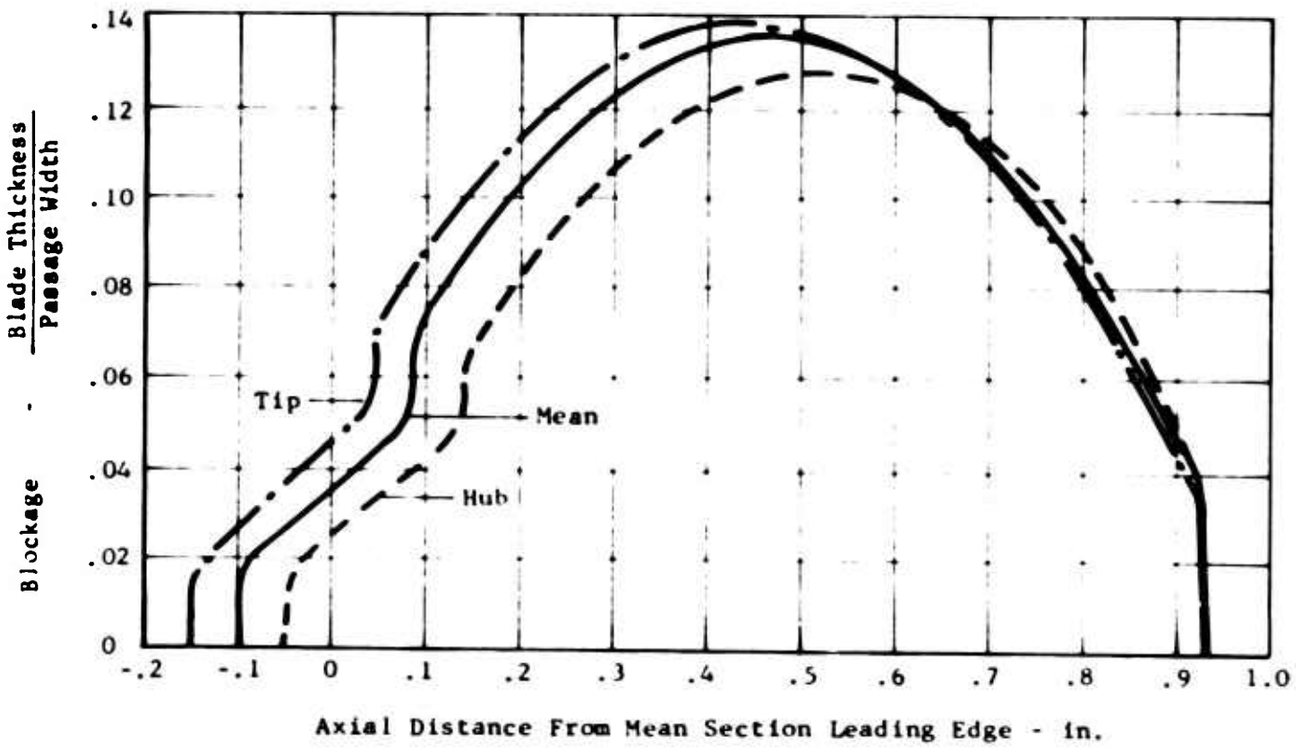

Figure 6. Blockage Due to Stator Blade Thickness.

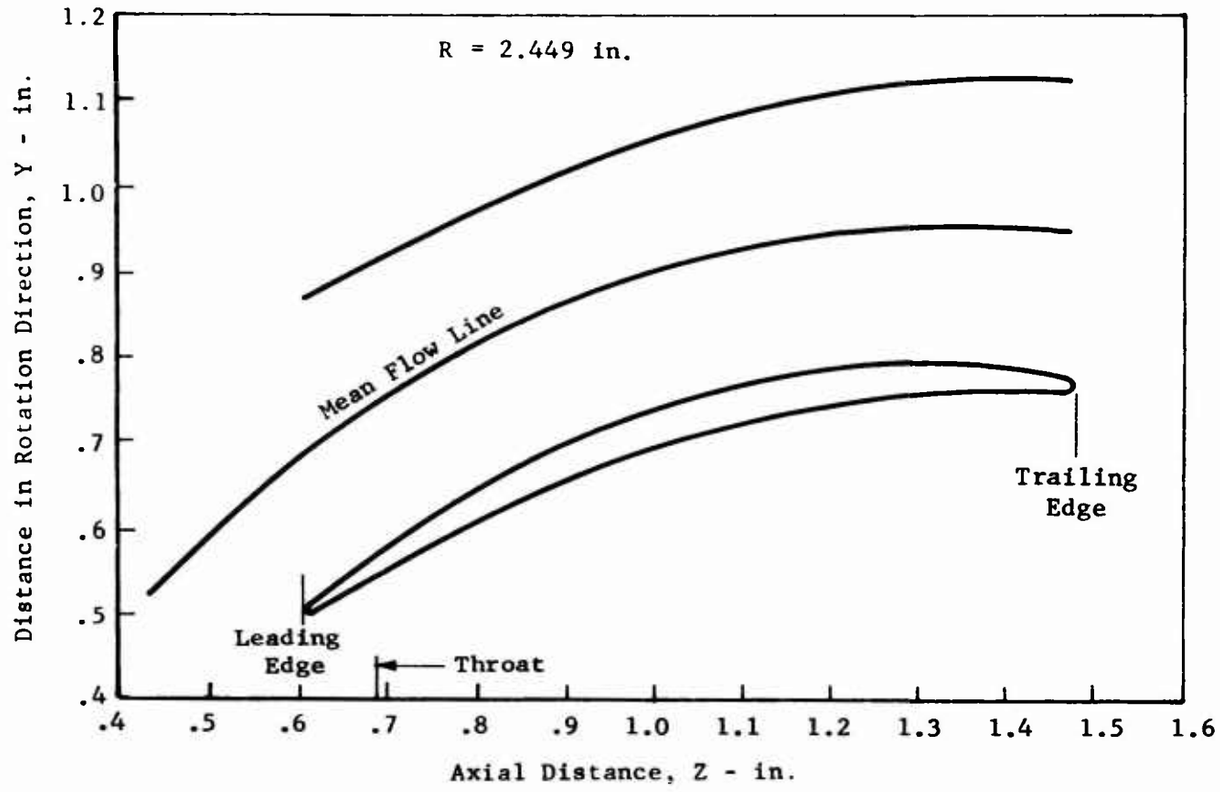

Figure 7. Redesigned Stator Hub Blade Section.

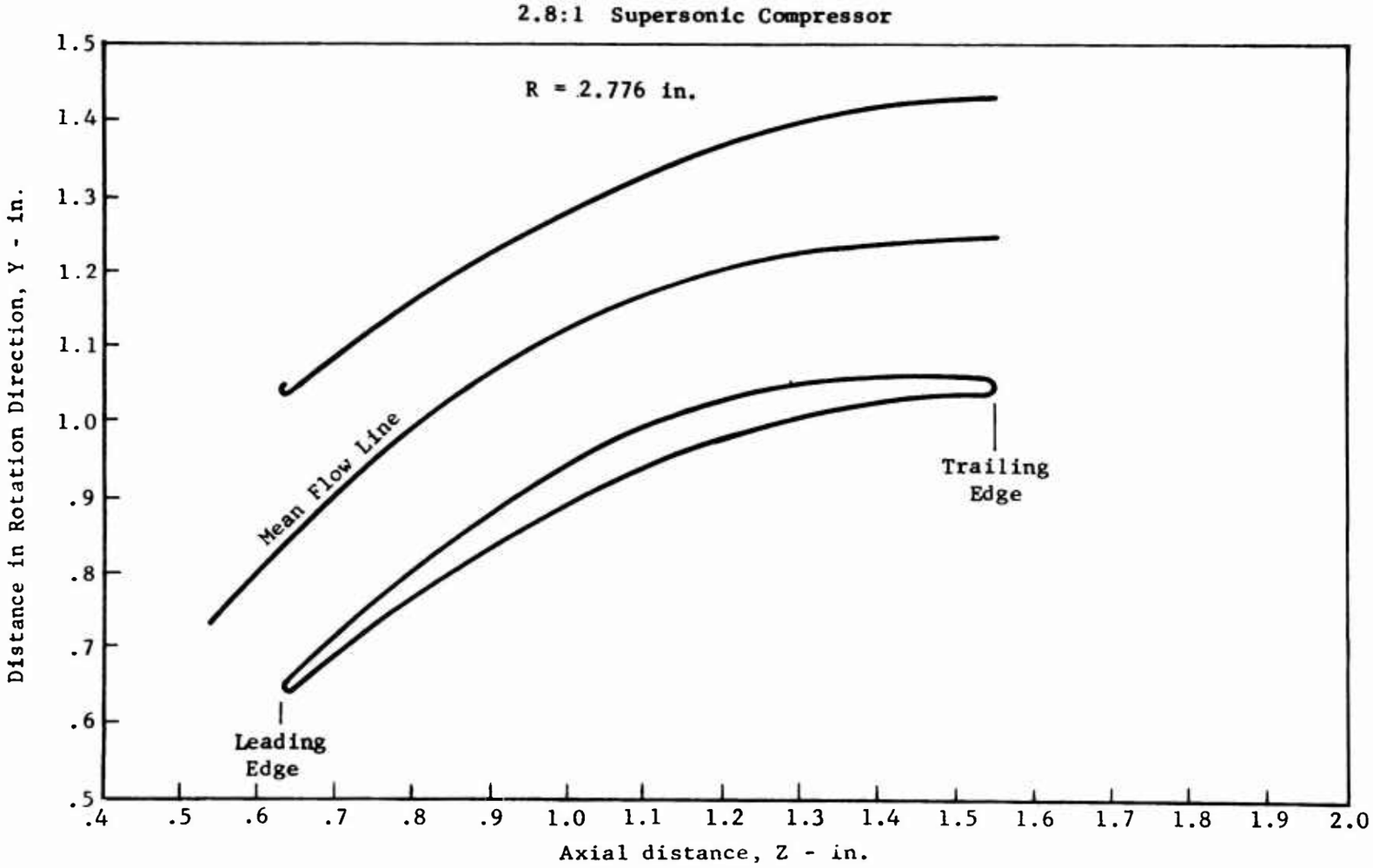

Figure 8. Redesigned Stator Mean Blade Section.

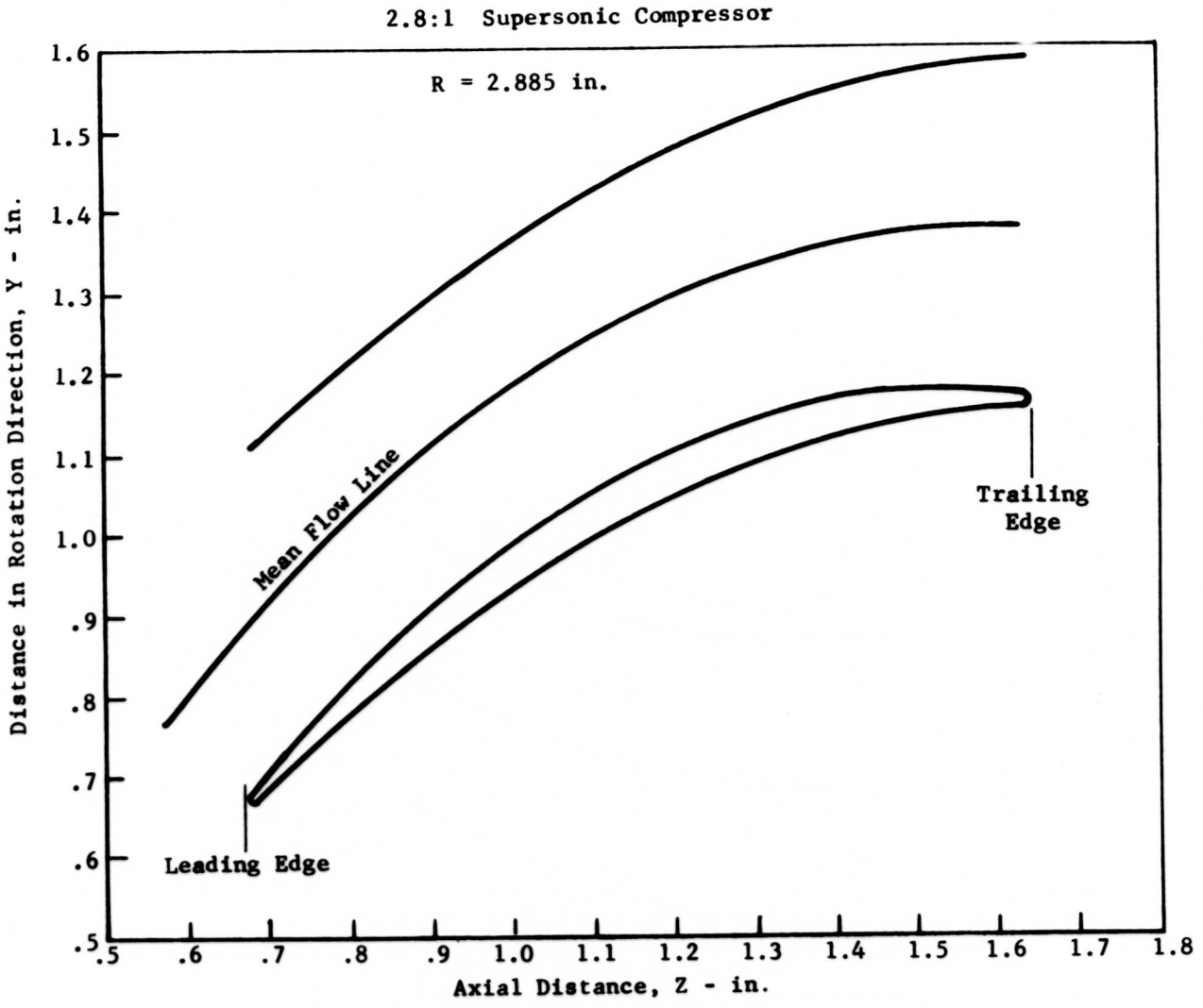

Figure 9. Redesigned Stator Tip Blade Section.

2.8:1 Supersonic Compressor

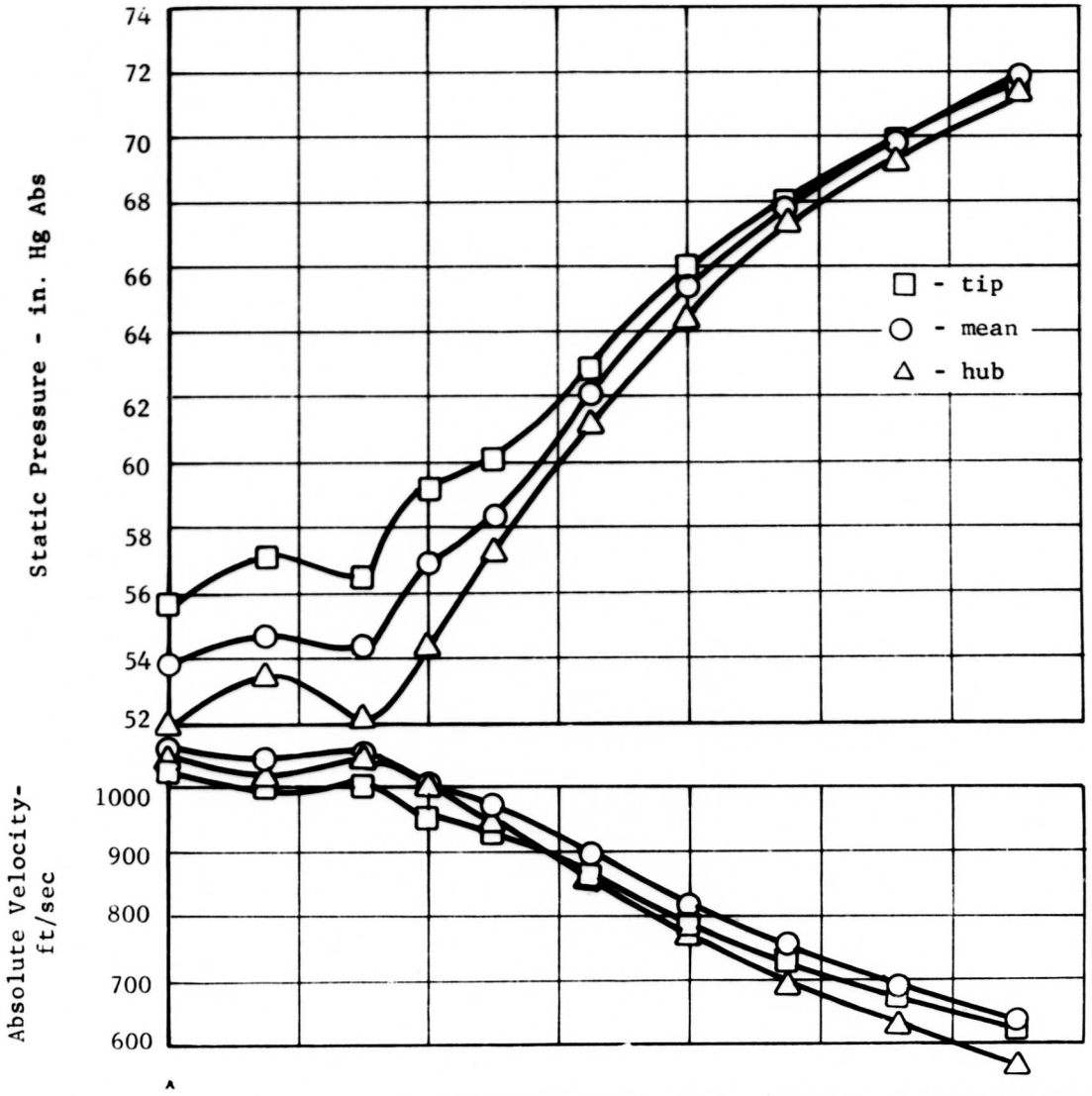

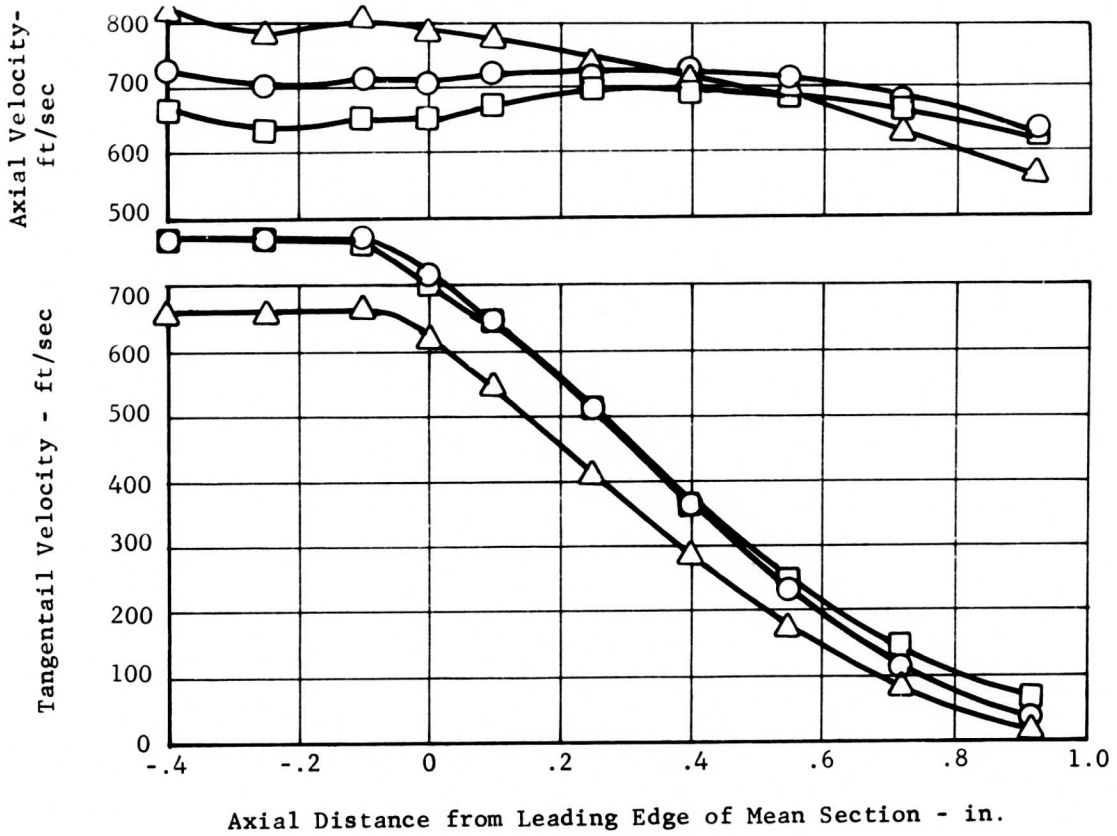

Figure 10. Predicted Stator Pressures and Velocities.

TABLE II. DESIGN POINT DATA FOR 2.8:1 SUPERSONIC COMPRESSOR WITH REDESIGNED EXIT STATOR

Station	Streamtube	Mach Number		Velocity (ft/sec)		Flow Angle (degrees)	
		Absolute	Relative	Absolute	Relative	Absolute	Relative
1	Tip	.584	1.599	631	1728	29.0	71.4
	Mean	.610	1.518	657	1636	31.3	69.9
	Hub	.629	1.428	676	1536	35.3	69.0
4	Tip	.798	.648	1004	815	48.9	35.9
	Mean	.845	.662	1051	825	46.8	29.3
	Hub	.900	.714	1104	876	43.3	23.6
5	Tip	.326	-	430	-	7.2	-
	Mean	.343	-	451	-	4.7	-
	Hub	.296	-	386	-	3.8	-
6	Tip	.271	-	357	-	8.7	-
	Mean	.285	-	374	-	5.6	-
	Hub	.246	-	321	-	4.6	-

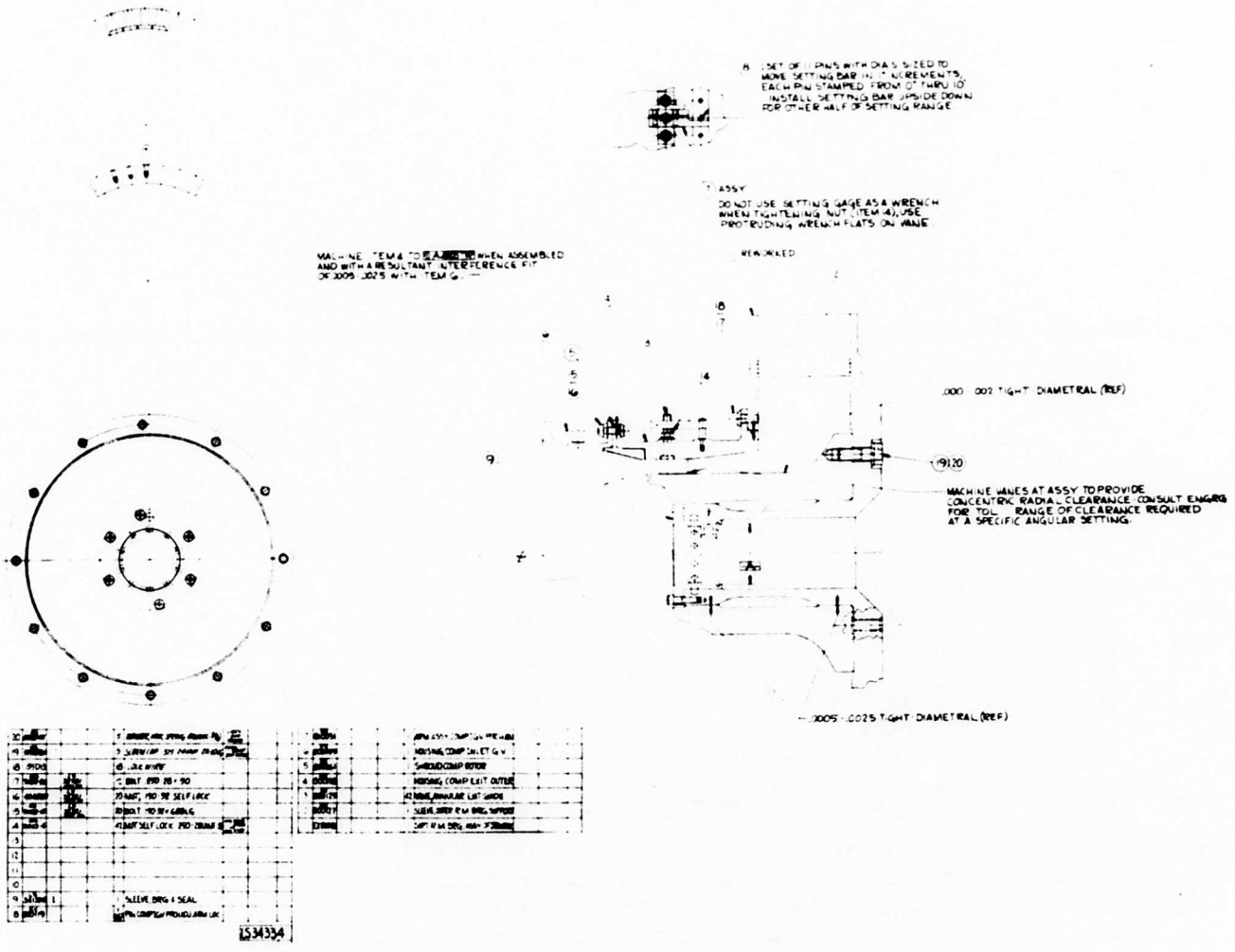

Figure 11. Layout of Redesigned Exit Stator Assembly.

integral blade and shroud configuration to an individual blade design with a cantilevered support. This also required a change in the support and pilot arrangement between the rear bearing and the front housing. In the previous design, the primary support and pilot arrangement from the rear bearing to the outer housing was directly through the integral exit stator blade and shroud assembly. Adjustable stator blades required that this support and piloting be carried from the bearing around through the rear main bearing support housing structure to the outer housing.

Outer Housing

The outer housing was designed to attach to the existing rotor shroud flange at the upstream end and rear support flange at the downstream end. The length between flange faces was increased only enough to eliminate the need for a .010-inch spacer used in the previous build. The rear flange pilot diameter was increased to provide an interference fit since the redesign made this one of the primary pilots for holding concentricity between the front and rear bearings.

This housing was made thick enough to contribute stiffness to the spring rate of the rear support system and to provide adequate pilot length for the stems of the stator vanes. The internal surface of the housing, which defines the tip shroud contour of the flow path, has a 2.902-inch constant radius from its leading edge to the station at the trailing edge of the stator vanes. Downstream of the vanes this radius increases at a 6-degree 24-minute cone angle. Pin holes are provided in the O.D. of the housing and located with respect to the vane support holes so that the same arm and pin arrangement used to set the inlet guide vane angles can be used to set the stator vanes.

Stator Vanes

The stator vanes are an integral airfoil, button and stem design.

The blade stem pilots through a radial hole in the outer housing, and the button seats in a counterbore at the housing I.D. contour. The stem is threaded and a lock nut is used to clamp the blade in place. The clamping force is 2300 pounds when the nut is torqued to 80-85 inch-pounds. This load results in 53,250 psi bearing stress on the button face. The 0.2 percent yield strength of the AMS 5613 material is 85,000 psi. The button surface on the blade side is contoured to closely match the cylindrical shroud and minimize the surface discontinuities. The button contour at the outer diameter is recessed slightly with respect to the shroud contour so that no protrusion of the button will occur when the blade is adjusted $\pm$ 10 degrees from the nominal setting. Parallel flats on either side of the end of the stem serve as the reference direction for the blade setting.

The airfoil section of the vane is constructed (stacked) so that the trailing edge is on a radial line from the axis which results in a tapered leading edge.

The structural analysis of the blade stresses due to the airloads gave the following results. The maximum shear stress at the junction of the airfoil and the button is 357 psi. The bending stress at the junction of the airfoil and the button is 10,194 psi. At the junction of the button and shank, the bending stress is 4375 psi. Both of these stresses include stress concentration factors. The shear forces and bending moments for the airfoils in the axial and tangential planes versus radius are given in Table III.

TABLE III. STATOR BLADE STRESS DATA

Radius (inches)	Shear Force		Bending Moment	
	Axial (pounds)	Tangential (pounds)	Axial (inch-pounds)	Tangential (inch-pounds)
2.902	-62.43	97.98	-14.27	22.38
2.808	-49.08	77.01	- 9.03	14.16
2.7139	-36.16	56.71	- 5.02	7.87
2.6670	-29.87	46.84	- 3.47	5.44
2.6199	-23.68	37.12	- 2.21	3.46
2.5259	-11.65	18.21	- 0.55	0.86
2.4316	0.0	0.0	0.0	0.0

The bending moments and shear forces are a maximum at the 2.902-inch radius, where the blade attaches to the button.

The C/I about the axis of minimum and maximum moments of inertia for airfoil sections at three radii are listed below.

Radius (Inches)	C/I (min)	C/I (max)
2.902	16100	1460
2.867	2056	121.9
2.667	770.6	6.7

The maximum C/I occurs at the 2.902-inch radius; consequently, the highest bending stress occurs at this location, which is the junction of the airfoil and the button. As previously indicated, the bending stress at this point is 10,194, which is well below the 0.2 percent yield strength of the material (85,000 psi).

Sleeve on Rear Main Bearing Support

The sleeve has been redesigned to provide the cylindrical hub passage wall and the necessary support at the rear bearing. A constant 2.432-inch radius is set at the O.D. of the sleeve from its leading edge to a point in the collector beyond the stage exit station. The sleeve is bolted to the rear plate of the rear main bearing support and further supported at two pilots with interference fits along the centerbody. This assembly provides a support system spring rate of 37 x 10^6 pounds per inch, which is

higher than that for the previous rig configuration (25×10^6 pounds per inch). These results were expected to preserve the satisfactory operation of the previous rig design, which was free of critical speeds.

FABRICATION

BLADES

The stator blades were machined individually as an integral airfoil, button and stem unit. The airfoil tooling was developed from 20 times size mylar airfoil sections and held within 0 to + .002 inch. The button end of the blade was machined to closely match the contour of the O.D. shroud but with sufficient clearance to permit an adjustment of ± 10 degrees from the nominal setting. Stock was left on the exposed end of the blade so that final machining to match the hub shroud contour could be performed as an assembly to minimize the blade to hub shroud clearance. The assembly machining of the exposed ends of the blades was performed by grinding a cylindrical radius .002 inch larger than the sleeve contour radius with the blades set at each of the 10-degree-closed and 8-degree-open settings. The calculated clearances at the leading and trailing edges of the stator at the various settings are given in Table IV.

TABLE IV. STATOR BLADE CLEARANCES

	Clearance (inches)			
	Leading Edge		Trailing Edge	
	O.D.	I.D.	O.D.	I.D.
Nominal Setting	.003	.002	.016	.007
10 degrees closed	.000	.002	.002	.019
10 degrees open	.005	-	.027	-
8 degrees open	-	.002	-	.002

Figures 12, 13 and 14 are photos of the stator vanes assembled in the outer housing.

The specified tolerance band for the blade thickness was .010 to .014 inch at the leading edge and .014 to .018 inch at a point .050 inch downstream of the leading edge. The final inspection data indicated that the majority of these blades were at the high limit.

HOUSING ASSEMBLY

Final machining of the housing and sleeve pilot diameters was accomplished during a step-by-step assembly process in order to maintain concentricities of the shroud contours and bearings within .001 inch.

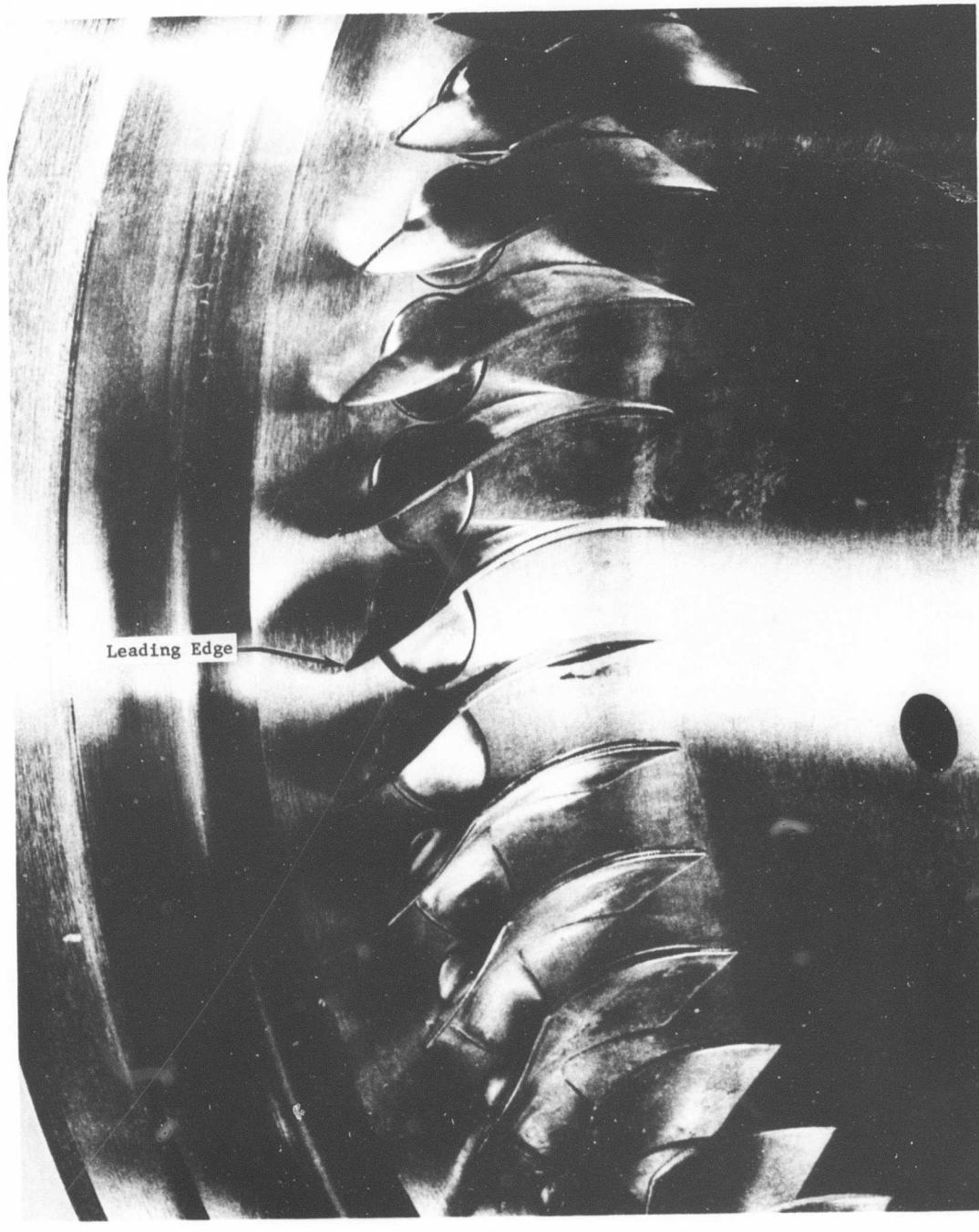

Figure 12. Redesigned Exit Stator and Outer Housing Assembly, Close-up View of Vanes.

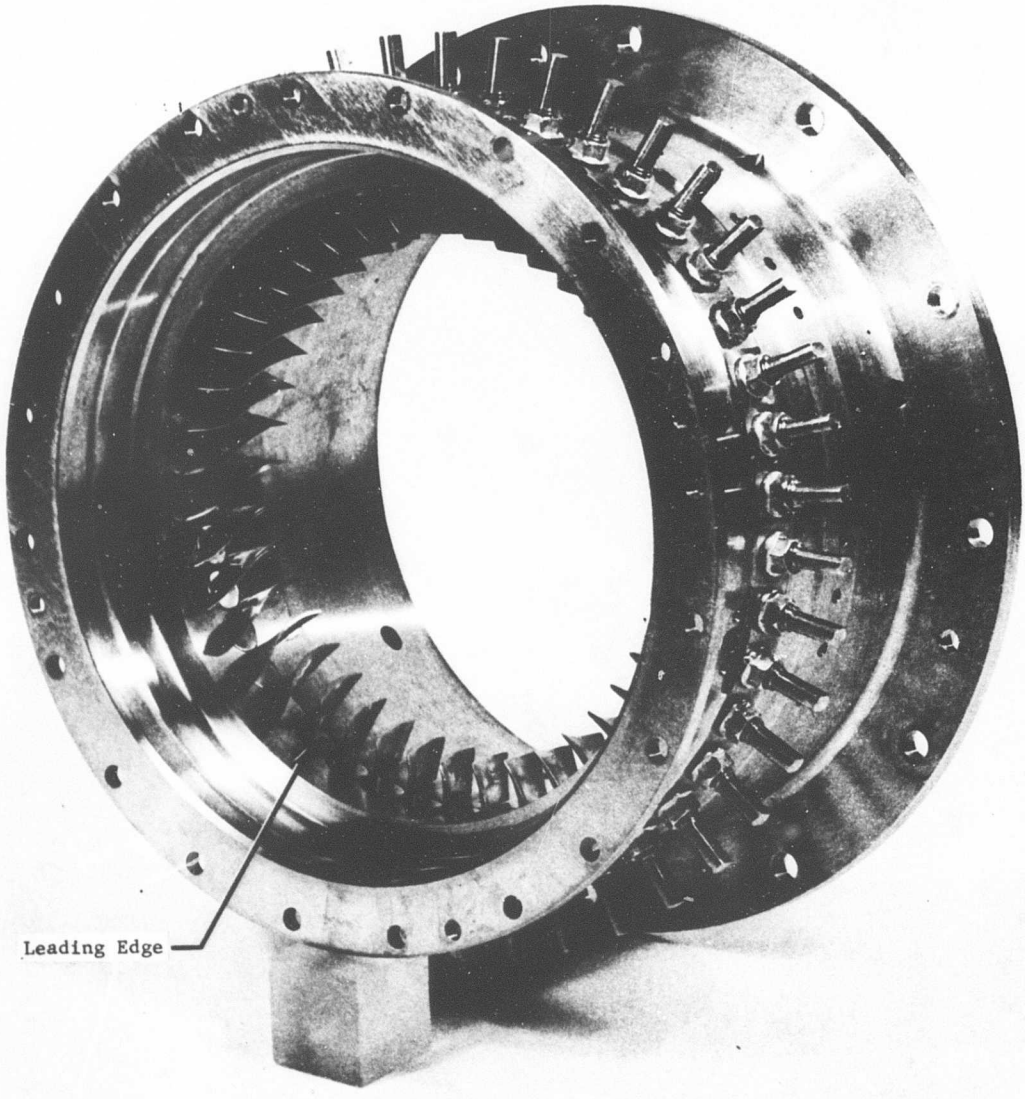

Figure 13. Redesigned Exit Stator and Outer Housing Assembly, Front View.

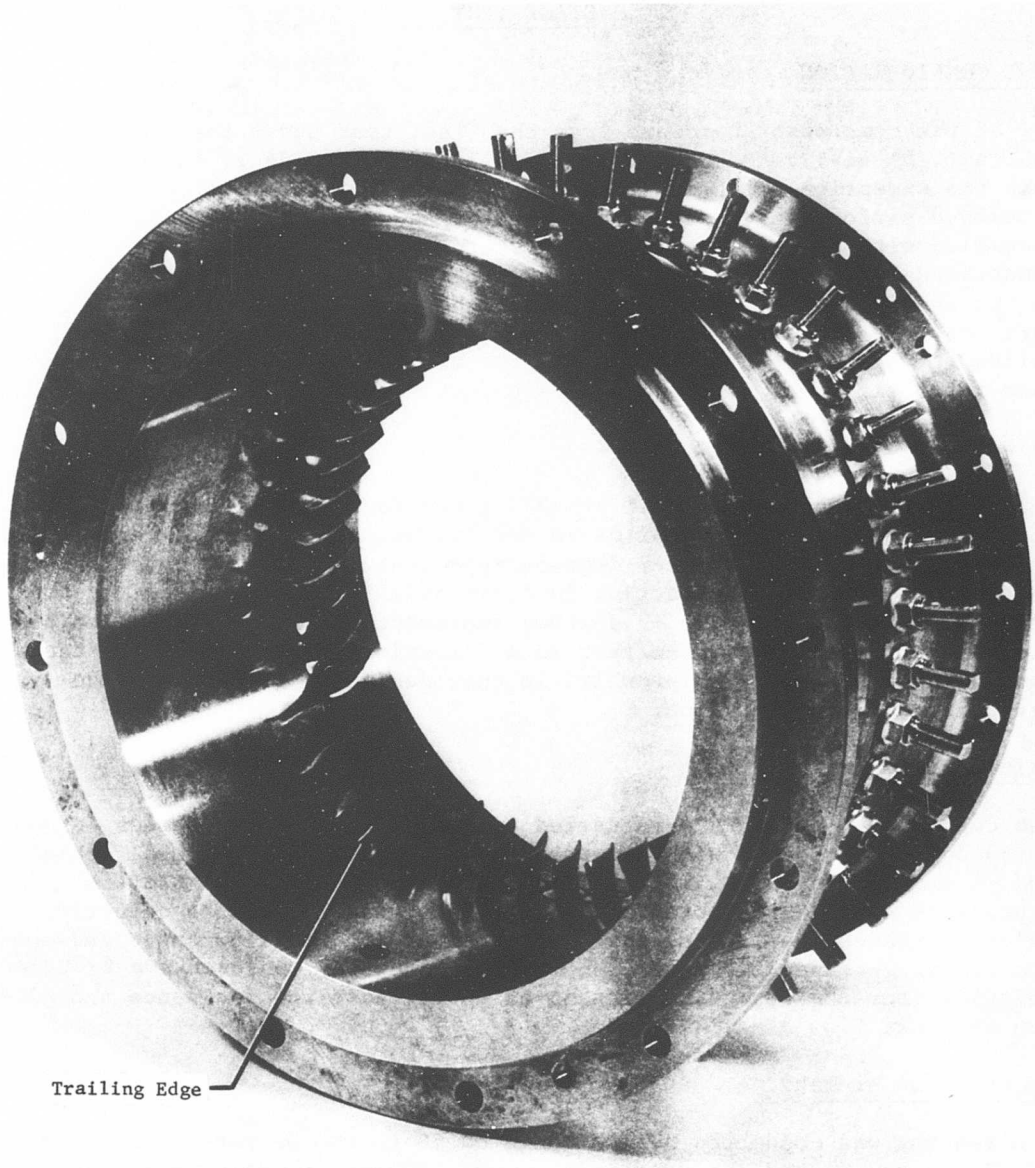

Figure 14. Redesigned Exit Stator and Outer Housing Assembly, Rear View.

STAGE TEST

TEST CONFIGURATION

All of the compressor hardware from the final test under the previous contract, DA 44-177-AMC-392(T), were utilized in builds 13 through 20 with the exception of the exit stator components. The inlet housings, developed airfoil inlet guide vanes, rotor and rotor shroud were reassembled with no changes. The exit stator assembly consisted of the redesigned outer housing, exit stator vanes, and support sleeve discussed in the previous sections. The pertinent hardware and assembly data for this test are summarized in Table V along with the data from the previous builds for reference. As indicated, the compressor was assembled with the same rotor tip clearance as in the previous test of builds 10 through 12.

Inlet Guide Vane Setting

The inlet guide vanes were set at -7 degrees (open) for builds 13 through 15, at design setting for builds 16 and 17, and at +2 degrees (closed) for builds 18 through 20. The -7 degrees represents a 7-degree rotation of the vane from the design setting in a direction so as to reduce the tangential prewhirl while the +2 degrees represents a 2-degree rotation of the vanes from the design setting in a direction so as to increase the tangential prewhirl. The prewhirl in this design is opposite to the direction of rotor rotation.

Exit Stator Setting

The exit stator settings were varied over a range from -8 degrees (open) to +6 degrees (closed) with intermediate settings of -4 degrees, design, and +4 degrees as shown in Table V. The -8 degrees in the stators represents an 8-degree rotation from the design setting in a direction which increases the leading edge incidence at a given flow angle and opens the stator entrance flow area, while the +6 degrees represents a 6-degree rotation from the design setting so as to decrease the incidence and close the entrance flow area.

Description of Test

The testing was conducted over a range of 50 to 100 percent of the design corrected speed, and the data points were obtained along constant speed lines. Builds 13 and 16 were investigated most thoroughly. The combinations of inlet guide vane and exit stator settings for these two builds were common to those tested in builds 11 and 12 of the previous program and therefore offered a direct comparison of the redesigned exit stator performance with that of the previous stator design. Data were obtained in the other builds to the extent that the effects of the changes in vane settings on the performance and operating characteristics were adequately defined. The surge line was investigated only at certain speeds and in certain builds. In builds 13 and 16, the surge data obtained at representative speed lines confirmed the respective surge lines established in

TABLE V. 2.8:1 SUPERSONIC COMPRESSOR EXPERIMENTAL HARDWARE DATA

	Build No.											
	10	10A	11	12	13	14	15	16	17	18	19	20
Contract	← DA 44-177-AMC-392(T) →				← DAAJ02-69-C-0085 →							
IGV:												
Type	Developed Airfoil											
Setting	-4°	-4°	-7°	Design	-7°			Design		+2°		
Rotor												
Serial No.	S/N 5											
Configuration No.	6											
Leading Edge:												
Expansion Angle	0.6° - 1.3° < Design											
Thickness	.006 - .012											
Condition	New				Unchanged							
Tip Clearance (Static)												
Leading Edge	.013											
Trailing Edge	.011											
Stator												
Serial No.	S/N 2				S/N-3							
Configuration No.	2				3							
Setting	Design				Design	-8°	+4°	Design	+4°	+6°	-4°	+4°

builds 11 and 12. Surge data were also obtained in builds 18 and 20, where the change in stator settings caused a significant shift in the compressor airflow.

Fixed probe and static pressure data were recorded at every test point. The tangential and radial traverse probe data at the stage exit (station 6) was taken at key performance points in builds 13 through 18. The rotor exit radial traverse probe was not installed in builds 13 through 18 to insure that the stage performance was not influenced by probe losses at the rotor exit. The rotor exit traverse probe was installed in builds 18 and 19, and traverse data were taken at key points. The probe was withdrawn to its minimum insertion while recording the fixed probe and stage exit traverse data for these two builds.

Post-test examination of the hardware showed the condition of all blading to be unchanged, and there was no evidence of rotor tip rub.

Instrumentation

The instrumentation for this test is described in the Appendix.

TEST RESULTS AND ANALYSIS

STAGE PERFORMANCE

Figures 15 through 22 are the experimental performance maps for the compressor stage with redesigned exit stator (builds 13 through 20).

Comparison With Previous Exit Stator

The peak stage performance data for builds 13 and 16 with the redesigned exit stator are summarized in Table VI and compared to the performance from builds 11 and 12 with the previous stator. The inlet guide vanes were at the -7 degrees setting in both builds 11 and 13 and at the design setting in both builds 12 and 16. The exit stators were at the design setting in all four of these builds.

The constant corrected speed lines of stage pressure ratio versus airflow for build 13 agreed with those of build 11 within 1 percent, and similarly build 16 agreed with build 12. A comparison of the peak pressure ratio data in Table VI illustrates this. The peak efficiencies in builds 13 and 16, however, were lower than the respective results from builds 11 and 12 by 2 to 2.4 percent at design speed and up to 5 percent at part speed. The difference in efficiency is evidenced by a higher temperature rise measured in builds 13 and 16.

Effect of Exit Stator Setting

The stage pressure ratio and efficiency were highest at the design exit stator setting (Figures 15 and 18).

At open or negative stator angle settings (-8 and -4 degrees), the part-speed wide-open throttle airflow and stage pressure ratio increased relative to the design setting (Figures 16 and 21). As the compressor airflow was throttled, however, the stage pressure ratio increased at a much slower rate and peaked below that of the design stator setting. At the negative settings, the compressor was throttled just short of the design setting surge line without encountering surge. The design speed airflow along the vertical characteristic was essentially the same at the negative stator settings as for the design setting, but the speed line departed from the vertical characteristic and peaked at lower stage pressure ratios.

At the closed or positive exit stator settings (+4 and +6 degrees), the part-speed wide-open throttle airflow was lower relative to the design setting (Figures 17, 19, 20 and 22). The speed lines for the positive settings fell below those at the design setting, and the stage pressure ratios peaked at lower values. The design speed airflow at the vertical characteristic was reduced significantly by the closed stator setting, and the peak stage pressure ratio was lower as it was at part speed. The surge line showed some movement toward lower airflows at these positive settings.

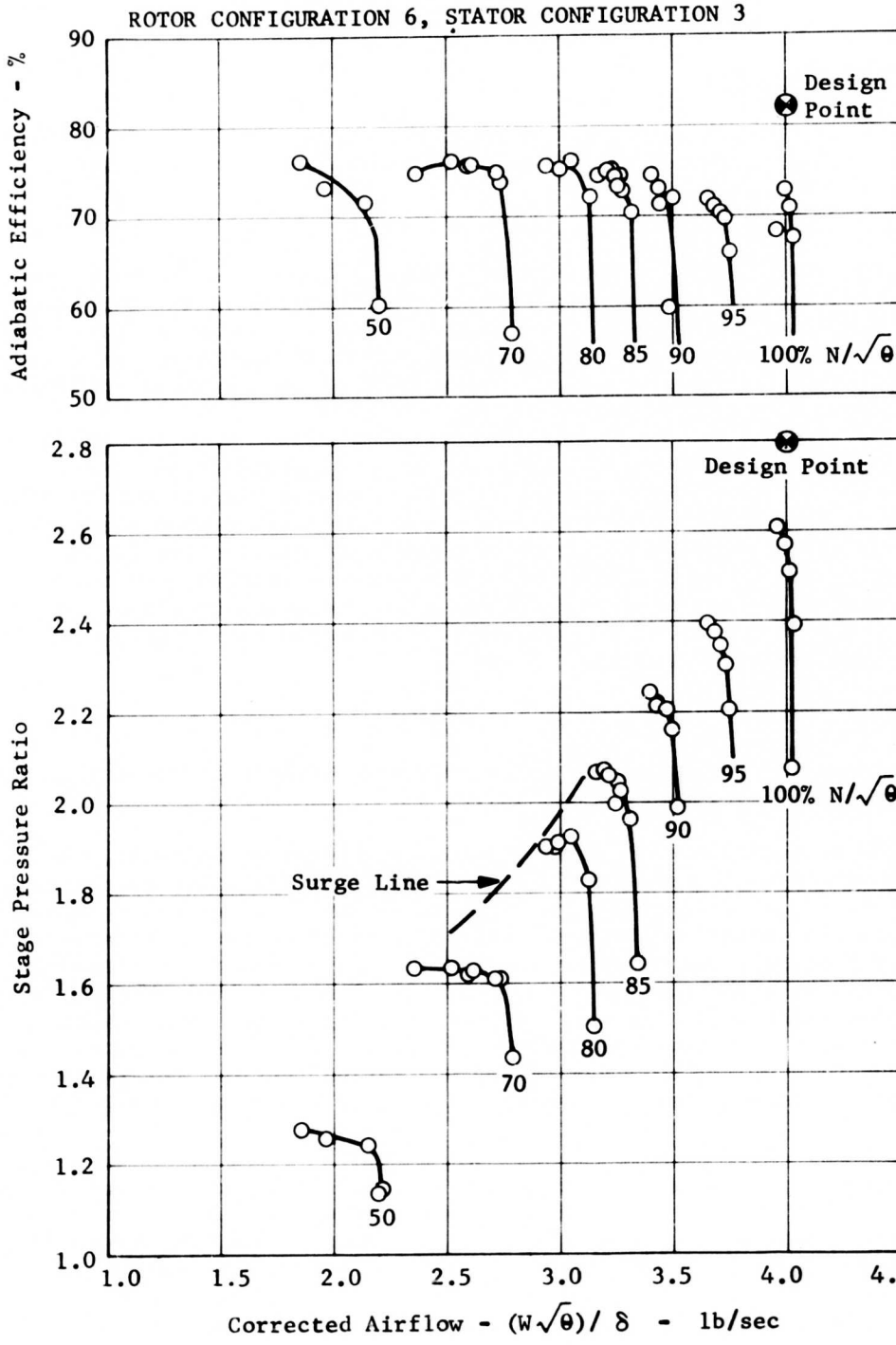

Figure 15. Compressor Stage Performance Map, Build 13, IGV at -7° Setting, Exit Stator at Design Setting.

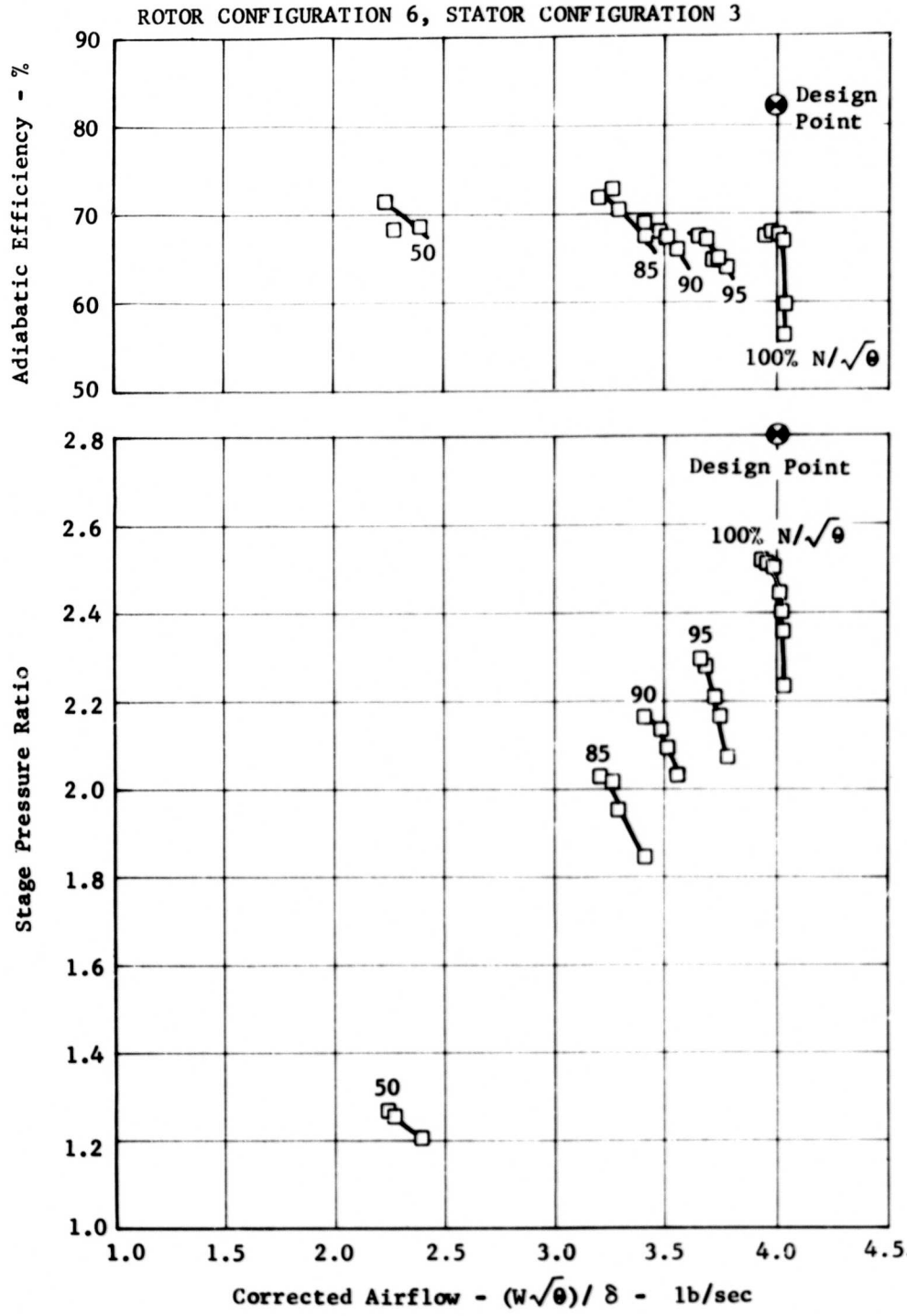

Figure 16. Compressor Stage Performance Map, Build 14, IGV at -7° Setting, Exit Stator at -8° Setting.

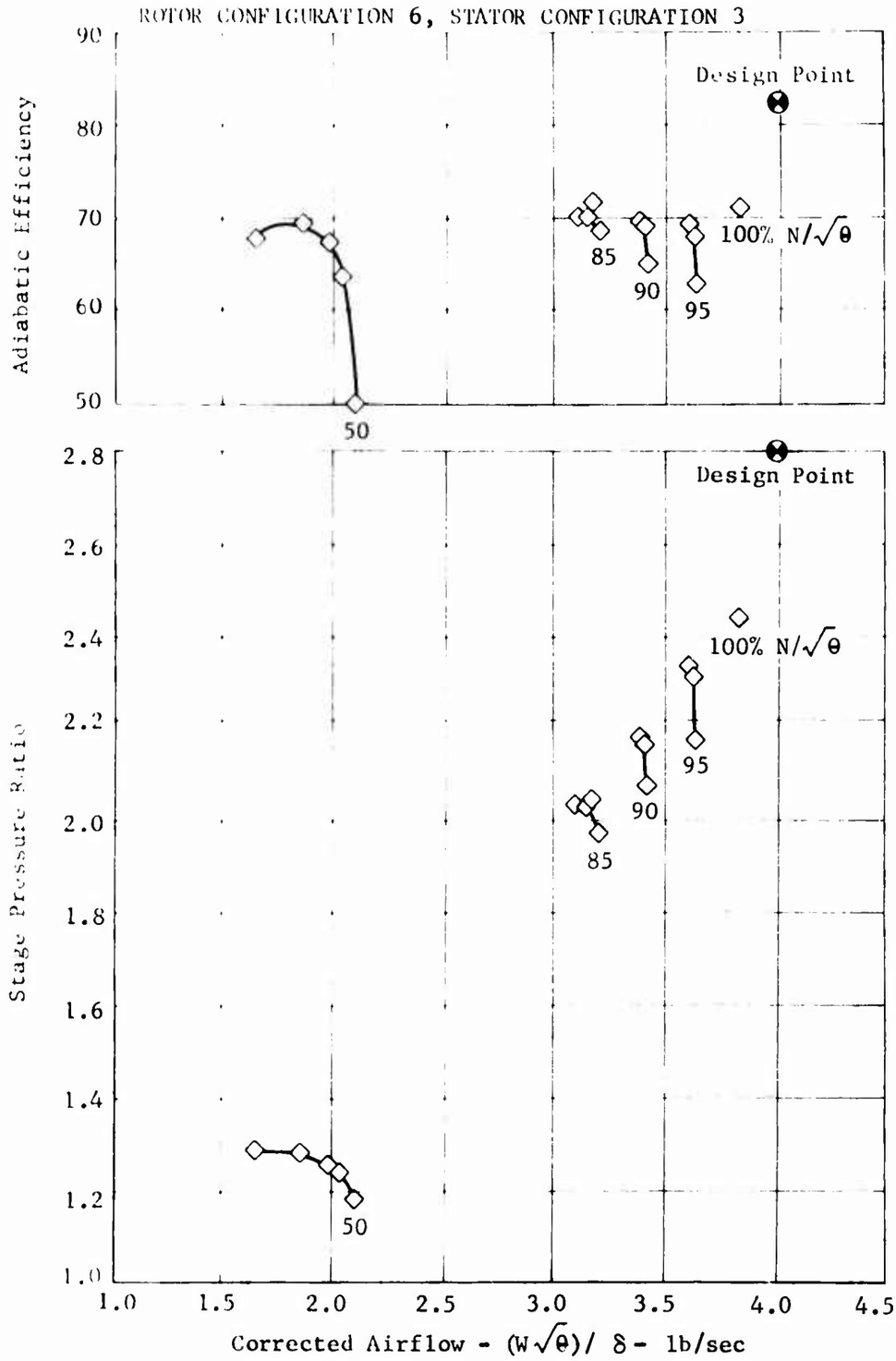

Figure 17. Compressor Stage Performance Map, Build 15, IGV at -7° Setting, Exit Stator at +4° Setting.

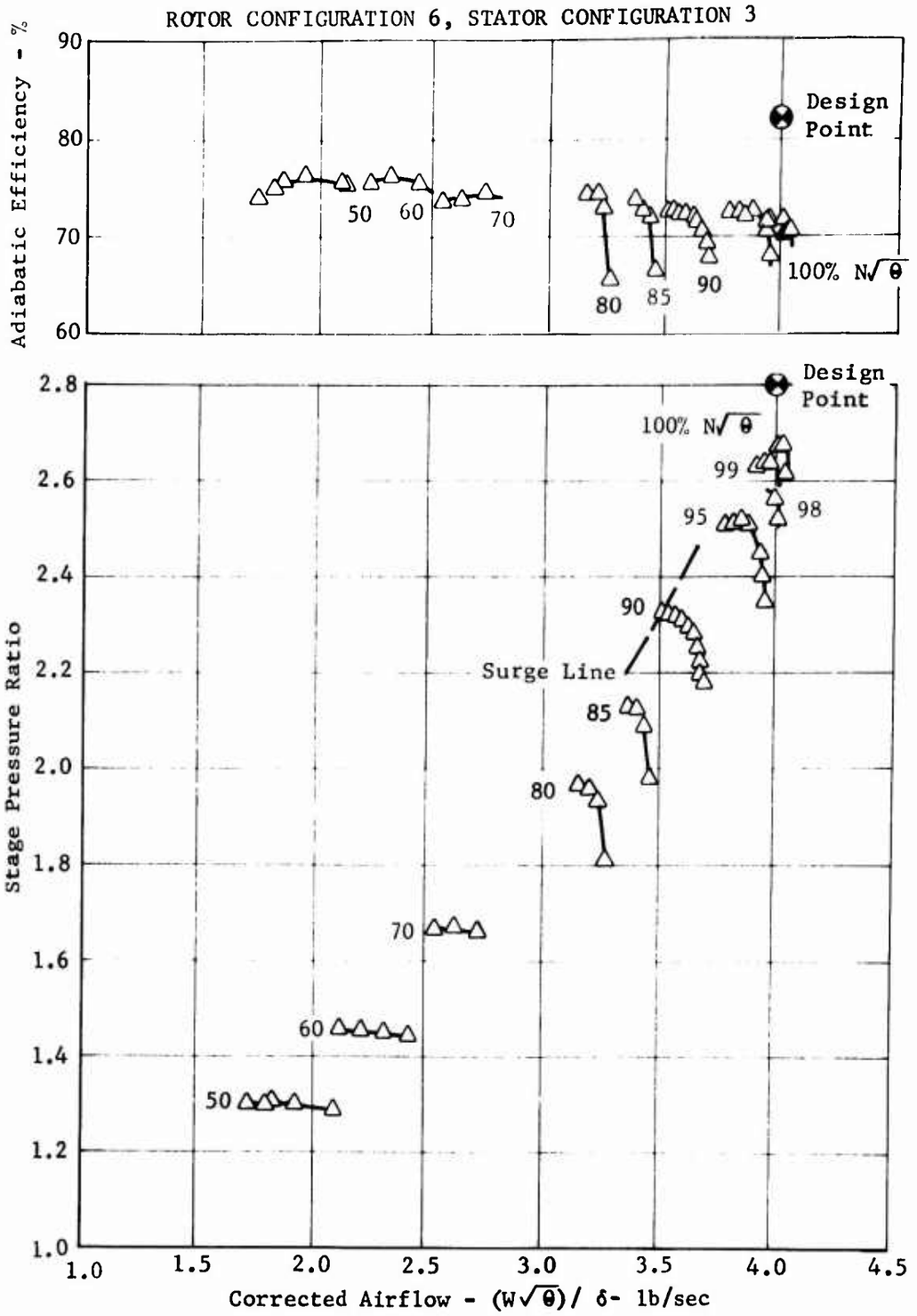

Figure 18. Compressor Stage Performance Map, Build 16, IGV at Design Setting, Exit Stator at Design Setting.

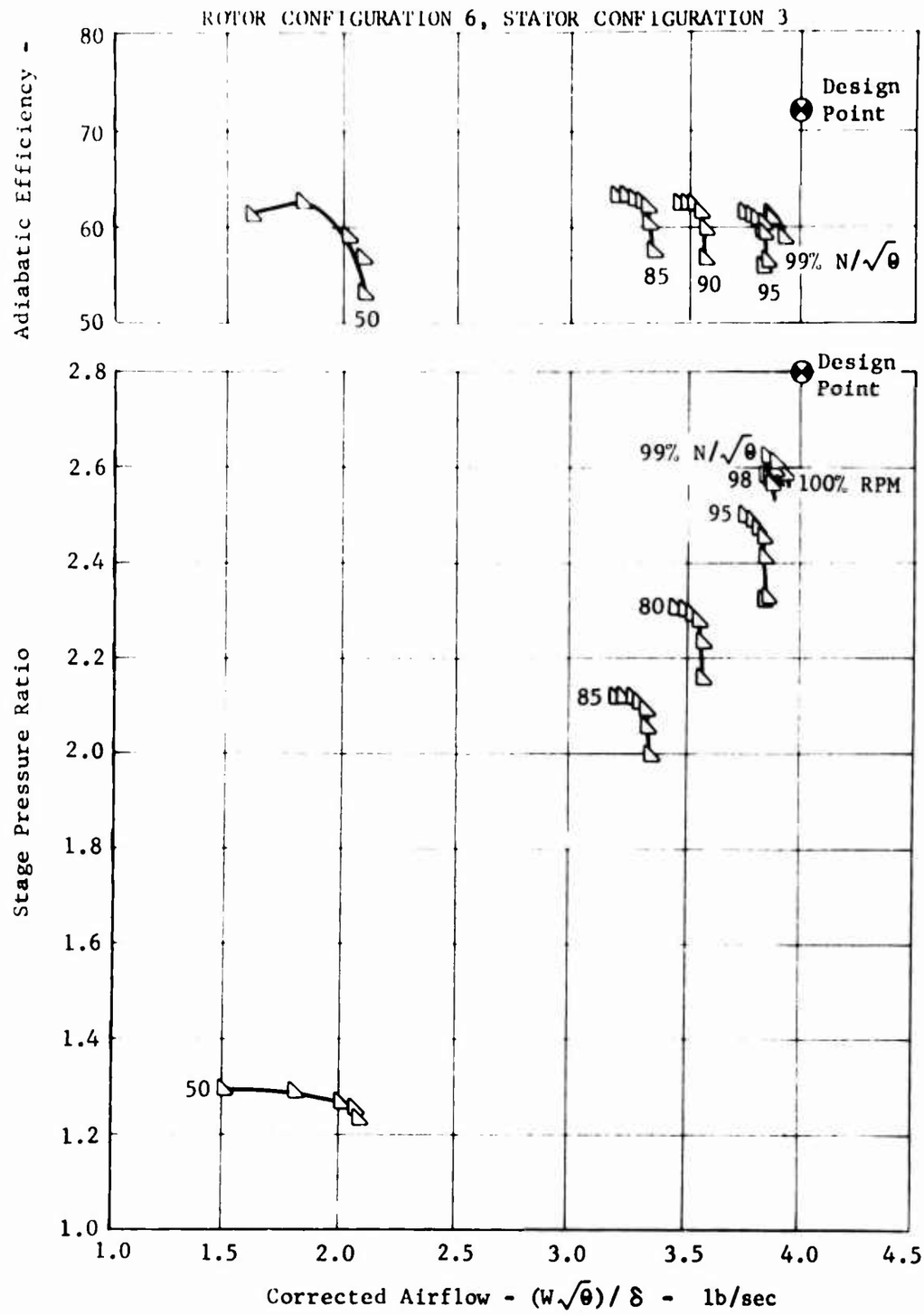

Figure 19. Compressor Stage Performance Map, Build 17, IGV at Design Setting, Exit Stator at +4° Setting.

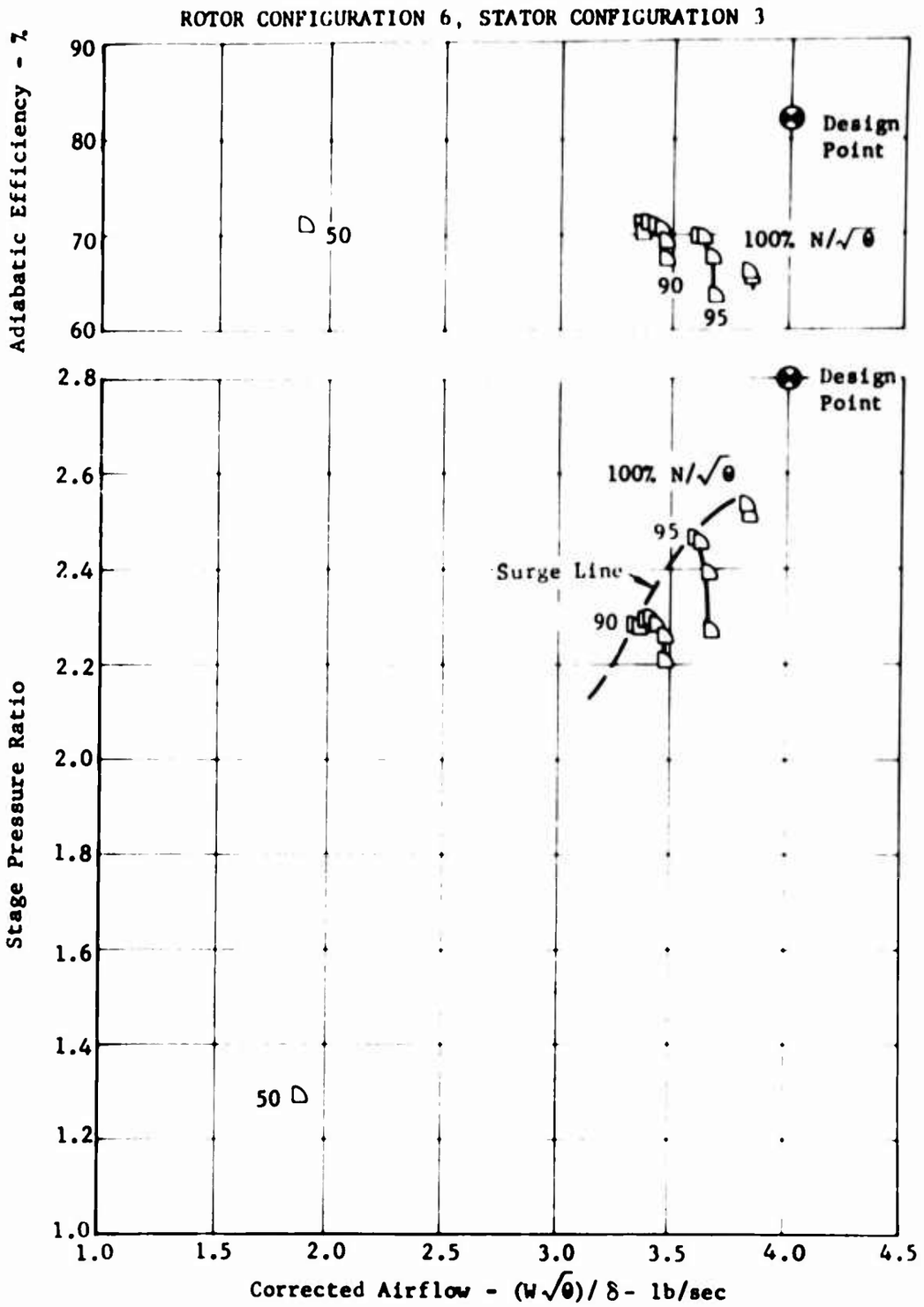

Figure 20. Compressor Stage Performance Map, Build 18, IGV at +2° Setting, Exit Stator at +6° Setting.

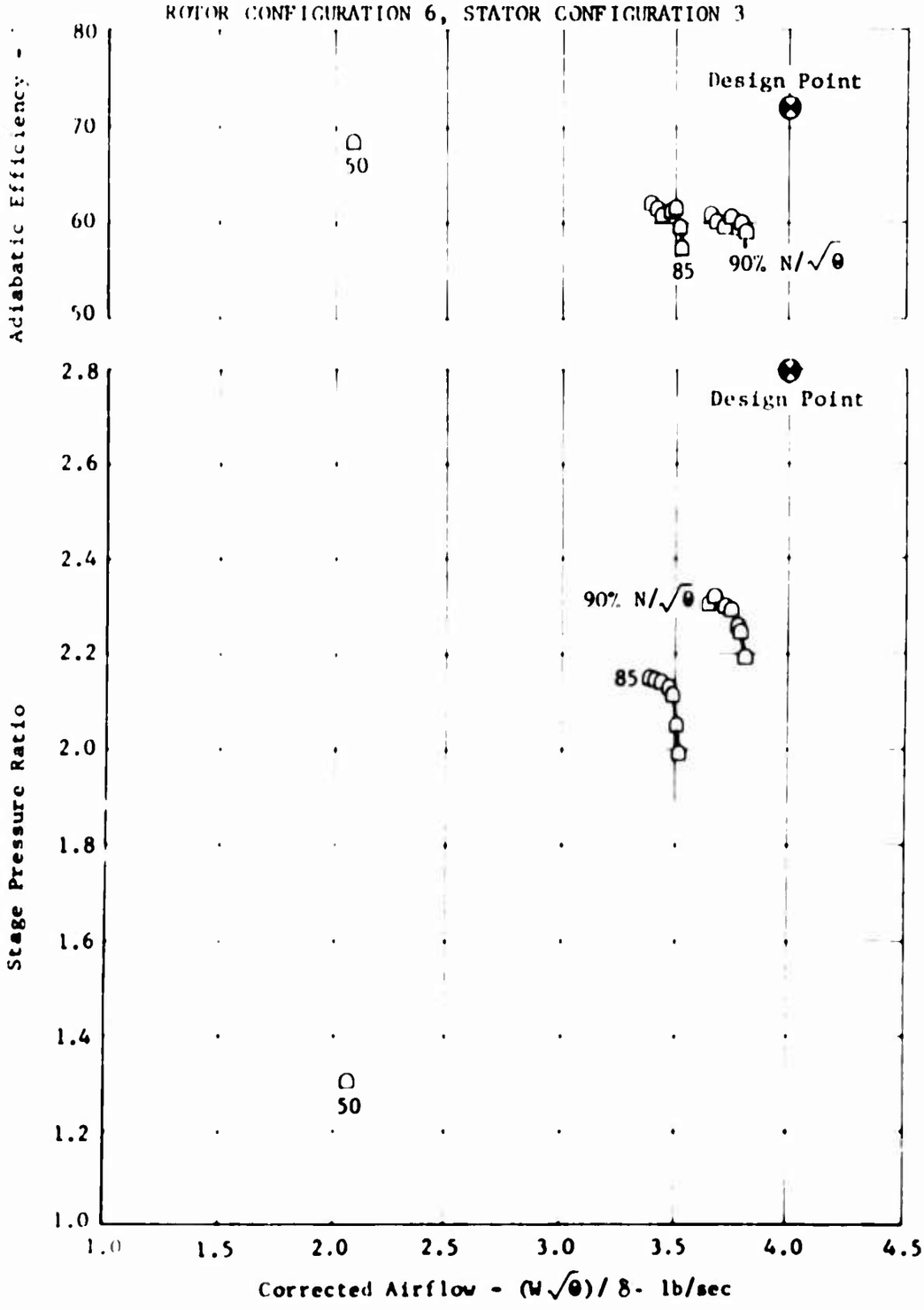

Figure 21. Compressor Stage Performance Map, Build 19, IGV at +2° Setting, Exit Stator at -4° Setting.

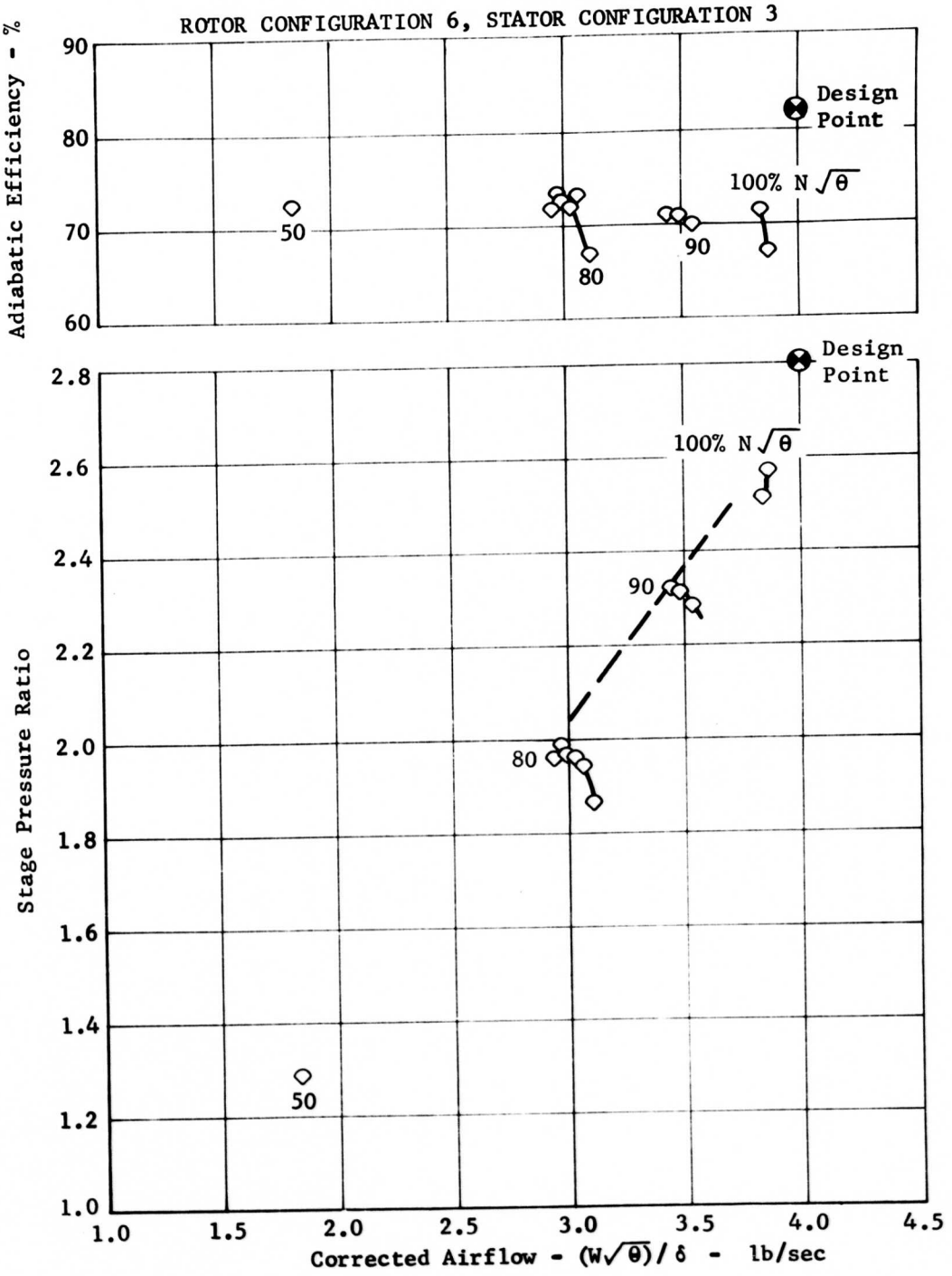

Figure 22. Compressor Stage Performance Map, Build 20, IGV at +2° Setting, Exit Stator at +4° Setting.

TABLE VI. STAGE PERFORMANCE DATA SUMMARY

				STAGE PRESSURE RATIO: % SPEED			STAGE EFFICIENCY %		
		BLADE SETTINGS							
	BUILD	IGV	STATOR	80	90	100	80	90	100
Predicted Peak		**Design**	**Design**	**1.84**	**2.26**	**2.80**	82.7	82.5	82.2
Data Peak With Stator #2	**11**	**-7°**	**Design**	**1.90**	**2.22**	**2.59**	80.0	76.7	74.8
Data Peak With Stator #2	**12**	**Design**	**Design**	**1.98**	**2.33**	**2.69**	78.0	75.4	73.8
Data Peak With Stator #3 (Redesign)	**13**	**-7°**	**Design**	**1.92**	**2.24**	**2.57**	76.8	74.5	72.8
Data Peak With Stator #3	**14**	**-7°**	**-8°**	**-**	**2.17**	**2.52**	-	68.9	67.6
Data Peak With Stator #3	**15**	**-7°**	**+4°**	**-**	**2.17**	**2.44**	-	69.4	71.0
Data Peak With Stator #3	**16**	**Design**	**Design**	**1.96**	**2.32**	**2.68**	74.4	72.6	71.4
Data Peak With Stator #3	**17**	**Design**	**+4°**	**-**	**2.41**	**2.61**	-	69.2	70.7
Data Peak With Stator #3	**18**	**+2°**	**+6°**	**-**	**2.29**	**2.53**	-	70.9	66.0
Data Peak With Stator #3	**19**	**+2°**	**-4°**	**-**	**2.30**	**-**	-	70.4	-
Data Peak With Stator #3	**20**	**+2°**	**+4°**	**1.99**	**2.32**	**2.58**	73.4	70.8	71.5

INLET GUIDE VANE AND ROTOR PERFORMANCE

The inlet guide vane and rotor performance established in the testing of builds 11 and 12 of the previous contract forms a reference base for the performance evaluation in this contract since the identical inlet guide vane and rotor hardware was used in both series of tests. No total pressure instrumentation was installed at the rotor exit in builds 13 through 18 and therefore the measured airflow, stage exit temperature and static pressure data at the exit of the IGV and along the rotor shroud were compared to the data in builds 11 and 12 to evaluate the performance. Radial total pressure traverses were made at selected points in builds 19 and 20.

Inlet Guide Vane Data

The performance of the inlet guide vanes in the current tests appears to be essentially the same as in the previous tests based on the close agreement of the induced airflow data at common inlet guide vane and exit stator settings. The airflow along the vertical characteristic of the 100 percent speed line agrees well within 1 percent both between builds 11 and 13 and between builds 12 and 16. Figure 23 compares the static pressures at the trailing edge of the inlet guide vane for builds 12 and 16. At the higher airflow the agreement is very close, but as the airflow decreases, the data from build 16 shows slightly lower pressures. Figure 24 compares these pressures for builds 11 and 13 and indicates slightly lower pressures in build 13. The differences could result from the minor inaccuracies in setting the guide vane angle (accuracy is well within 1 degree). It should be noted that the proximity of the pressure taps to the blades changes as the blade setting is varied, becoming closer to the blade at off-design negative settings.

Rotor Data

The rotor performance data show some deviation from that obtained in the previous program. The most pronounced change is the fact that the measured temperature rise is 5 to 10 degrees higher, which reflects a degradation in stage efficiency. Figures 25 and 26 compare the temperature rise data of the current and previous tests. The possible sources of the increased temperature rise are (1) a radial redistribution of flow attributable to the redesigned exit stator configuration, (2) small differences in tip clearance within the accuracy of repeating a setting, and (3) small differences in guide vane angle within the accuracy of repeating the vane setting. The potential contribution of the latter two to the increased temperature rise is considered to be small.

Figure 27 compares the inlet guide vane and rotor pressure ratio data of the current and previous builds. Builds 19 and 20, in which the current rotor pressure ratio data were measured, represent an inlet guide vane setting of +2 degrees. These data are compared to those from build 12, which represents a design inlet guide vane setting since a +2 setting was

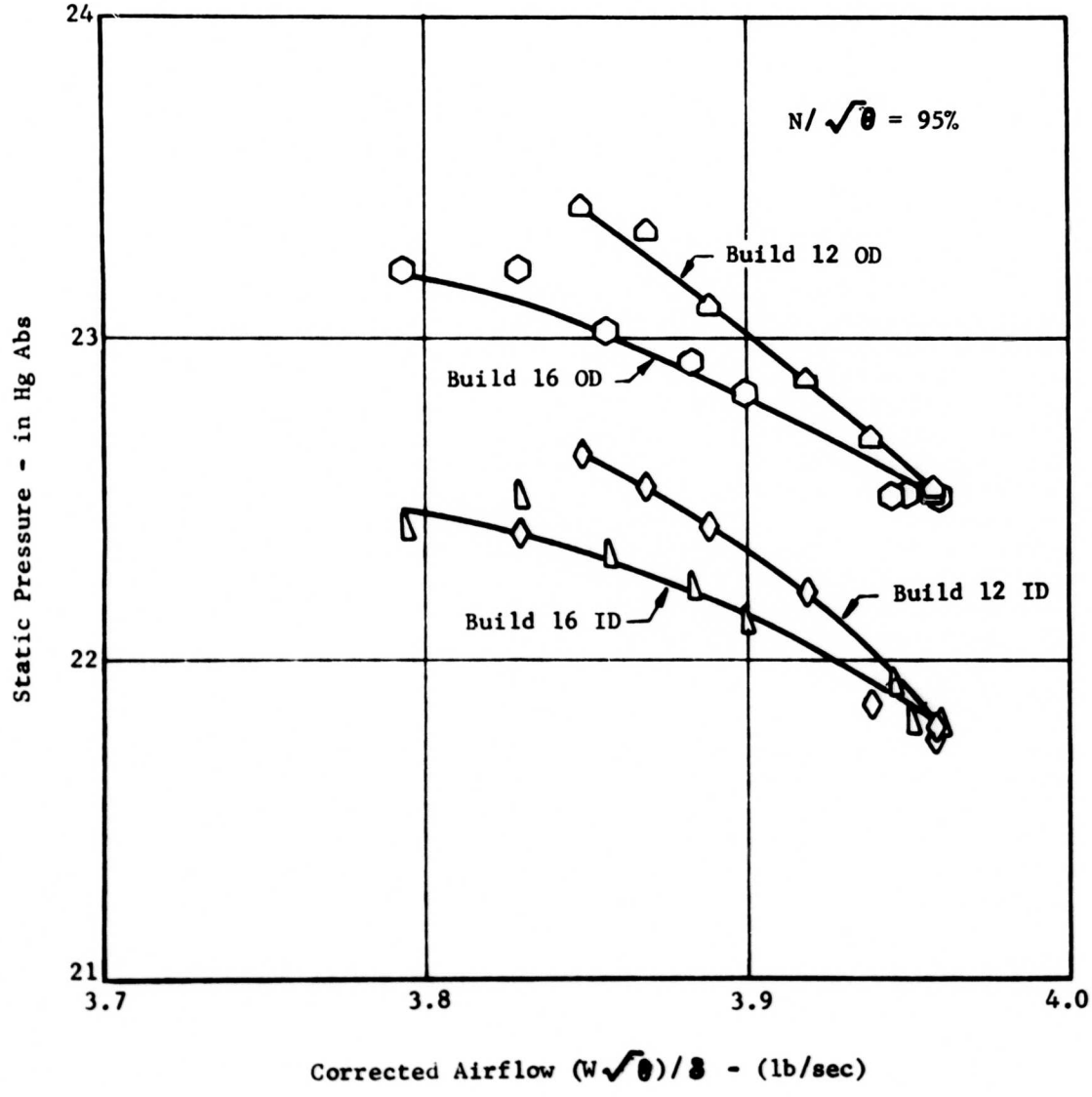

Figure 23. Comparison of Measured Inlet Guide Vane Trailing Edge Static Pressure for Builds 12 and 16.

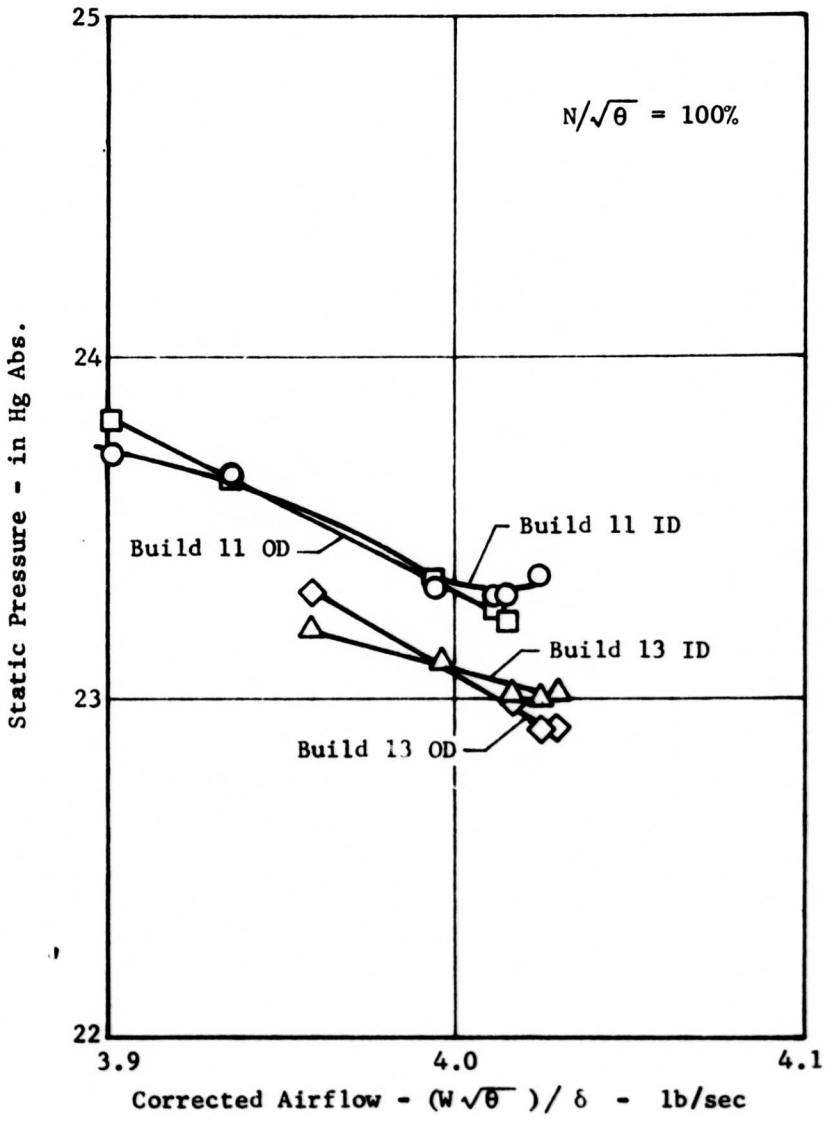

Figure 24. Comparison of Measured Inlet Guide Vane Trailing Edge Static Pressure for Builds 11 and 13.

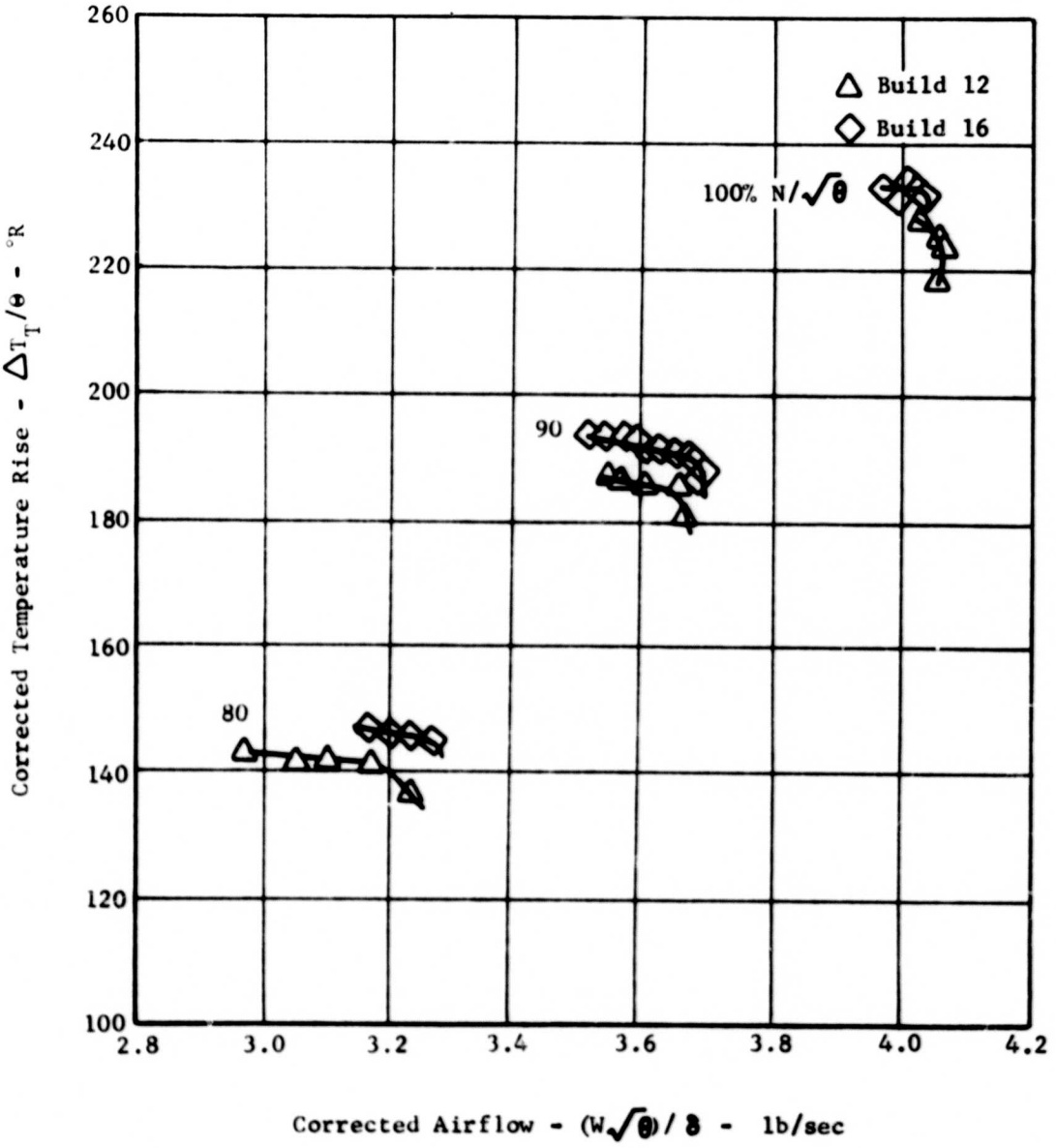

Figure 25. Comparison of Measured Temperature Rise for Builds 12 and 16.

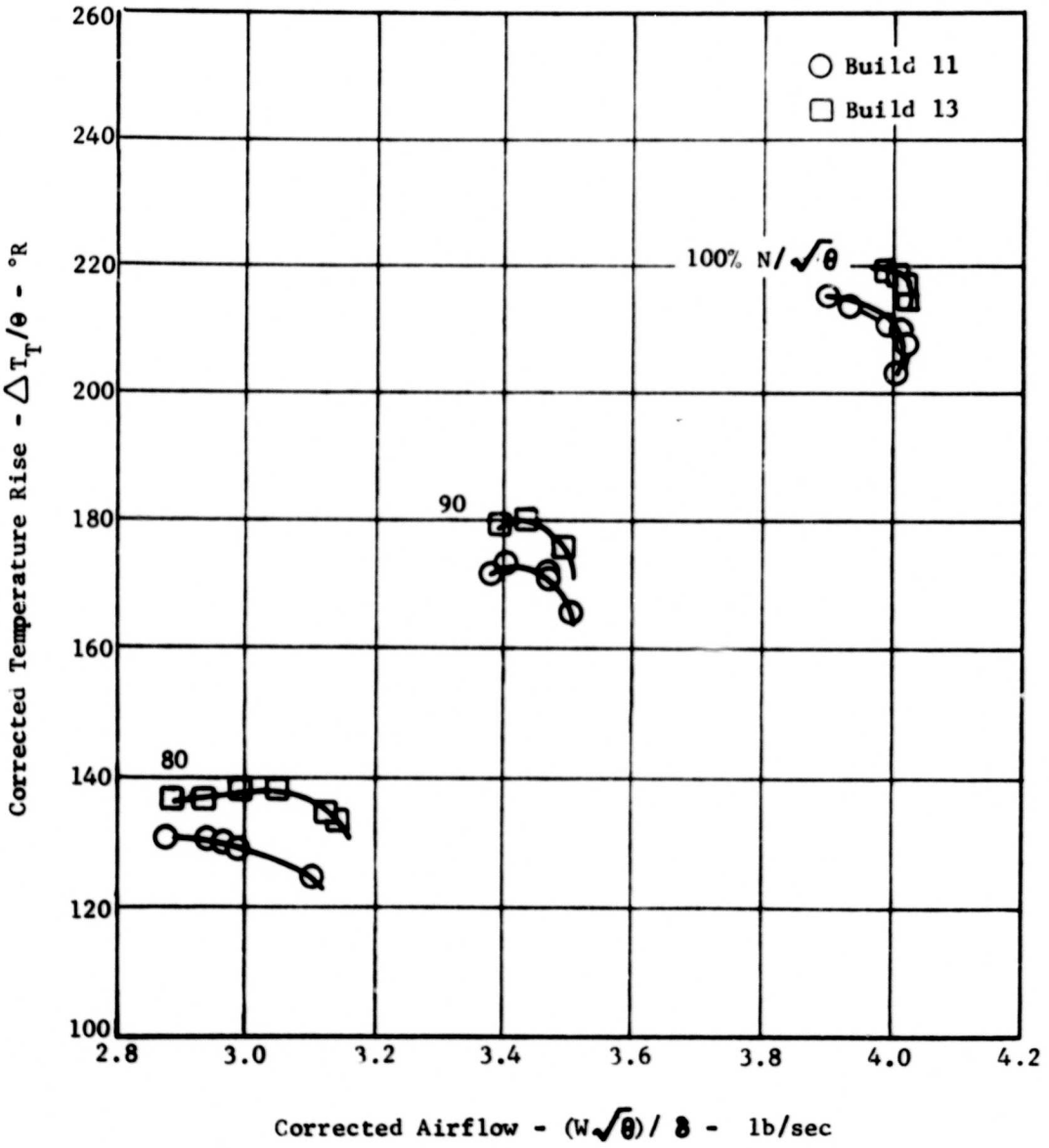

Figure 26. Comparison of Measured Temperature Rise for Builds 11 and 13.

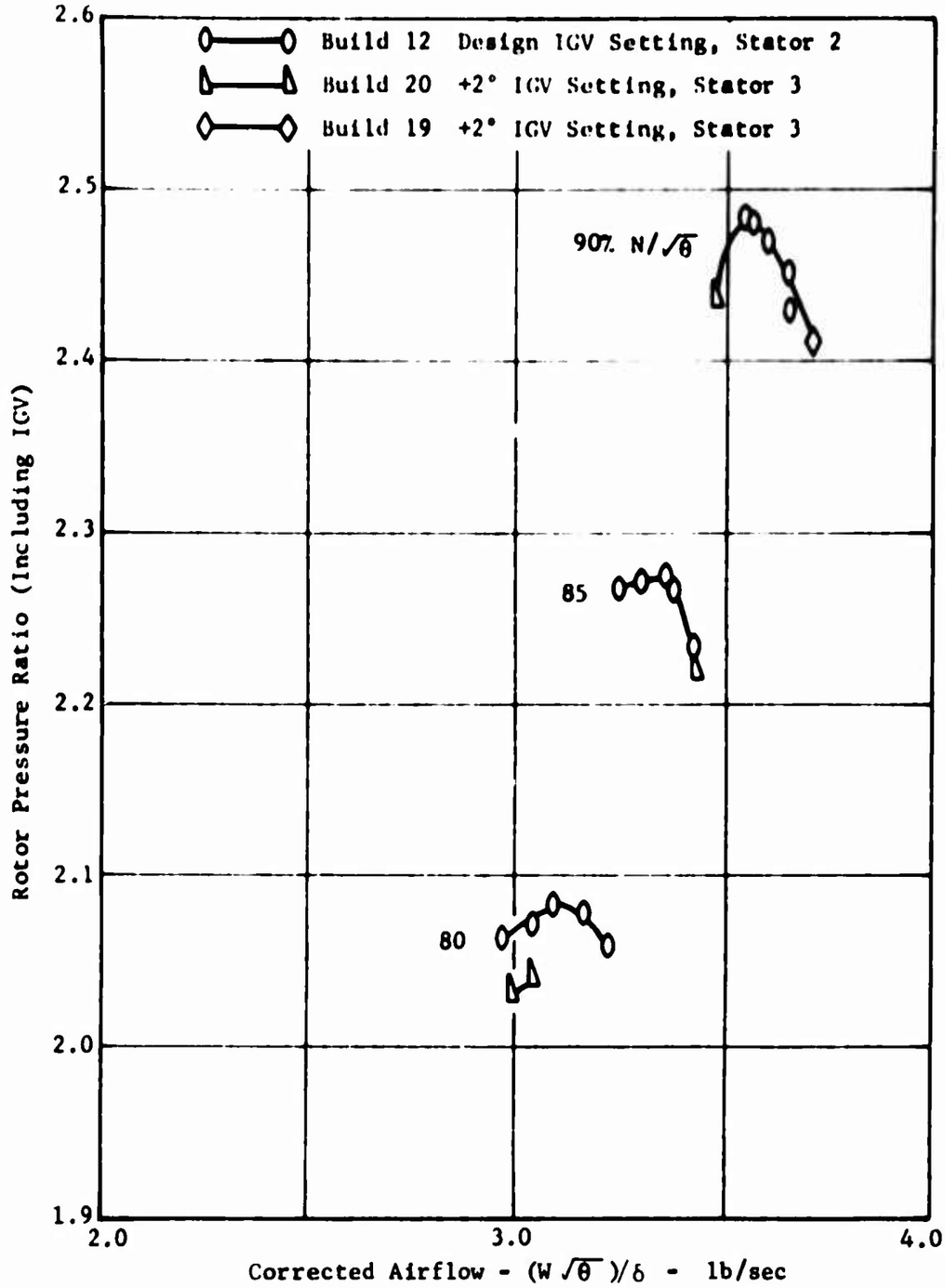

Figure 27. Comparison of Rotor Pressure Ratio for Builds 12, 19 and 20.

not included in the previous test. The data points from the current test show a consistent trend with the data from build 12 at the 85 and 90 percent speeds, but there is no point near the previous peak performance at those speeds. The 80 percent speed data indicate a small degradation of pressure ratio in the current tests. This small pressure ratio difference may be due to the difference in inlet guide vane setting or could be attributable to the same sources discussed for the increased temperature rise.

Figure 28 shows that the static pressure ratio across the rotor at the shroud is slightly lower in the current test as compared to the previous test. This difference is probably due to the configuration of the redesigned stator since the meridional turning of the flow path to an axial direction occurs at the rotor exit.

The pressure differences in the IGV and rotor performance between the data from the current tests (builds 13-20) and those from the previous tests (builds 11 and 12) are relatively small. The IGV and rotor performance data from builds 11 and 12 can be used without excessive error for the purpose of evaluating the performance of the redesigned exit stator for data points at which no rotor exit pressure traverse is available.

Figure 29 shows the vector diagrams for a test point in build 20 at which a rotor exit pressure traverse was taken. The vector diagram data were calculated from measured static pressures at the IGV exit and rotor exit, the measured total pressure profile at the rotor exit, the temperature rise based on the measured total temperature profile at the stage exit, and the assumed flow angles and total pressure at the IGV exit.

EXIT STATOR PERFORMANCE

Both the overall stage data and the exit stator data indicate that the redesign has not resulted in any significant improvement in the performance of the exit stator and duct assembly. The comparison of the overall stage performance has been discussed in a previous section, and the close agreement in overall stage pressure with both the previous stator and the redesigned stator is illustrated in Table VI. The detailed exit stator data are discussed in the following sections.

Stator Entrance Conditions

The results from the previous program indicated that total pressure probes installed between the rotor trailing edge and the stator leading edge might have had an excessive influence on the flow in that region. Consequently, no stagnation probes were installed in this region for builds 13 through 18 and the static pressures along the hub and tip shrouds were the only data measured in the vaneless space between the rotor and stator. A radially traversing impact tube was installed in builds 19 and 20, and the total pressure profiles just ahead of the stator leading edge were measured at selected test points.

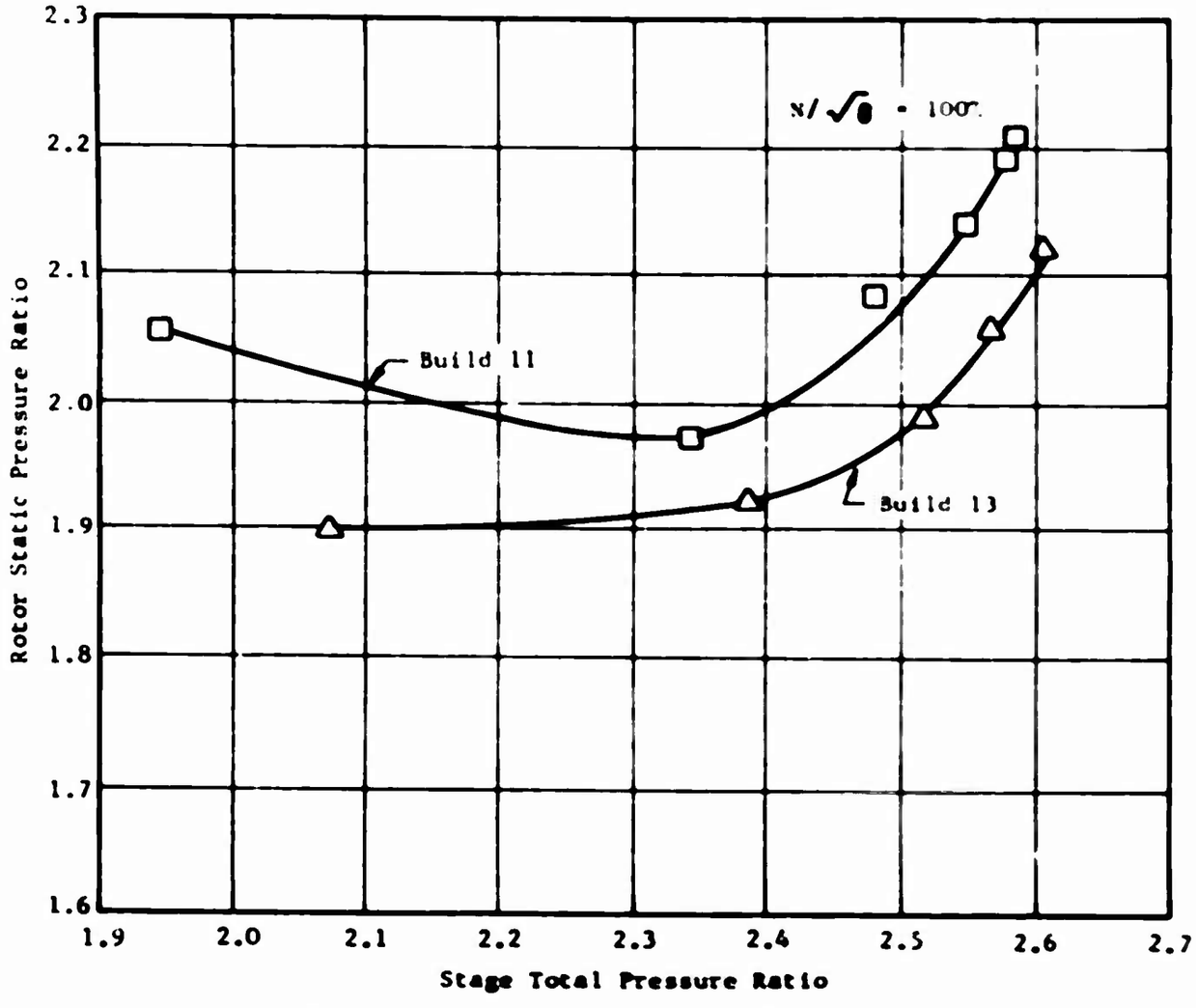

Figure 28. Comparison of Rotor Static Pressure Ratio at the Shroud for Builds 11 and 13.

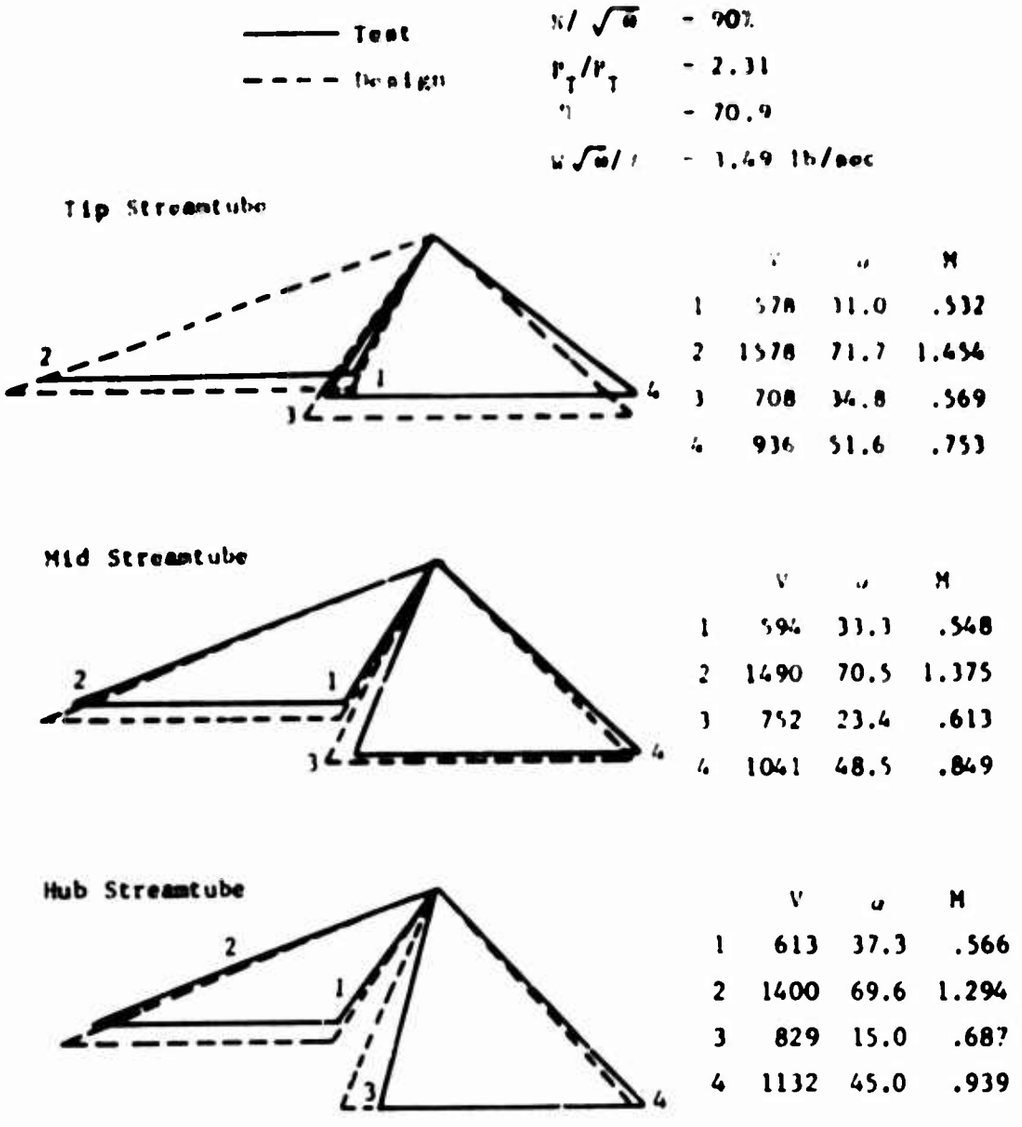

Tip Streamtube

	V	α	M
1	578	11.0	.532
2	1578	71.7	1.454
3	708	34.8	.569
4	936	51.6	.753

Mid Streamtube

	V	α	M
1	594	33.3	.548
2	1490	70.5	1.375
3	752	23.4	.613
4	1041	48.5	.849

Hub Streamtube

	V	α	M
1	613	37.3	.566
2	1400	69.6	1.294
3	829	15.0	.687
4	1132	45.0	.939

Figure 29. Build 20 Test Data, Vector Diagrams, IGV at +2° Setting, Exit Stator at -4° Setting.

The static pressure decreases rapidly from the rotor trailing edge to the stator leading edge as shown for build 13 in Figure 30. This condition was present in the test with the previous exit stator also, as apparent from the build 11 data in Figure 30. The data in Figure 30 indicate that the tip shroud static pressure was somewhat lower for build 13 at the rotor trailing edge but was in close agreement for build 11 at the stator leading edge. The hub shroud static pressure was in close agreement at the rotor trailing edge but was higher than for build 11 near the stator leading edge. The difference in pressure at the hub shroud could be due to the change in meridional flow path included in the redesign and to the absence of the rotor exit impact pressure probes from build 13. In both cases, however, the static pressure gradient is indicative of a flow acceleration in this vaneless space region. Figure 31 shows the Mach number versus axial distance in the vaneless space based on the measured static pressures for build 13 and the hub and tip total pressure data from build 11. Although it is recognized that the total pressure does not remain constant in this region due to mixing losses, the assumption of constant total pressure used in the calculation of the Mach number provides a reasonable approximation. The results indicate that the Mach number of the flow leaving the rotor is below 0.9 but at the stator leading edge is sonic or above. This apparent acceleration and the resultant high Mach number at the stator leading edge are considered to be primary factors in the high stator and duct losses.

Three conditions which could contribute to static pressure gradient in the vaneless space are (1) total pressure losses, (2) boundary layer thickening or separating at the hub or shroud walls, and (3) propagation of blade leading-edge blockage effects forward into the vaneless space. Total pressure losses are not considered the primary contributor because very high levels of loss, well above the overall measured stator and duct loss, are required to satisfy mathematical requirements of the static pressure axial gradient, the continuity equation, and the conservation of angular momemtum. The wake-mixing mechanism is judged insufficient to produce such losses, therefore, the hub and shroud boundary layer and the stator blade blockage effects are considered to be more plausible causes of the flow acceleration.

Figure 32 presents a typical radial total pressure profile from the traverse data taken in build 20. The profile is consistent with the data from build 12, showing a uniformly decreasing pressure from hub to tip in the region measured. Probe limitations prevented obtaining pressures close enough to the end walls to investigate the profile in the boundary layers. The total pressure profile very close to the wall would have to be established in order to evaluate the boundary layer influence on the flow acceleration since the change in effective flow area associated with the acceleration is on the order of 1 percent.

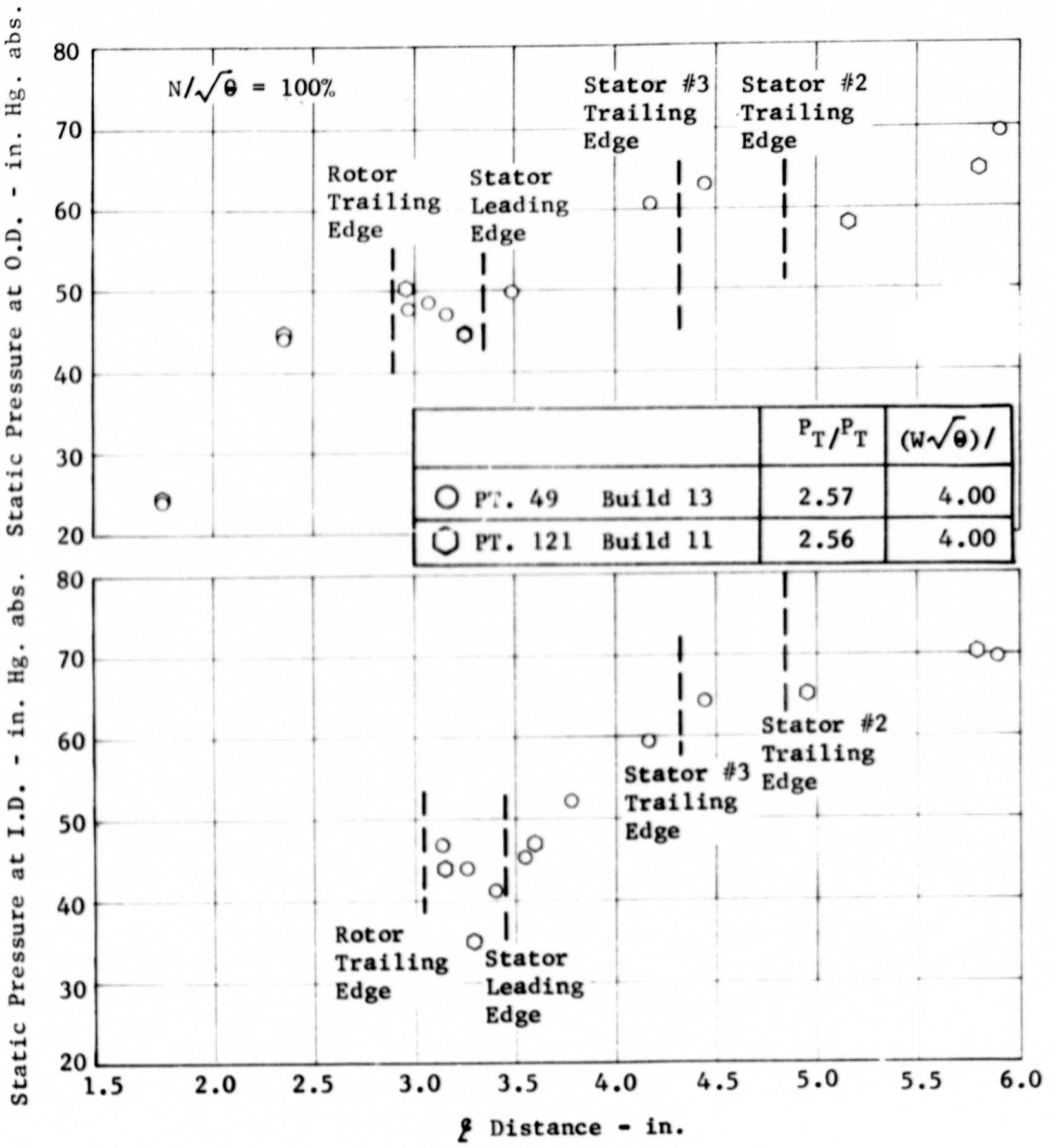

Figure 30. Static Pressure Distribution Versus Axial Distance Through Compressor, Comparison of Builds 13 and 11.

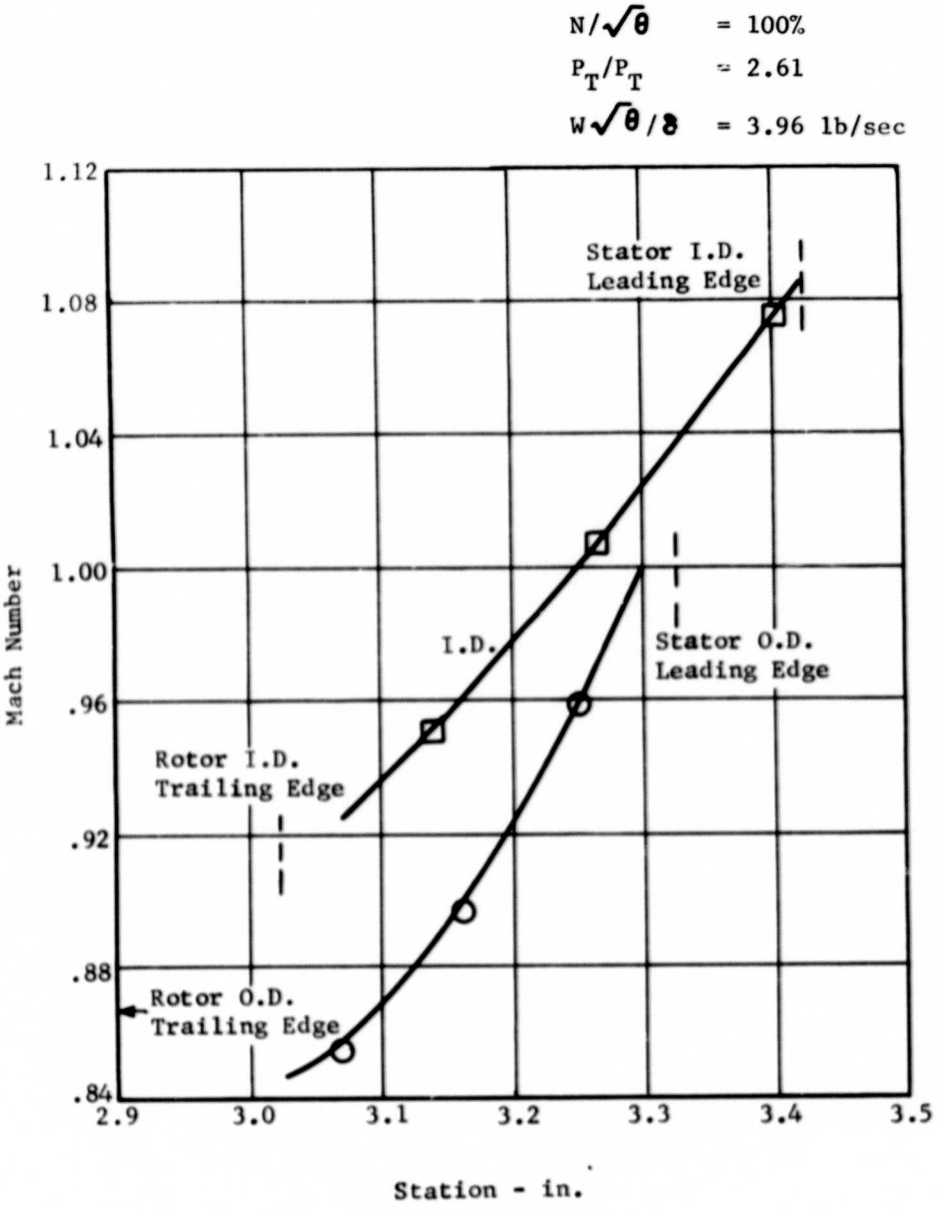

Figure 31. Mach Number in Vaneless Space Aft of Rotor for Build 13.

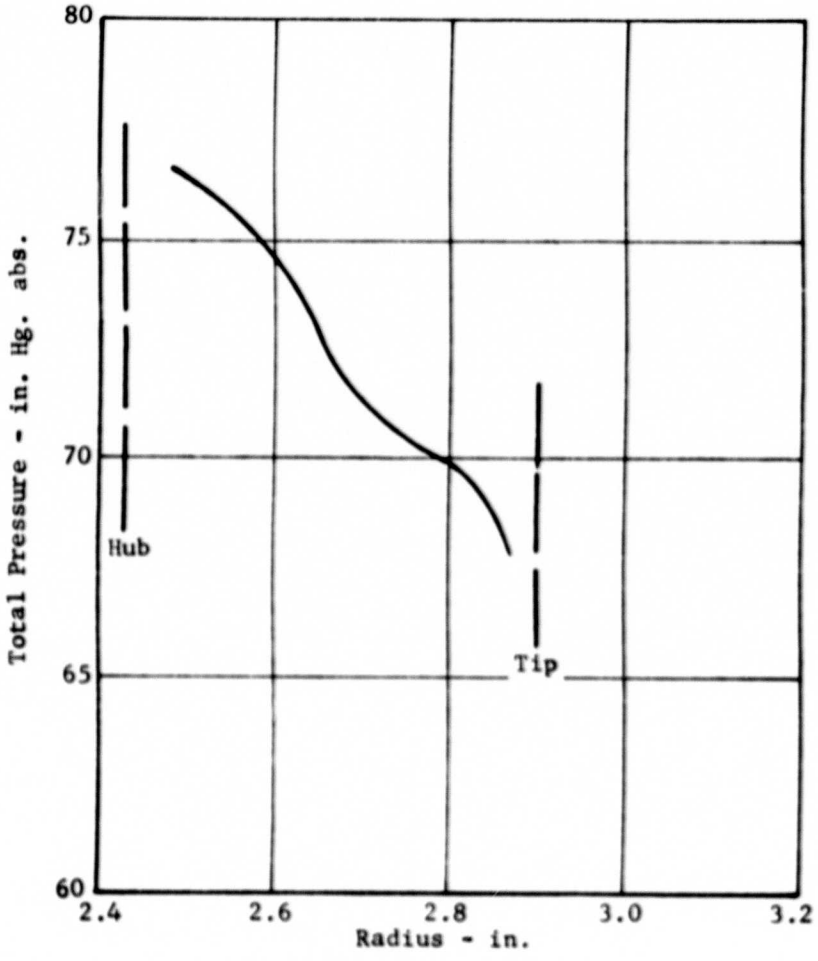

Figure 32. Build 20 Rotor Exit Pressure Traverse Data for $N/\sqrt{\theta}$ = 90 Percent, $(W\sqrt{\theta})/\delta$ = 3.49 lb/sec, and P_T/P_T = 2.31.

Stator incidence could not be evaluated directly since no instrumentation was available for sensing the flow angle at the stator leading edge. The vector triangle solutions discussed under the section on rotor performance provide an implied stator incidence. The accuracy of the incidence calculation is uncertain, in view of the rapidly changing conditions in the vaneless space between the rotor and stator. For example, assuming a constant total pressure in the vaneless space, the flow angle which satisfies the static pressure at the rotor trailing edge can be 10 degrees or more higher than the angle which satisfies the static pressure near the stator leading edge.

Stator Duct Losses and Diffusion

The parameter used to evaluate the stator and duct performance is the ratio of the total pressure loss to the entering total pressure. The total pressure difference between the traverse probe location just upstream of the stator leading edge and the stage exit measurement plane at station 5 constitutes the stator and duct loss. Total pressure traverse data just upsteam of the stator leading edge was taken at selected points in builds 19 and 20. The losses at those test points are based on the measured stator entrance pressure data from this test and are indicated by an asterisk in Table VII. The stator entrance total pressure data from the previous program (builds 11 and 12) were used to establish the losses for all other test points. The stator entrance data from build 11 were used to determine the stator losses of builds 13, 14 and 15, representing an inlet guide vane setting of -7 degrees and, from build 12 for the stator losses of builds 11 and 17, representing design inlet guide vane setting. The builds 11 and 12 stator entrance data were chosen to agree closely in corrected speed and airflow with the test point being evaluated. The significantly reduced airflows experienced at the +6-degree exit stator setting in build 18 could not be matched with data from the previous builds, and therefore the stator losses were not evaluated for this build.

The stator and duct losses at the peak performance points are presented in Table VII. The data from builds 13 and 16, which represent the design exit stator setting at the -7-degree and at the design inlet guide vane settings respectively, indicate design speed stator losses from 8.1 to 9.6 percent. This performance for the redesigned stators is in close agreement with the 6.5 to 9.0 percent losses measured with the previous exit stators. In making this comparison, it should be noted that the error in the losses for the redesigned stator, associated with using the stator entrance pressure from the previous builds, could easily be 0.5 percent. The data from build 14 indicate that the loss increased to almost 12 percent at the -8 degree stator setting. The data from build 19 indicate that the loss at 90 percent speed is 4.9 percent for the -4-degree stator setting. The loss for the previous stator under comparable conditions was 6 percent, which indicates a small improvement at the -4 degree setting. The data from build 20 indicate that the loss at 90 percent speed is 5.0 percent for the +4-degree stator setting. The airflow for the build 20 point is somewhat lower than that of the build 19 point, which implies that the build 20 loss is associated with a lower mach number and the +4-degree setting is a higher loss

TABLE VII. EXIT STATOR PRESSURE LOSS DATA

Build No.	% $N/\sqrt{\theta}$	$\frac{W\sqrt{\theta}}{\delta}$	P_T/P_T Stage	Stator Loss $\Delta P_T/P_T$ H	M	T	AV
13	100	3.96	2.61	.059	.085	.116	.087
14	100	3.96	2.51	.111	.116	.131	.119
15	98	3.83	2.44	.121	.141	.174	.148
16	100	4.03	2.68	.069	.066	.108	.081
16	100	3.98	2.64	.100	.084	.105	.096
19	90	3.67	2.30	.035	.072	.056	.054
19	90	3.72	2.29	.027*	.052*	.069*	.049*
20	90	3.49	2.31	.060*	.049*	.040*	.050*
20	90	3.49	2.31	.061	.056	.091	.062

* Losses based on total pressure measurement at rotor exit for this test point.

setting. The stator setting for minimum loss appears to be in the region between -4 degrees and design. A more detailed analysis of the relationship between stator losses and incidence could not be made due to the uncertainty in establishing the stator incidence.

The static pressure rise through the redesigned stator and duct is compared with that for the previous stator in Figure 30 and with the design case in Figure 33. The redesigned stator and duct achieved a higher degree of diffusion as evidenced by the 2.5-inches of mercury higher average static pressure at the stage exit. The static pressure entering the redesigned stator is approximately 11 inches of mercury below the design value. This discrepancy decreases to approximately 7 to 8 inches of mercury just downstream of the leading edge and to 6 inches of mercury at the trailing edge of the exit stator. The flow within the stator passage, therefore, appears to be diffusing as expected. The static pressure rise along the annular diffuser downstream of the vanes is within 1 inch of the expected static pressure rise.

Stage Exit Conditions and Stator Deviation

The radial total temperature and total pressure profiles for the build 13 design speed peak performance point are presented in Figure 34. The total pressure profile differs from the previous build 11 primarily at the tip, where the pressure is significantly lower for the redesigned stator. The temperature profile follows the same trend as in build 11, but the temperature is higher as discussed previously. Figure 35 shows the design speed total pressure profiles across the blade wakes at the stage exit (station 5). The profiles show the greatest variation at the hub and the smallest at the tip, as was the case for the previous design, and similarly the maximum variation is within 5 percent of the average value. The mean total pressures of the blade wake profiles, as established at station 5 from the 10 element rakes, were from 0.5 to 1.0 percent higher than the numerical average of this rake data. These mean values were in agreement with the traversing probe data measured at station 6. The average total pressure at the stage exit was determined as the average of the mean values measured at the hub, mid and tip sections. This average total pressure satisfied continuity at the stage exit for the average flow angle and a blockage of 6%. The data from the other builds showed no significant change in the profiles.

The stage exit flow angle versus radius measured at station 6 is shown in Figure 36 for build 13. The results indicate a flow angle of 19.7 degrees at the tip as compared to a design angle of 8.7 degrees. The deviation as measured at the stage exit is therefore 11 degrees higher than the design value. The measured flow angle at the hub is 5.5 degrees, which is less than 1 degree higher than the design value of 4.6 degrees. The increase in flow angle which occurs along the annular diffuser may have been in excess of the predicted value at the outer wall and thus may account for part of the high tip deviation at the stage exit. The deviation at the tip section of the blade trailing edge, however, is projected to be greater than 15 degrees compared to a design value of 8.5 degrees.

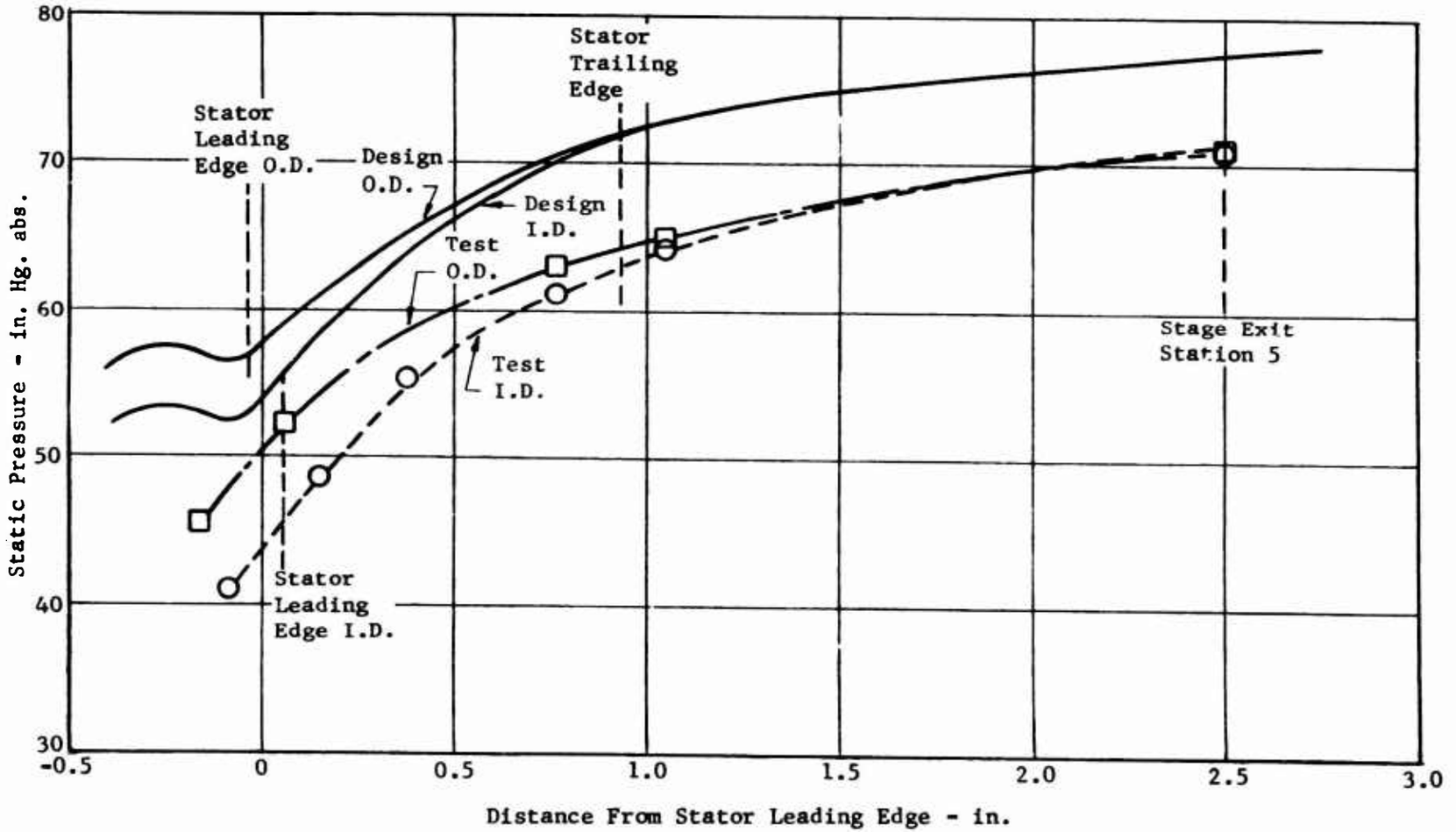

Figure 33. Build 13 Static Pressure Rise Through the Exit Stator and Duct for $N/\sqrt{\theta}$ = 100 Percent, $(W\sqrt{\theta})/\delta$ = 3.96 lb/sec, and P_T/P_T = 2.61.

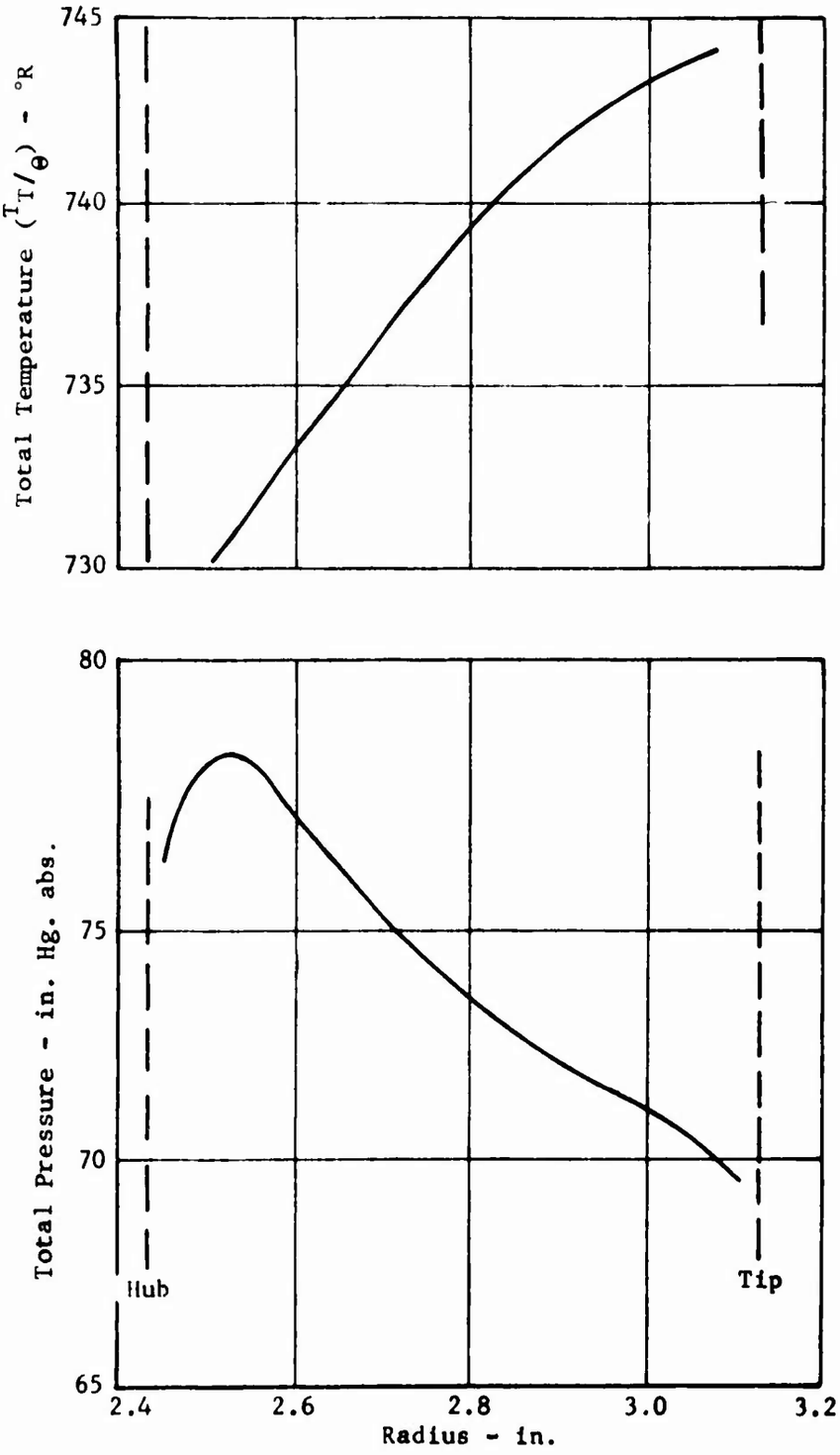

Figure 34. Build 13 Test Data, Radial Temperature and Pressure Profiles at Stage Exit Station 6 for $N/\sqrt{\theta}$ = 100 Percent, $(W\sqrt{\theta})/\delta$ = 4.02 lb/sec, and P_T/P_T = 2.52.

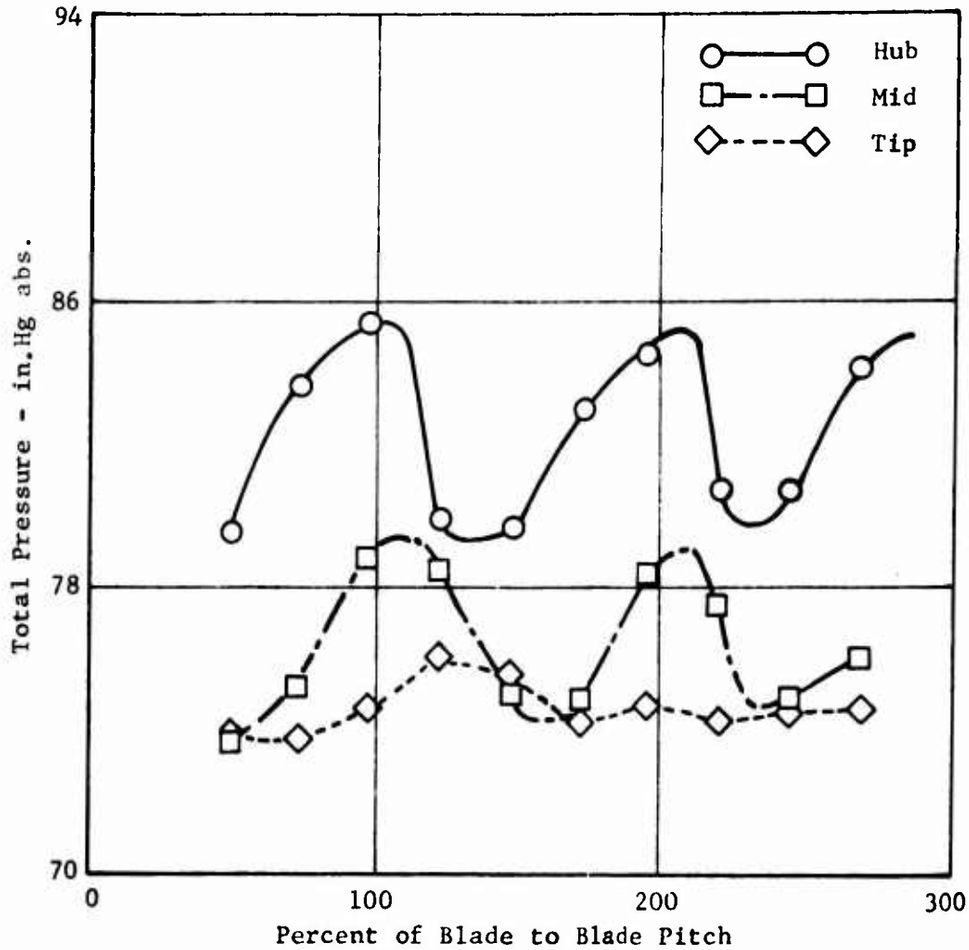

Figure 35. Build 13 Test Data, Total Pressure Profiles Across Blade Wakes at the Stage Exit Station 5 for $N/\sqrt{\theta}$ = 100 Percent, $(W\sqrt{\theta})\,\delta$ = 3.96, lb/sec, and P_T/P_T = 2.61.

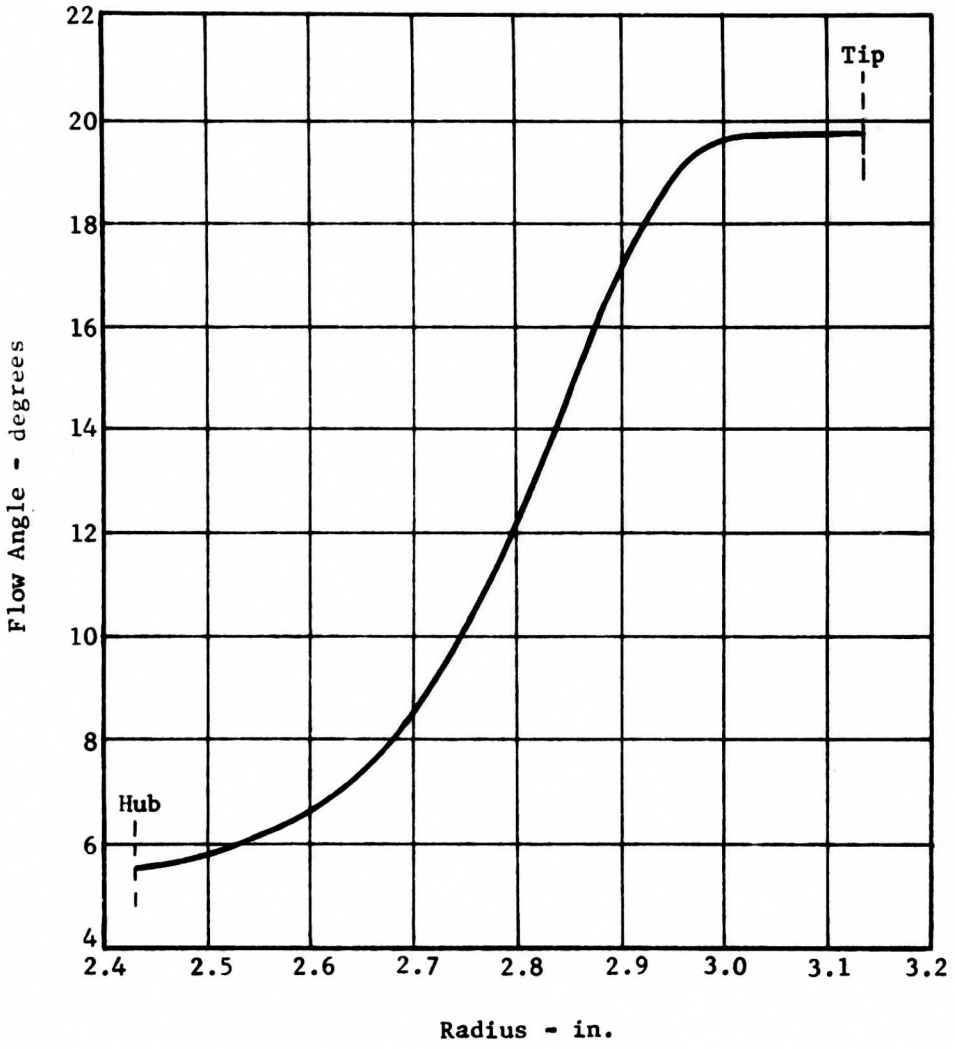

Figure 36. Build 13 Test Data, Flow Angle Versus Radius at Stage Exit Station 6 for $N/\sqrt{\theta}$ = 100 Percent, $(W\sqrt{\theta})/\delta$ = 4.02 lb/sec and P_T/P_T = 2.52.

The radial variation in Mach number at the stage exit (station 6) is given in Figure 37 for build 13. The average stage exit Mach number for this point is .329 compared to a design value of .322.

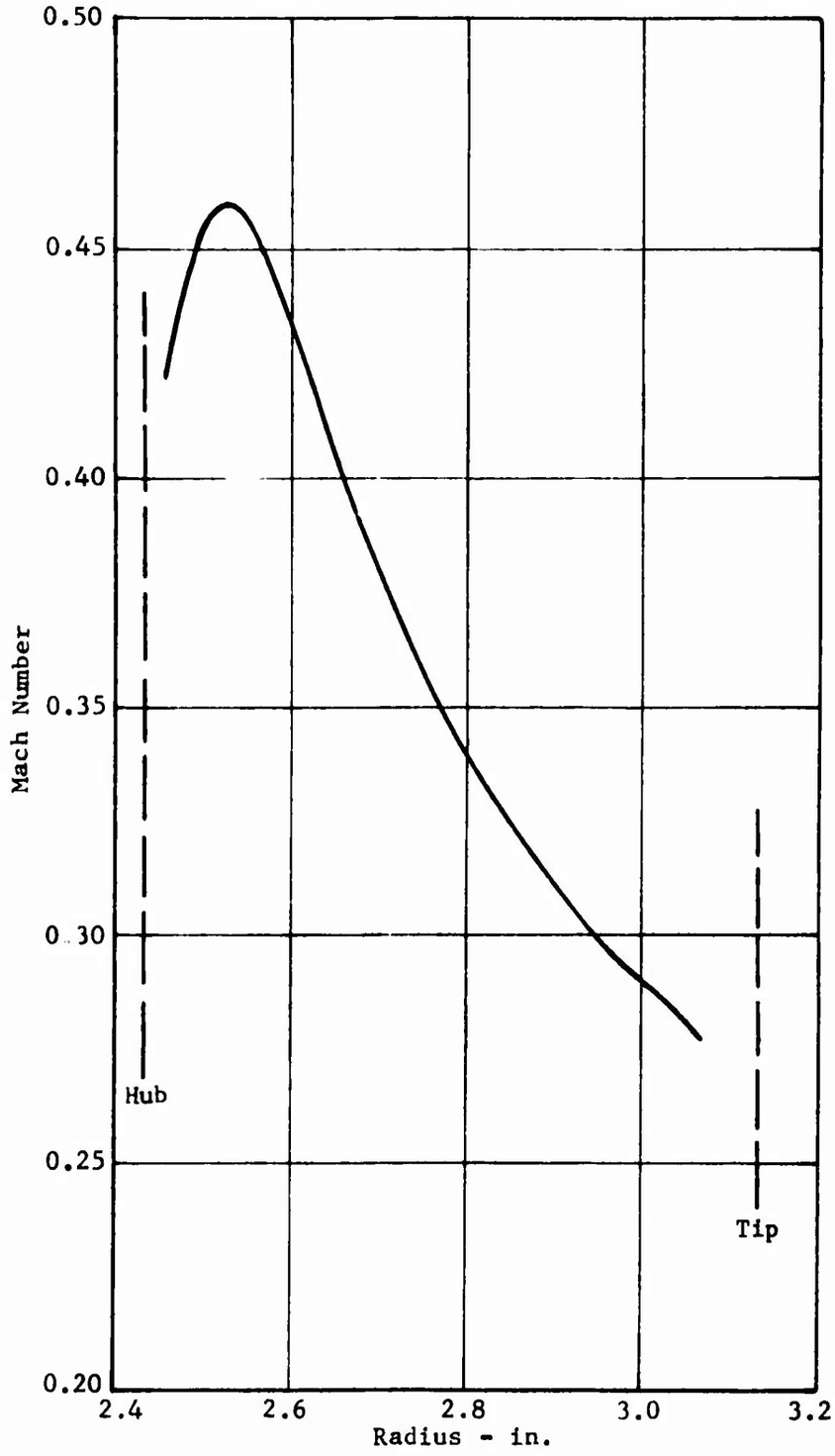

Figure 37. Build 13 Test Data, Radial Mach Number Profile at Stage Exit Station 6 for $N/\sqrt{\theta}$ = 100 Percent, $(W\sqrt{\theta})/\delta$ = 4.02 lb/sec, and P_T/P_T = 2.52.

CONCLUSIONS

1. The redesigned exit stator with the annular flow path did not improve the performance of the 2.8:1 supersonic compressor stage.

2. Adjusting the exit stator vane shifted the surge line at the closed settings but offered no improvement in performance over the design setting.

3. The change in exit stator configuration had a significant effect on the rotor work but only a minor effect on the rotor pressure ratio.

4. The flow acceleration from the rotor exit to the stator leading edge noted in the previous test was also present in this test.

5. This flow acceleration has a primary influence on the stator losses and is responsible for the fact that the losses were insensitive to the change in stator configuration.

RECOMMENDATIONS

1. Investigate the source of the flow acceleration from the rotor exit to the stator entrance to establish design modifications which will eliminate this condition.

2. Continue development of the 2.8:1 supersonic axial boost compressor incorporating design modifications which offer a solution to the flow acceleration problem and the associated high exit stator losses.

3. Continue to investigate the effect of exit stator configuration on the rotor work or temperature rise.

LITERATURE CITED

1. Muller, C.H., Litke, W., Sabatiuk, A., and Weiser, H., SINGLE-STAGE AXIAL COMPRESSOR COMPONENT DEVELOPMENT FOR SMALL GAS TURBINE ENGINES(U), Volume I-Design (U), USAAVLABS Technical Report 68-90A, March 1969 (Confidential).

2. Muller, C.H., and Cox, L., SINGLE-STAGE AXIAL COMPRESSOR COMPONENT DEVELOPMENT FOR SMALL GAS TURBINE ENGINES, Volume II-Rotor Development, USAAVLABS Technical Report 68-90B, May 1969.

3. Muller, C.H., and Cox, L., SINGLE-STAGE AXIAL COMPRESSOR COMPONENT DEVELOPMENT FOR SMALL GAS TURBINE ENGINES, Volume III-Supersonic Compressor Stage Development, USAAVLABS Technical Report 68-90C, June 1969.

4. Sagi, C., and Johnston, J., THE DESIGN AND PERFORMANCE OF TWO-DIMENSIONAL, CURVED DIFFUSERS, ASME Transactions, pp. 715-731, December 1967.

5. Reneau, L., and Johnston, J., A PERFORMANCE PREDICTION METHOD FOR UNSTALLED, TWO-DIMENSIONAL DIFFUSERS, ASME Transactions, pp. 643-654, September 1967.

6. Wright, L., and Novak, R., AERODYNAMIC DESIGN AND DEVELOPMENT OF THE GENERAL ELECTRIC CJ 805-23 AFT FAN COMPONENT, ASME Paper 60-WA-270.

7. Welliver, A.D., and Acurio, J., ELEMENT DESIGN AND DEVELOPMENT OF SMALL CENTRIFUGAL COMPRESSOR (U), USAAVLABS Technical Report 67-30, August 1967 (Confidential).

APPENDIX

TEST PLAN

OBJECTIVE

The objective of the stator redesign program is to evaluate the performance of exit stators designed for a cylindrical flow path and their effect on the overall performance of the 2.8:1 supersonic axial compressor stage. The compressor stage consists of the inlet, inlet guide vanes, rotor, and exit stators. The inlet guide vanes and the exit stators are adjustable. The stage performance goals are:

Pressure Ratio	2.8:1
Adiabatic Efficiency	82.2 percent
Weight Flow	4.0 pounds per second
Design Speed	50,700 revolutions per minute

APPROACH

The 2.8:1 supersonic compressor was designed and its development was initiated under Contract DA 44-177-AMC-392(T). The demonstrated performance of the combined inlet, inlet guide vanes, and rotor for build 11 of that program was within two points of the efficiency goal at within 1-1/2 percent of the pressure ratio and airflow goals as indicated by the following data:

INLET, INLET GUIDE VANES AND ROTOR

	Design Goals	Demonstrated	
Build No.		11	12
Inlet Guide Vane Setting	Design	-7°	Design
Pressure Ratio	2.98:1	2.85:1	2.91:1
Adiabatic Efficiency (Percent)	85.2	83.9	80.7
Corrected Airflow (Pounds per Second)	4.0	3.94	4.02

The losses of the integral fixed exit stators and "S" shaped interconnecting duct included in those tests, however, resulted in a stage efficiency 7 to 8 points below the design goal.

The exit stator assembly redesign performed under the current program provides adjustable exit stator vanes in a cylindrical duct followed by an annular diffuser of optimum divergence angle (see Figure 1). The entire 2.8:1 compressor stage, consisting of the inlet, inlet guide vanes, and rotor from build 11 of the previous contract, and the new exit stator assembly will be tested to evaluate the stator and overall stage performance.

The inlet guide vanes will be set at -7° and the exit stators will be at the design setting for the initial testing. The exit stator setting will be varied first and then the inlet guide vane setting will be varied to determine the effects on design speed performance. Compressor characteristics will then be generated along 60, 80, 90 and 100% speed lines for the IGV and exit stator setting combination which exhibited best performance.

Instrumentation will be provided (as detailed in the following sections) which will permit evaluation of the (1) overall stage pressure ratio, adiabatic efficiency and airflow, (2) the exit stator losses, and (3) the static pressure rise between the rotor trailing edge and the stator leading edge, within the stator passages and in the exit diffuser.

The data points in the 90 to 100% speed range, which represent peak pressure ratio and efficiency for a given speed, will be analyzed to establish vector diagrams that satisfy the experimental data. The experimental vector diagrams will be compared to the design conditions to pinpoint any deficiencies.

TEST CONFIGURATIONS

Compressor

A. The compressor build will include the inlet guide vanes and the 2.8:1 pressure ratio rotor from builds 10-12 of Contract DA 44-177-AMC-392(T) and the redesigned exit stator assembly. The compressor will be mounted to and powered by the steam-driven Rover turbine on test stand WX25R. See Figures 1 and 38.

B. The inlet guide vanes will be set in the -7° position (7 degrees less prewhirl than at the design setting) and the exit stators at their design setting initially, but repositioning may be required as indicated by the test results.

C. The rotor blade tip clearance will be set at .011 inch at the trailing edge, which is the same as in builds 10-12. The same rotor shroud from builds 10-12 will be used.

D. An external air supply will be used to pressurize the cavity between the front oil seal and the rotor labyrinth seal. This pressurization serves to balance the axial forces on the rotor to minimize bearing loads and to provide a pressure differential across the oil seal to eliminate oil leakage.

Test Equipment

A. Air Inlet System - The air inlet system consists of an air filter, a calibrated air bottle, a convergent adapter, and approximately seven feet of straight ducting.

B. Exit Air System - The compressor exit scroll is connected to a close-couple valve with a divergent adapter. The exhaust air from the close-couple valve is ducted and dumped into the vertical stack of the steam exhaust system.

C. Turbine Thrust Balance System - Pressurized air is supplied to the downstream side of the turbine balance piston to reduce the thrust load on the bearing. An automatic system maintains the air pressure equal to the stream pressure at the exit of the turbine stator.

D. Oil System - Oil is supplied from a pump to three inlet points on the compressor and turbine at the pressure of 30.0 psi. The inlet points feed respectively: (1) compressor front bearing, (2) compressor rear main bearing and turbine front main bearing, and (3) turbine rear main bearing. The oil from the compressor front main bearing collects in the compressor sump while the remaining oil collects in the turbine sump. The return oil from both sumps is scavenged with a common pump.

INSTRUMENTATION

Compressor Speed

A magnetic pickup is set to sense 12 lobes on the front compressor shaft nut. The signal is fed into an eput meter for direct rpm readout. The signal is also fed into an oscilloscope and the rpm is periodically checked against a known frequency calibration signal.

Compressor Airflow

The pressure differential across a standard calibrated air bottle is measured on an inclinometer to determine the compressor airflow. The air bottle is located at the entrance of the compressor inlet air system.

Compressor Pressures

The compressor pressures to be measured include fixed total pressure probes, traversing yaw probes, and static pressure taps. All of the pressures except those from the traversing probe are recorded on manometer banks which are photographed. The data from the traversing probe are recorded on X-Y plotters. The locations and ranges of all pressures are detailed in Table VIII and illustrated in Figures 39 through 43.

A. Inlet Total Pressure - The inlet total pressure is measured by a five-element total pressure rake located in the inlet ducting upstream of the compressor. The probe elements are located at the centers of equal areas along the zero-degree radial position from the duct centerline to the I.D.

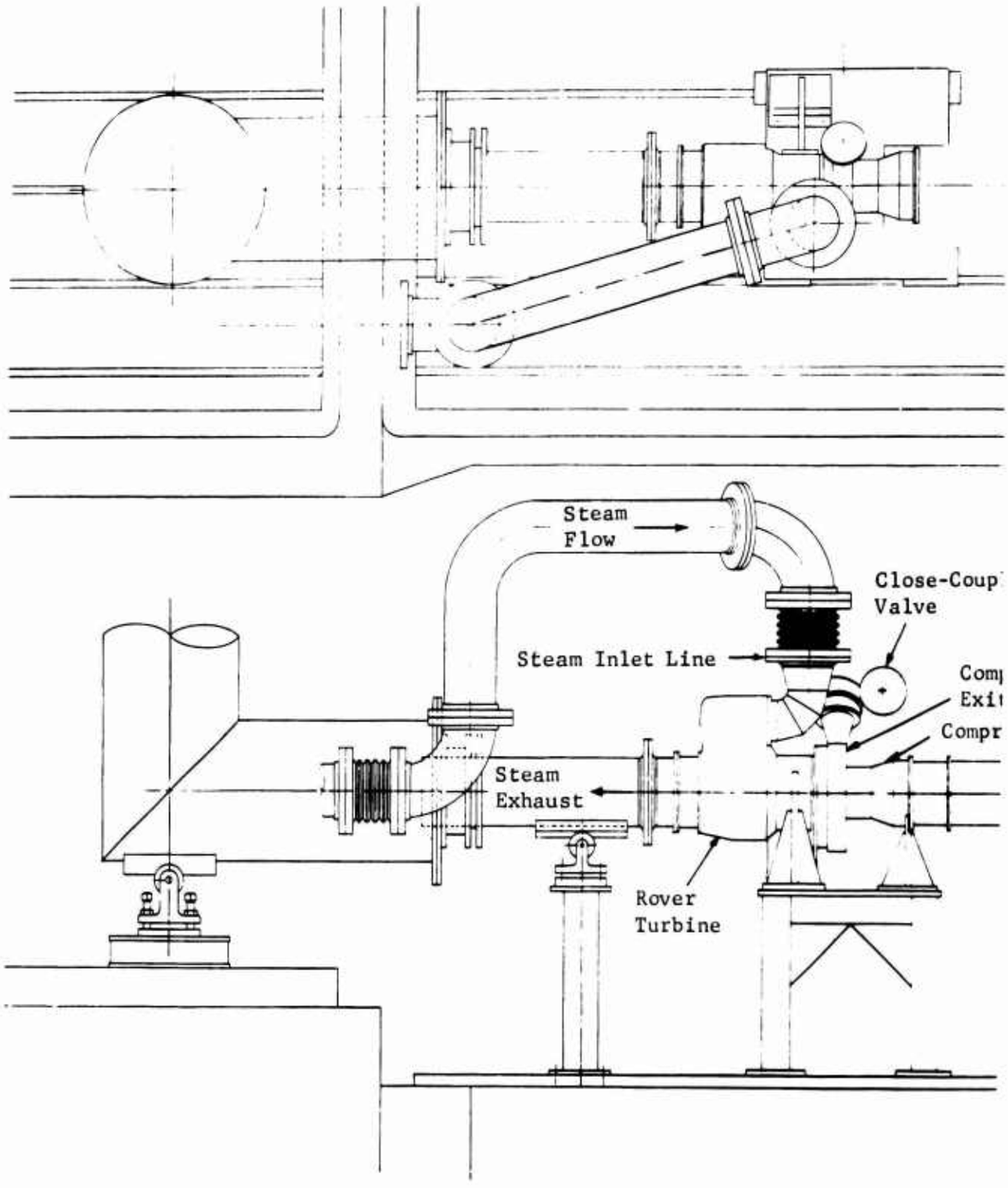

Figure 38. Compressor Test Rig Installation.

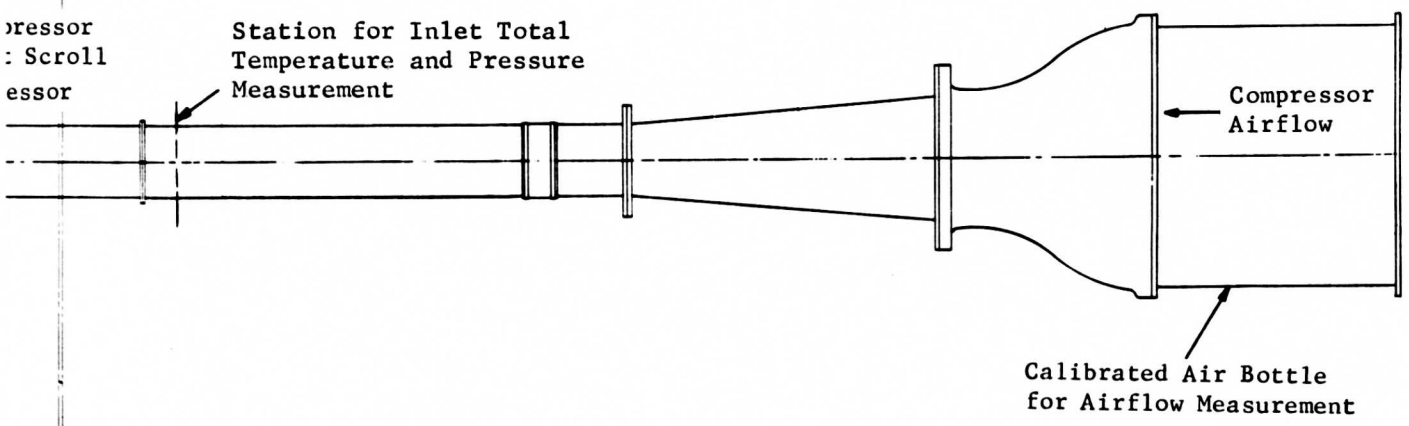
Station for Inlet Total
Temperature and Pressure
Measurement
Compressor
Airflow
Calibrated Air Bottle
for Airflow Measurement

TABLE VIII. STAGE TEST - INSTRUMENTATION

Instrumentation	Location			Operating Range	Quick-Look Board
	Axial	Circumf.	Radial		
5 Inlet Totals (Pressures, Temperatures)	Inlet Duct	0°, 180°	1.21", 2.09" 2.68", 3.18", 3.62	-60 to 0 in. Hg. Gage	
Static Pressure in Labyrinth Cav.				-60 to 0 in. Hg. Gage	
3 Statics	Leading Edge IGV	6°, 122°, 238°	Flow Path O.D.	-60 to 0 in. Hg. Gage	
3 Statics	Leading Edge IGV	6°, 122°, 238°	Flow Path I.D.	-60 to 0 in. Hg. Gage	
3 Statics	Trailing Edge IGV	6°, 122°, 238°	Flow Path O.D.	-60 to 0 in. Hg. Gage	1 Pressure
3 Statics	Trailing Edge IGV	6°, 122°, 238°	Flow Path I.D.	-60 to 0 in. Hg. Gage	
3 Statics	Leading Edge-Rotor	40°, 166°, 274°	Flow Path O.D.	-60 to 0 in. Hg. Gage	
3 Statics	Mid Chord Rotor	27°, 153°, 261°	Flow Path O.D.	0 to 60 in. Hg. Gage	
3 Statics	Trailing Edge-Rotor	14°, 140°, 248°	Flow Path O.D.	0 to 60 in. Hg. Gage	1 Pressure
1 Static	.245" Upstream Leading Edge Exit Stator	15°	Flow Path O.D.	0 to 60 in. Hg. Gage	
3 Statics	.155" Upstream Leading Edge Exit Stator	16°, 136°, 256°	Flow Path O.D.	0 to 60 in. Hg. Gage	
1 Static	.065" Upstream Leading Edge Exit Stator	17°	Flow Path O.D.	0 to 60 in. Hg. Gage	
1 Static	.320" Upstream Leading Edge Exit Stator	19°	Flow Path I.D.	0 to 60 in. Hg. Gage	
3 Statics	.185" Upstream Leading Edge Exit Stator	19°, 139°, 259°	Flow Path I.D.	0 to 60 in. Hg. Gage	
1 Static	.050" Upstream Leading Edge Exit Stator	21°	Flow Path I.D.	0 to 60 in. Hg. Gage	
2 Statics	.170" Downstream Leading Edge Exit Stator	21°, 147°	Flow Path O.D.	0 to 60 in. Hg. Gage	
2 Statics	.855" Downstream Leading Edge Exit Stator	28°, 154°	Flow Path O.D.	0 to 60 in. Hg. Gage	

TABLE VIII - Continued

Instrumentation	Location			Operating Range	Quick-Look Board
	Axial	Circumf.	Radial		
1 Static	.105" Downstream Leading Edge Exit Stator	23°	Flow Path I.D.	0 to 60 in. Hg. Gage	
1 Static	.335" Downstream Leading Edge Exit Stator	25°	Flow Path I.D.	0 to 60 in. Hg. Gage	
1 Static	.720" Downstream Leading Edge Exit Stator	27°, 153°	Flow Path I.D.	0 to 60 in. Hg. Gage	
2 Statics	.111" Downstream Trailing Edge Exit Stator	28°, 154°	Flow Path O.D.	0 to 60 in. Hg. Gage	
2 Statics	.111" Downstream Trailing Edge Exit Stator	27°, 153°	Flow Path I.D.	0 to 60 in. Hg. Gage	
3 Statics	Station 5	30°, 150°, 270°	Flow Path O.D.	0 to 60 in. Hg. Gage	
3 Statics	Station 5	30°, 150°, 270°	Flow Path I.D.	0 to 60 in. Hg. Gage	
2 Pitot (Adjustable Yaw Angle)	Station 4	230°, 310°	Adjustable	0 to 100 in. Hg. Gage	1 Probe
3 Tangential Ten Element Pitot Rake	Station 5	40° 160° 280°	.300" from O.D. .500 from O.D. .100 from O.D.	0 to 100 in. Hg. Gage	
2 Radial Five Element Pitot Rake	Station 5	80°, 236°	.100" Spacing	0 to 100 in. Hg. Gage	1 Rake
3 Radial Five Element Thermocouple Rakes	Station 6	20°, 140° 253°	.100" Spacing	50 to 500°F	
Traversing Probe (Total Pressure) (Total Temperature) (Yaw Angle)	Station 6	279°	Variable	0 to 45 psia 50 to 500°F 30° to -30°	
Traversing Probe (Total Pressure) (Total Temperature) (Yaw Angle)	Station 6	152°	Variable	0 to 45 psia 50 to 500°F +30 to -30°	
Traversing Probe Variable (Total Pressure) (Total Temperature) (Pitch Angle)	Station 6	Variable 200°-242°	0.300 from Flow Path O.D.	0 to 45 psia 50 to 500°F +30 to -30°	

2.8:1 Supersonic Compressor Redesigned Exit Stator

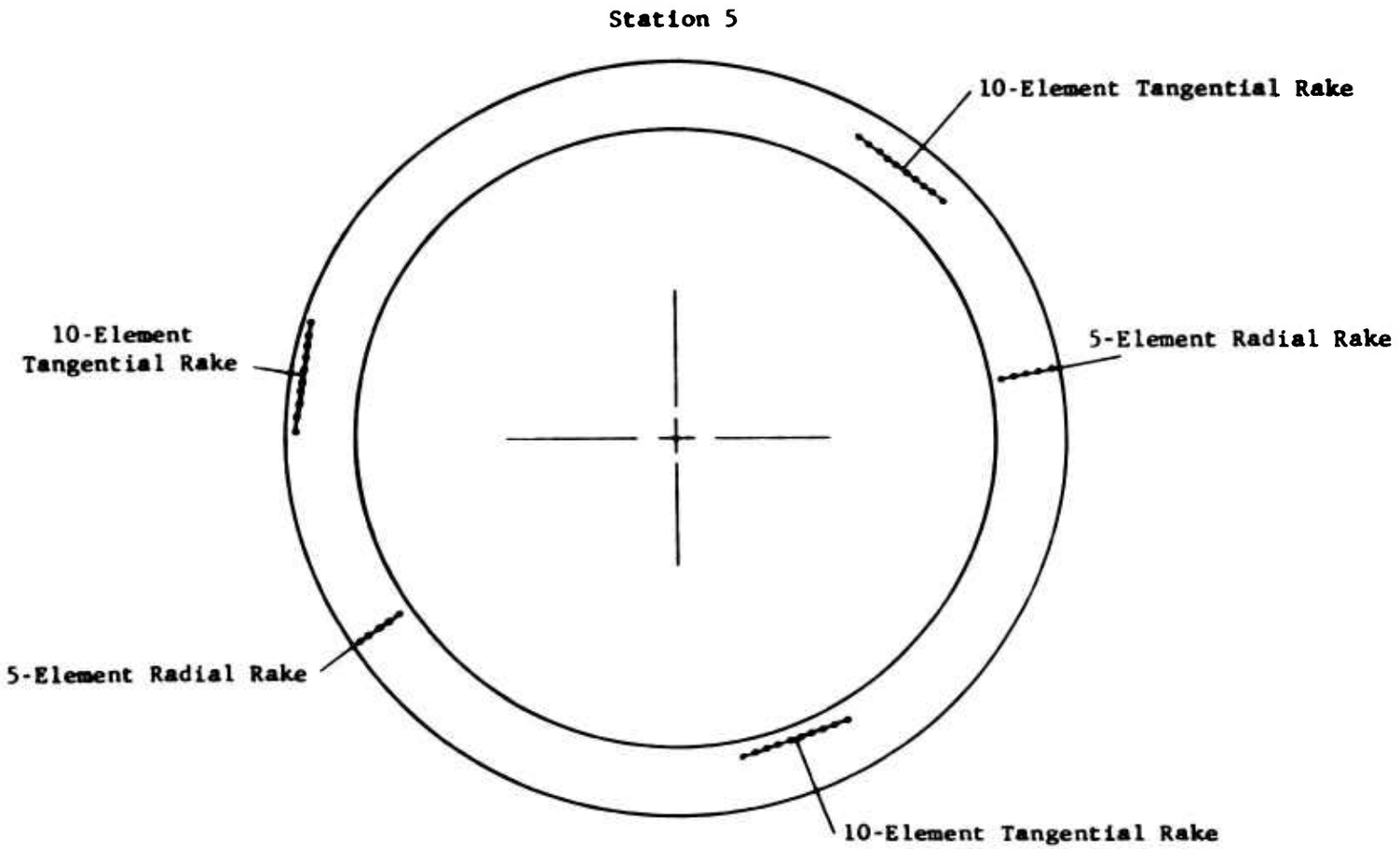

Figure 39. Total Pressure Instrumentation.

2.8:1 Supersonic Compressor Redesigned Exit Stator

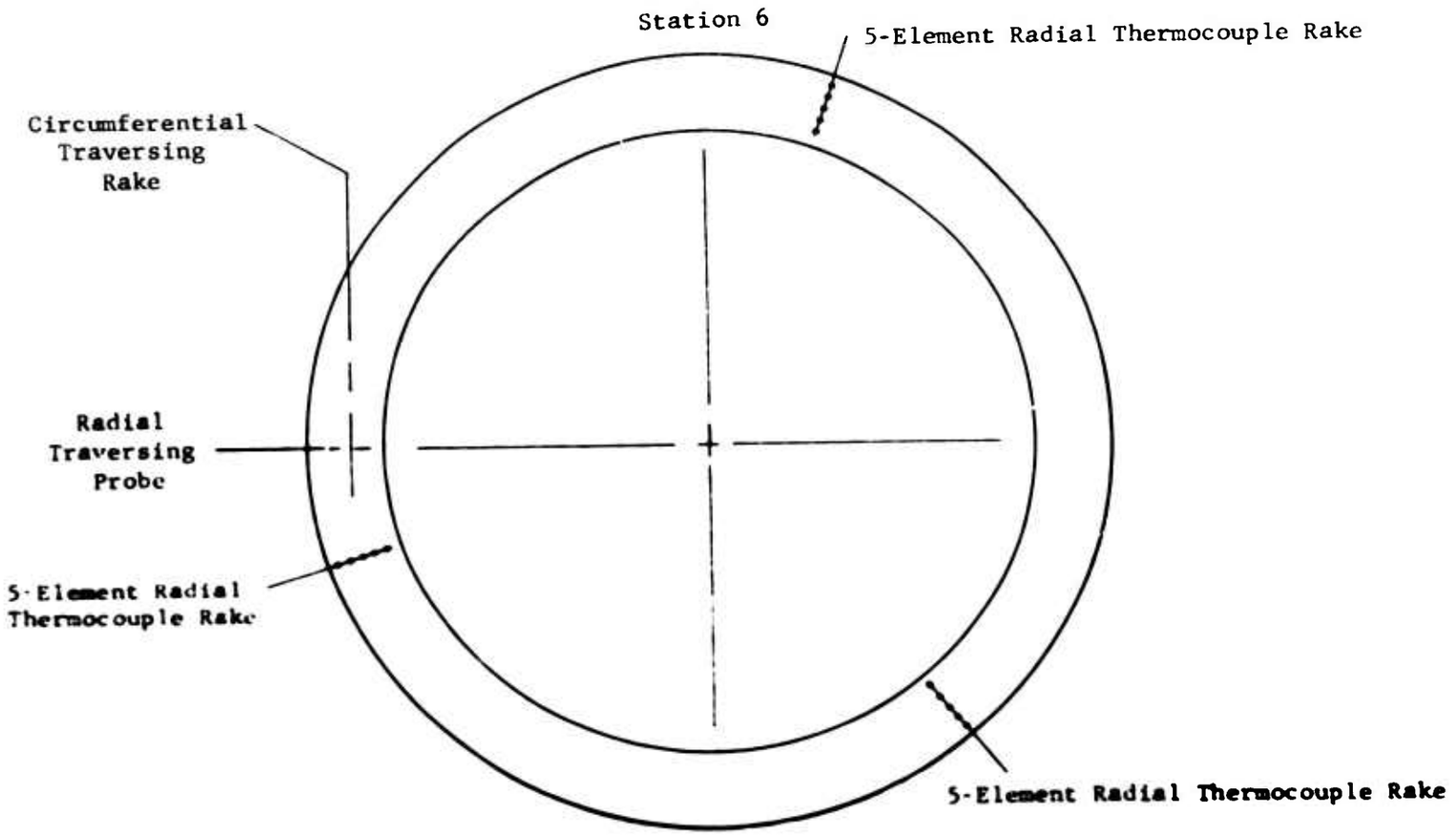

Figure 40. Temperature Instrumentation and Traversing Probes.

Supersonic Compressor 2.8:1 Pressure Ratio

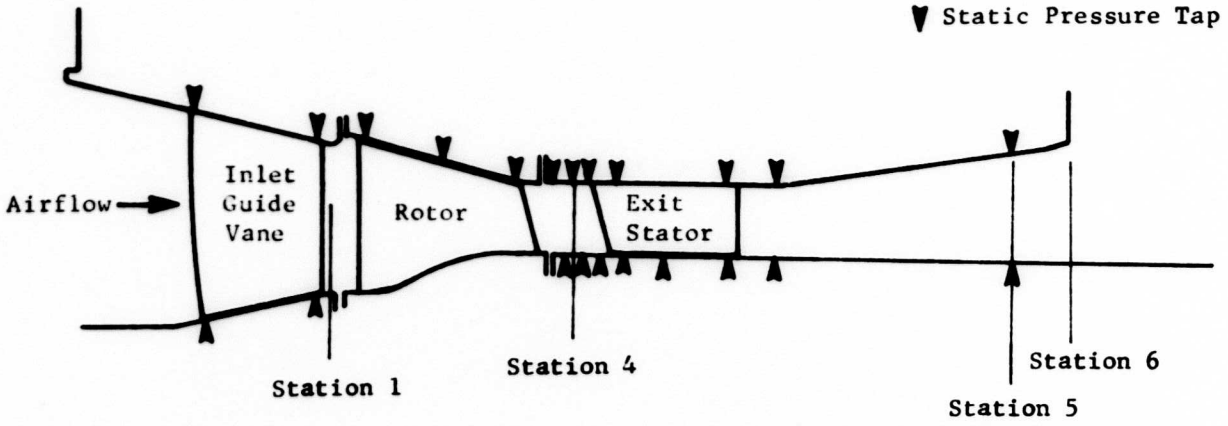

Figure 41. Static Pressure Locations Along Flow Path for Redesigned Exit Stator.

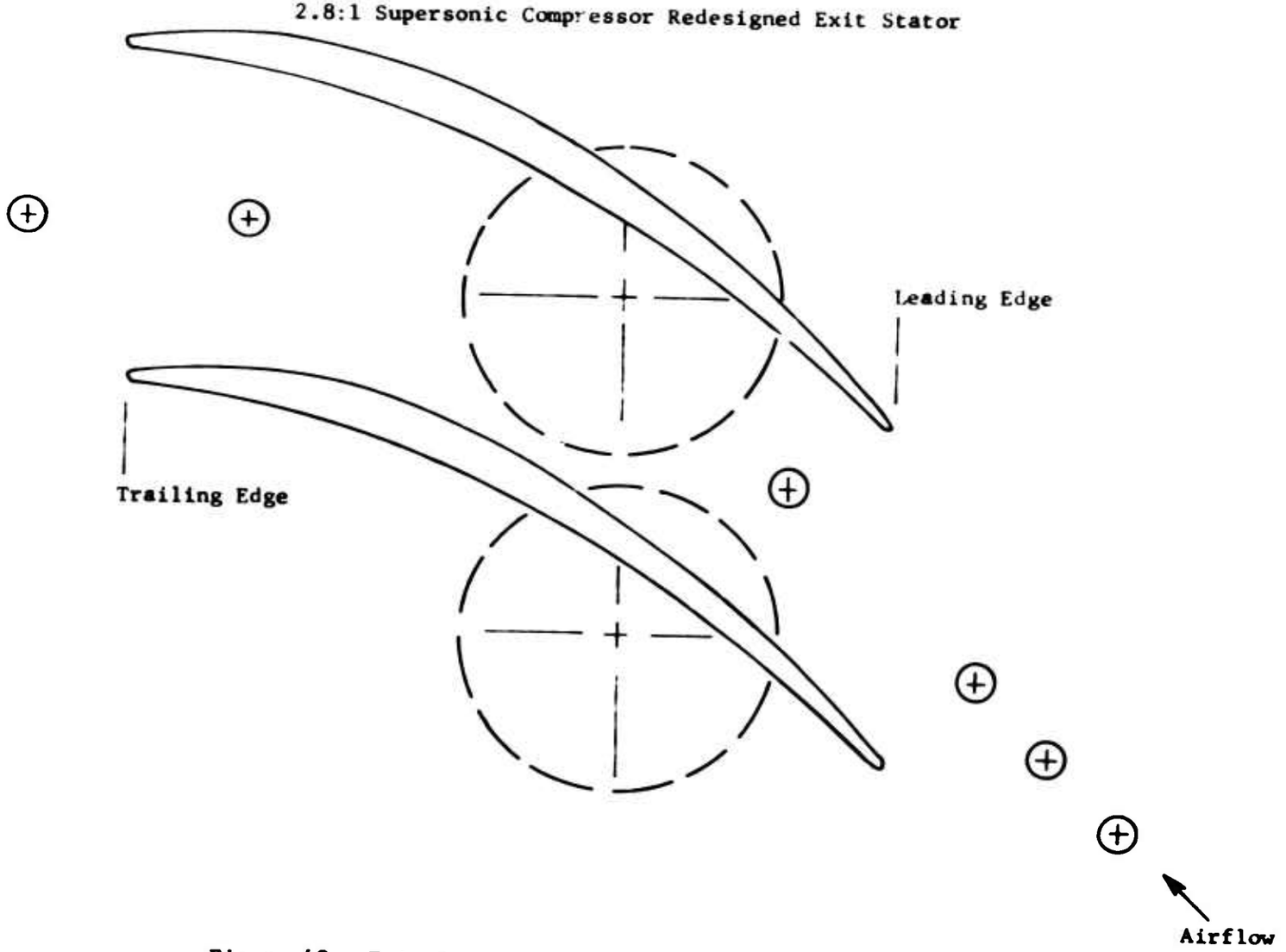

Figure 42. Exit Stator O.D. Static Pressure Instrumentation.

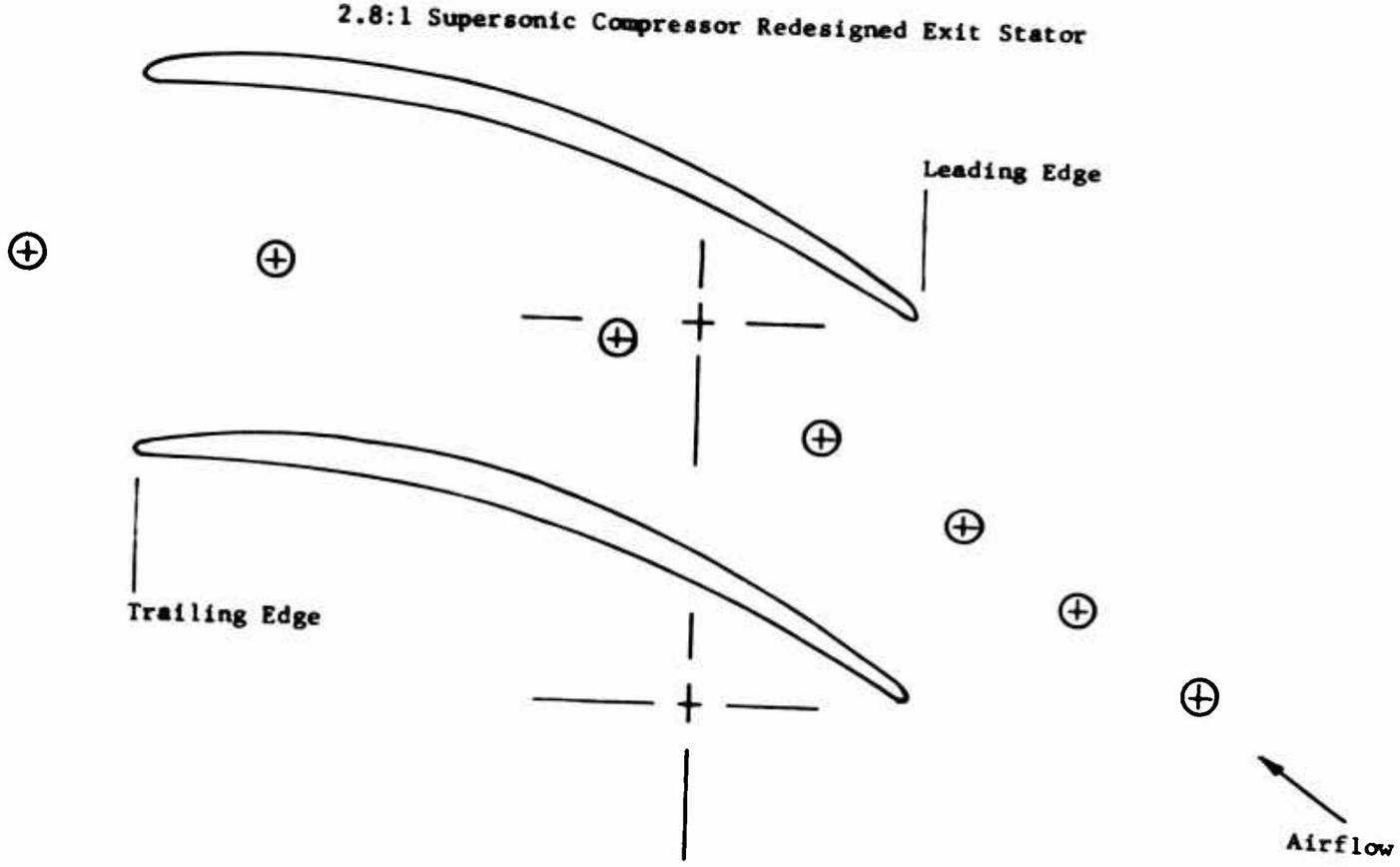

Figure 43. Exit Stator I.D. Static Pressure Instrumentation.

B. Rotor Exit Total Pressure - The rotor exit total pressure will be measured with two adjustable single-element total probes at station 4 (see Figure 41). The yaw angle and radial depth will be adjustable for these probes. The total probes will be mounted in plugs which will be removable from the compressor housing. By substituting uninstrumented plugs, the compressor performance can be checked with no probe obstruction between the compressor rotor and the exit stator.

C. Stage Exit Total Pressure - The stage exit total pressure is measured with an array of fixed-position total probes and traversing yaw probes. The fixed probe measurements are made at station 5, which represents the exit plane of the compressor stage. The traversing probe measurements are made at station 6, which is just downstream of station 5 (see Figure 41).

The fixed total pressure probes will consist of three 10-element tangential rakes and two 5-element radial rakes (see Figure 39). The probes of the tangential rakes are aligned perpendicular to the trailing edge of the vanes to establish the total pressure profiles across the vane wakes. Each of the tangential probes is set at a different radial depth to determine the profiles for the hub, mean and tip streamtubes. The radial probes have their elements aligned along a radial direction to measure the pressure profile in a radial direction (hub to tip).

The traversing yaw probe senses and automatically aligns the probe along the flow yaw angle and is capable of a continuous traverse from the tip to the hub of the annular passage. During a traverse the total pressure, yaw angle, and total temperature are recorded on X-Y plotters as a function of radius. Both radial and circumferential traverses will be made to supplement the fixed-probe radial and tangential data (see Figure 40).

D. Static Pressures - Static pressure taps are located on the O.D. and I.D. of the flow path in the inlet section, at the leading and trailing edges of each of the blade rows, and at the stage exit plane. Both O.D. and I.D. static pressure taps have been located at three axial stations between the rotor trailing edge and the stator leading edge to evaluate the change in velocity in this region. Static taps have also been located within the stator blade passages to investigate the stator diffusion (see Figures 41, 42 and 43). Static pressure measurements just aft the stator trailing edge and at the stage exit plane will permit evaluation of the static pressure rise in the annular diffuser.

Compressor Temperatures

The compressor temperatures include fixed-probe temperatures and a traversing-probe total temperature. The fixed-probe temperatures are read out from a multiple-selector Brown recorder, while the traversing-probe temperature is recorded on a X-Y plotter. The detailed locations of the thermocouples are presented in Table VIII.

A. Inlet Total Temperature - The inlet temperature is measured by a 5-element total temperature I.C. thermocouple rake which is located and spaced the same as the inlet total pressure rake.

B. Stage Exit Total Temperature - The stage exit total temperature is measured with an array of fixed-position thermocouples and a total temperature thermocouple on the traversing yaw probe. These measurements are made at station 6, which is just downstream of the stage exit plane (see Figure 40).

The fixed thermocouples include three radial 5-element rakes (see Figure 40). These rakes will have unshielded thermocouple elements. Temperature measurements from tests of builds 10-12 showed satisfactory agreement between the stagnation type thermocouples and the unshielded rakes, both of which were installed in those builds.

The traversing thermocouples are a part of the same traversing yaw probes as described for the total pressure.

Vibration

Vibration pickups are located so as to record the vertical and horizontal vibrations at the front compressor support, turbine front support, and turbine rear support. The vibrations are recorded in units of acceleration (g's) since the displacement values are less than 0.1 mil.

Oil Temperature and Pressures and Flow Rate

The oil temperature is recorded at the inlet and outlet of the compressor rig, and the temperature rise is monitored as an indication of satisfactory bearing operation. The oil flow rates to each of the three rig supply lines are monitored continuously. The pressure differential of calibrated orifices is measured to indicate the flow rates.

Steam Pressure

The steam pressure is recorded upstream of the control valve and at the inlet steam jacket for the turbine.

PRETEST INSPECTIONS

Dimensional Inspection

Dimensional inspection of the hardware is performed prior to and during assembly to establish and check critical dimensions, clearances, and airfoil geometry.

Blade Natural Frequencies

The blade natural frequencies for the compressor rotor were measured prior to builds 10-12, and the speeds at which interference might occur with rig excitations have been defined.

Rotor Balancing

The compressor and turbine rotors and shaft assemblies will be check-balanced to insure a balance of within .001-.003 ounce-inch at 2500 rpm prior to assembly.

Magnaflux

The compressor rotor was given a Magnaflux inspection prior to assembly for builds 10-12.

TEST PROCEDURES

Table IX presents the scheduled test points. The following sequence of steps describes the normal test procedure:

1. All subsystems such as the oil system and the balance air systems are started and checked for proper operation prior to opening the steam control valve and starting the compressor.

2. The steam control valve is then activated and the compressor speed is brought slowly up to the first test speed with the close-coupled valve for the compressor air system in the wide-open position (maximum airflow). The vibration meter is monitored continuously throughout the test.

3. The inlet temperature is noted after it has stabilized, and the speed is then adjusted to the desired corrected speed ($N/\sqrt{\theta}$).

4. After all the instruments are stabilized, a complete set of data is recorded, including a photograph of the manometer banks and full traverse from tip to hub with the traversing yaw probe.

5. A constant speed line is then developed by closing the close-couple valve while maintaining speed, until the next scheduled reduced weight flow is attained. Step four is then repeated. Four to five test points are planned for each speed line. The final test point on a given speed line is obtained by closing the close-couple valve until compressor surge is audible. The weight flow at which surge is first detected is noted, and the close-couple valve is opened until a weight flow slightly above surge is attained. This point is then taken as the last data point on the speed line.

6. The close-couple valve is set wide open, and the compressor is then accelerated to the next highest speed. The process is repeated for each of the scheduled speed lines up to 100% speed. In the range of 90 to 100% speed where the speed lines are expected to exhibit almost constant weight flow, the constant speed line is developed by closing the close-couple valve to meet prescribed increments of increased pressure ratio rather than increments of reduced weight flow.

TABLE IX. SCHEDULED STAGE TEST POINTS

% Speed	$W\sqrt{\theta}/\delta$		P/P
60	Wide-open throttle		
	2.4		
	2.3		
	2.2		
	Surge Point		
80	Wide-open throttle		
	3.1		
	3.0		
	2.9		
	Surge Point		
90	Wide-open throttle		1.80
			2.1
			2.15
			2.22
	Surge Point	~	2.30
100	Wide-open throttle		2.08
			2.3
			2.5
			2.6
	Surge Point	~	2.8

The above points are estimated based on previous performance and are intended as a guide. Deviation from predicted performance may require adjustment of the data points to be run.

DATA PRESENTATION

Compressor Map

The standard compressor map in which the adiabatic efficiency and total-to-total pressure ratio are plotted against corrected weight flow for each of the corrected speed lines will be generated and compared to the experimental maps from previous builds and the design conditions. This map will be based on the average compressor inlet conditions and the average stage exit conditions (measured at station 5). The corrected conditions and efficiency are computed as follows:

$$\text{Corrected weight flow} = \frac{Wa\sqrt{\theta}}{\delta}$$

where Wa = actual measured airflow in pounds per second

$$\sqrt{\theta} \quad \sqrt{\frac{T_{inlet}}{T_{reference}}}$$

T_{inlet} = Average total temperature at the compressor inlet (°R)

$T_{reference}$ = 519°R

$$\text{Corrected speed} = N/\sqrt{\theta}$$

where N = Actual measured speed in rpm

$\sqrt{\theta}$ = same as above

$$\text{Percent speed} = \frac{(N/\sqrt{\theta}\ \text{measured})}{(N/\sqrt{\theta}\ \text{design})} \times 100$$

where $(N/\sqrt{\theta})$ measured = same as above

$(N/\sqrt{\theta})$ design = 50,700 rpm

$$\text{Pressure ratio} = P_{T_5}/P_{T_0}$$

where P_{T_5} = total pressure integrated from hub to tip of the velocity vector leaving the stage exit plane

P_{T_0} = integrated total pressure at the compressor inlet.

$$\text{Adiabatic Efficiency} = \frac{\Delta H'}{\Delta H} \times 100$$

where $\Delta H'$ = The isentropic enthalpy rise for the measured pressure ratio (BTU/lb)

ΔH = The actual enthalpy rise based on the average measured total temperatures at the compressor inlet (T_{inlet}) and the total temperature of the stage exit velocity vector integrated from hub to tip. (BTU/lb)

Stage Exit Conditions

The following stage exit parameters will be presented as a function of radius from hub to tip:

Total pressure
Total temperature
Mach number
Flow angle with respect to axial

The circumferential pressure profile spanning two exit stator blades at the stage exit plane will also be presented.

Vector Diagrams

The velocity vector diagrams representing the inlet and outlet conditions for the inlet guide vanes, rotor, and exit stator will be presented for three streamtube positions and will be compared to the design vector diagrams.

DATA ANALYSIS

A data analysis computer program will be used to construct the streamline paths, mass flow weighted pressure ratio, and efficiency and vector diagrams which satisfy the test results. The inputs for this program are the measured inlet and outlet radial profiles of total pressure and total temperatures, the measured weight flow, and the compressor geometry. The program computes a solution which satisfies these inputs and radial equilibrium for both tangential velocities and meridional streamline curvature. In addition to the parameters discussed above, numerous other parameters are calculated by the program such as streamtube diffusion factors, loss coefficients, incidence and deviation angles.

The data analysis will be run for key test points such as peak pressure ratios and peak efficiencies in the 90 to 100 percent speed range and for any other points which may give some insight to deficiencies in the design. In each case, adjustments will be made to the program inputs until the solution best satisfies all of the measured data (e.g., static pressures and total temperature and pressure profiles). This solution will then be used to analyze deficient areas and to resolve what modifications will improve the performance. The compressor design techniques and empirical data will also be reevaluated based on these results.

UNCLASSIFIED

Security Classification

DOCUMENT CONTROL DATA - R & D

(Security classification of title, body of abstract and indexing annotation must be entered when the overall report is classified)

1. ORIGINATING ACTIVITY (Corporate author)

Curtiss-Wright Corporation
Wood-Ridge, New Jersey

2a. REPORT SECURITY CLASSIFICATION

None

2b. GROUP

3. REPORT TITLE

SINGLE-STAGE AXIAL COMPRESSOR STATOR REDESIGN INVESTIGATION

4. DESCRIPTIVE NOTES (Type of report and inclusive dates)

Final

5. AUTHOR(S) (First name, middle initial, last name)

Charles Muller

6. REPORT DATE	7a. TOTAL NO. OF PAGES	7b. NO. OF REFS
October 1970	92	7

8a. CONTRACT OR GRANT NO.	9a. ORIGINATOR'S REPORT NUMBER(S)
DAAJ02-69-C-0085	
b. PROJECT NO. Task 1G162203D14413	USAAVLABS Technical Report 70-56
c.	9b. OTHER REPORT NO(S) (Any other numbers that may be assigned this report)
d.	CW-WR-69-072.F

10. DISTRIBUTION STATEMENT

This document is subject to special export controls, and each transmittal to foreign governments or foreign nationals may be made only with prior approval of U.S. Army Aviation Materiel Laboratories, Fort Eustis, Virginia 23604.

11. SUPPLEMENTARY NOTES	12. SPONSORING MILITARY ACTIVITY
	U.S. Army Aviation Materiel Laboratories Fort Eustis, Virginia

13. ABSTRACT

This report describes the results of a program to redesign the exit stators of a 2.8:1 pressure ratio supersonic axial compressor, and to fabricate and test the redesigned stators to evaluate the effect of the redesign on the overall stage performance. This compressor is intended to serve as a boost stage in axial centrifugal compressors with overall pressure ratios of 16:1 for small gas turbine engines. The redesign was undertaken to provide an essentially cylindrical flow path aft of the rotor. This redesign eliminates an "S" shaped duct in the exit stator assembly of the original design. The measured performance showed no improvement over the original design, and indicated a two-point degradation in efficiency. The demonstrated exit stator and duct total pressure loss at design speed and stator setting was consistent with that demonstrated by the previous exit stators. Variation in the angle setting of the adjustable stator blades caused some movement of the surge line and flow range of the compressor, but offered no improvement in peak performance relative to the design setting.

DD FORM 1 NOV 68 1473 REPLACES DD FORM 1473, 1 JAN 64, WHICH IS OBSOLETE FOR ARMY USE.

UNCLASSIFIED

Security Classification

14 KEY WORDS	LINK A		LINK B		LINK C	
	ROLE	WT	ROLE	WT	ROLE	WT
supersonic flow						
compressor blades						
axial flow compressors						
gas turbine engines						
stator blades						